H-SPACE 2017 SELECTED PAPERS

2017, Budapest, Hungary

SELECTED PAPERS OF 3rd INTERNATIONAL CONFERENCE ON RESEARCH, TECHNOLOGY AND EDUCATION OF SPACE

H-SPACE 2017

organized by
Federated Innovation and Knowledge Centre of Budapest University of Technology and Economics and Hungarian Astronautical Society

Edited by László Bacsárdi and Kálmán Kovács

Magyar Asztronautikai Társaság

EGYESÜLT INNOVÁCIÓS ÉS TUDÁSKÖZPONT

Selected papers of 3rd International Conference on Research, Technology and Education of Space

February 9-10, 2017, Budapest, Hungary
at Budapest University of Technology and Economics

Organized by
Federated Innovation and Knowledge Centre of
Budapest University of Technology and Economics
and
Hungarian Astronautical Society

Editors
László Bacsárdi and Kálmán Kovács

MANT 2017

Selected papers of the 3rd International Conference on Research, Technology and Education of Space (H-SPACE2017)
February 9-10, 2017, Budapest, Hungary
BME building 'I', Hall IB 026
Magyar tudósok krt. 2., Budapest, H-1117 Hungary

Készült a BME VIK, a BME EIT, a MANT és a the urban institute Zrt. támogatásával
Szerkesztők: Dr. Bacsárdi László és Dr. Kovács Kálmán

Kiadja:
a Magyar Asztronautikai Társaság
1044 Budapest, Ipari park u. 10.
www.mant.hu
Budapest, 2017

Felelős kiadó: Dr. Bacsárdi László főtitkár

ISBN 978-963-7367-16-8

WELCOME from the Organizing Committee

The year of 2016 was determinative for Hungary in connection with space activities. It was the first year of Hungary's full ESA membership that raised high attention on the topic. On international level we saw that ESA ExoMars Program reached Mars and NASA's Juno spacecraft started orbiting Jupiter.

This year annual International Conference on Research, Technology and Education of Space has been held the 3rd time. The host was the BME Space Forum operated by the Federated Innovation and Knowledge Centre (EIT) of the Faculty of Electrical Engineering and Informatics at the Budapest University of Technology and Economics (BME) – in cooperation with the Hungarian Astronautical Society.

The organization of the conference comes at a time of growing opportunities arising from ESA recently granting full membership to Hungary and the need for a joint presentation of space activities pursued at BME. The selection of the date of the event pays tribute to the successful deployment to orbit and mission of the first Hungarian satellite, Masat-1.

The main topic of this year's conference was "Integrated space systems, missions and concepts". Naturally, our leading topic continues to be the roles of small satellites in space research and smart services, which covers applications and services from Earth Observation to future Smart City solutions. The agenda of the conference addresses scientific, technological and educational issues of space research and space activities. The conference was open for both local and international professionals and provides an opportunity to showcase Hungarian scientific, technological, educational and outreach activities, related to space.

The Organizing Committee had internationally recognized members: Prof. József Ádám, Dr. Tibor Bálint, Prof. László Pap, Prof. Gábor Stépán and Dr. Fruzsina Tari. We are grateful for their contributions to the success of the conference.

We appreciate the support of our sponsors, since their contribution made the offer of free-of-charge participation possible.

On the first day of the conference, we welcomed Prof. Amnon Ginati, ESA's Senior Advisor to the Directorate of Telecommunications and Integrated Applications. On the second day, Lluc Diaz joined us from ESA Technology Transfer Program Office.

The conference had three main sections: Science and Technology I, Science and Technology II and Education and Outreach (English and Hungarian). This was the first year when we organized a poster session with a number of great presentations.

After the conference, a special educational and scientific event was held named as SpacePaprika Workshop. The workshop was organized by the Space Generation Advisory Council (SGAC), the Budapest University of Technology and Economics (BME), the Hungarian Astronautical Society (MANT), and the Scientific Association for Infocommunications (HTE). During the workshop, a new Hungarian scientific experiment which could be placed onboard of the ISS has been discussed.

We issued a book of abstracts for the conference. During the conference, we had 1 keynote lecture, 2 invited lectures and 24 technical presentations from which 14 authors have submitted a full paper. These papers are included in this proceedings.

Dr. Kálmán Kovács
chair
Director of EIT BME

Dr. László Bacsárdi
co-chair
Secretary General of MANT

Final Conference Program

February 9-10, 2017
Budapest,
BME building 'I', Hall IB 026
Address: Magyar tudósok krt. 2., Budapest, H-1117, Hungary

February 9, Thursday

14:00–14.20 Opening

János Józsa, Rector of Budapest University of Techology and Economics (BME)
Fruzsina Tari, Hungarian Space Office, Ministry of National Development
Amnon Ginati, Directorate of Telecommunications and Integrated Applications, ESA
László Pap, National Council for Telecommunications and Information Technology of Hungary
János Solymosi, President of Hungarian Astronautical Society

14:20–15:20 Section of Science and Technology I/A

Keynote talk:
Space Eco-System Investment: Shaping the Future of the Space Economy
Amnon Ginati, ESA's Senior Advisor to the Directorate of Telecommunications and Integrated Applications

Philae's landing and autonomous operation control on a comet – challenges, achievements and lessons learnt
András Balázs, Wigner Research Centre for Physics of Hungarian Academy of Sciences (HAS)

Introducing E-GNSS navigation in the Hungarian Airspace: the BEYOND experience and the relevance of GNSS monitoring and vulnerab
Rita Markovits-Somogyi, HungaroControl Zrt.

15:20–16:15 Poster session with coffe break

Analyzing energy efficiency of sensor networks deployed on the surface of a Solar System Body
Roland Béres, Department of Networked Systems and Services, BME

Analyzing the Quantum Efficiency in Satellite-based Quantum Key Distribution Network
András Kiss, Institute of Informatics and Economics, University of Sopron

Comparative analysis of tropospheric delay models using reference data derived from ray tracing
Ildikó Juni, Department of Geodesy and Surveying, BME

Follow-up psychological status monitoring of the crew members of Concordia research station at Antarctica based on speech
Gábor Kiss, Department of Telecommunications and Media Informatics, BME

HABIT – instrument on ExoMars rover to detect microscopic liquid water
Ákos Kereszturi, Research Centre for Astronomy and Earth Sciences, HAS

Simulated Mars Rover Model Competition - More than a decade as a research area
Pál Gábor Vizi, Wigner Research Centre for Phyiscs, HAS

16:15-18:00 Section of Science and Technology I/B

Invited talk:

Performing chemistry in space, industrial and academic aspects: challenges and recent progress
Ferenc Darvas, ThalesNano Inc.

The Alphasat Scientific Experiment: Propagation Measurements and Statistics in the Ka/Q Band
Bernard Adjei-Frimpong, Department of Broadband Infocommunications and Electromagnetic Theory, BME

Developing a VLF transmiter for LEO satellites: Probing of Plasmasphere and RADiaton Belts - the POPRAD proposal
János Lichtenberger, Department of Geophysics and Space Sciences, Eötvös Loránd University

SATCOM developments for ESA
János Solymosi, BHE Bonn Hungary

An analysis of entanglened-based solutions on Earth-satellite channel
Ákos Korsós, Department of Networked Systems and Services, BME

Plasmaspheric density measurements based on guided VLF wave propagation
János Lichtenberger, Department of Geophysics and Space Sciences, Eötvös Loránd University

February 10, Friday

9:00–9:30 Opening of the second day

László Jakab, Dean of Faculty of Electrical Engineering and Informatics, BME
Marisa Michelini, President of the International Research Group on Physics Teaching
László Bacsárdi, Secretary General of Hungarian Astronautical Society

9:30–10:35 Section of Science and Technology II/A

Long talk:
Novel materials for aerospace hardware
Pál Bárczy, Admatis Kft.

Hexavalent Chromium free Coatings for Space Metallic Hardwares
Kalaivanan Thirupathi, University of Miskolc and Matmod Limited

10:35–11:00 Coffee break

11:00–12:00 Section of Science and Technology II/B,
Education/Outreach I/A *(in English)*
High speed integrated space streaming swarms as mission concepts
Pál Gábor Vizi, Wigner Research Centre for Phyiscs, HAS

RadMag development for the RADCUBE mission
Attila Hirn, Centre for Energy Research, HAS

Optical spectroscopy for high school and university students
Daniele Buongiorno, URDF - Università degli Studi di Udine

12:00–13:00 Lunch break

13:00–15:15 Section of Science and Technology II/C, **Education/Outreach I/B** *(in Hungarian)*

Invited talk:
How Space is Shaping our World
Lluc Diaz, Technology Transfer Office, ESA

Inspiring space enthusiast students and young professionals
István Arnócz, Space Generation Advisory Council

Space research and mini-satellites in secondary high school
Mária Pető, Székely Mikó High School, St. Goerge

About Space Weather in High Schools
Annamária Komáromi, Eötvös Loránd University

Funding opportunities of the EUROPLANET 2020
Melinda Dósa, Wigner Research Centre for Phyiscs, HAS

„Csillagszekér" Planetarium in education - experiences
Attila Szing, Stratolab Kft.

ESERO HUNGARY, the Hungarian Education Office of ESA
László Veress, Orion Space Generation Foundation

15:05-15:15 Closing remarks
Kálmán Kovács, Director of Federated Innovation and Knowledge Centre, BME

15:30-19:00 SpacePaprika Workshop
Students and Young Professionals Workshop (Invitation only, in Hungarian)

Content

A separate book of abstracts contains all of the abstracts accepted for the conference. During the conference, we had 1 keynote lecture, 2 invited lectures and 24 technical presentations from which 14 authors have submitted a full paper. These papers are included in this proceedings.

The Alphasat Scientific Experiment: Propagation Measurements and Statistics in the Ka/Q Band

Bernard Adjei-Frimpong
Budapest University of Technology and Economics
Broadband Infocommunications and Electromagnetic Theory(BME-HVT)
Budapest, Hungary
bernard.frimpong@hvt.bme.hu

Laszlo Csurgai-Horvath
Budapest University of Technology and Economics
Broadband Infocommunications and Electromagnetic Theory (BME-HVT),
Budapest, Hungary
laszlo.csurgai@hvt.bme.hu

***Abstract*—The increasing demand for bandwidth in radio communication in both terrestrial and satellite domain is becoming a serious challenge. This demand can be met by moving the communication channels to a higher frequency band. The Ku band is already exhausting its capacity, and the higher Q band is fast becoming the preferred choice for satellite communication. Hence for both research and commercial purposes it is important to effectively explore the Q band. This high frequency band is subject to attenuation, depolarization and signal scintillation due to different atmospheric effects.**

In 2013, in cooperation with Inmarsat the European Space Agency (ESA) launched the Alphasat communication satellite which also includes four technological experiments. One of them is the Aldo Paraboni payload, supported by ESA in the framework of the ARTES 8 Telecom program and the Italian Space Agency (ASI). The Alphasat scientific experiment is transmitting coherent beacon signals at Ka-band (19.701 GHz) and Q-band (39.402 GHz). The Q-band beacon covers the whole of Europe while the Ka-band beacon coverage additionally includes North Africa. This satellite supports Europe-wide experiments which investigate the atmospheric propagation effects occurring in the higher frequencies.

In view of this, BME-HVT has developed a ground station to help answer the basic questions that may arise when exploring the Ka/Q band. The station receives signal from the satellite to characterize the Satellite-Earth propagation channel in the Ka/Q band. The beacon receiver station is operating since 2014, collecting signal power data, and additionally records relevant meteorological data as well.

This paper gives an overview of the design and the components of the receiver station at BME-HVT. It reports on the experimental activities which have been carried out so far and describes the planned long term measurements, where the measured propagation statistics will be related to meteorological data from the weather station. The received data is then analysed and the first and second order attenuation statistics are compared with appropriate ITU-R models. We provide yearly and annual time series as well to demonstrate the attenuation events mainly induced by rain.

Keywords—propagation, Ka-band, Q-band, attenuation statistics, Alphasat

I. INTRODUCTION

Satellite communication at frequencies below 15GHz has become congested, and there are increasing demands for wide range broadband communication services. The demand for broadband service can be achieved by moving communication channels to a higher frequency band. However, at these frequencies communications are sensitive to atmospheric impairment which will result in attenuation due to rainy weather. This requires characterization of the channel, determined by statistical analysis of measurements to formulate a propagation impairment Mitigation Technique [1]. ESA launched the Alphasat communication satellite in 2013, with TDP5 Aldo Parabone payload for a research group across Europe to develop the Ka/Q beacon receivers for signals from the Alphasat. The Ka/Q beacon operates in the frequency of 19.701GHz and 39.402GHz respectively. These experiments aims at coordinating the propagation measurements across centres in Europe where the beacon receivers have been installed [1]-[7].

In view of this, the research group at BME-HVT a participant is also conducting experiments on the Alphasat with a receiver installed at our premises. The initial design was a Ka-receiver for Alphasat Beacon signal, rather it turns out that the Q-band system is achievable. Therefore, the decision of our research group was to build not only the Ka-band, but also the complete Q-band system as well.

The Ka/Q-band beacon receiver measures signals at 19.701 and 39.4GHz respectively [5]. These measurements are still ongoing and will enhance future research development activities at the department. A tracking system serves to keep the satellite on track. The station is also equipped with a meteorological station for weather monitoring and additional data collection.

The Ka/Q-band experimental data presented in this paper were collected by the BME-HVT beacon receiver station in Budapest/Hungary. The statistical results are relating to a whole year measurement that will be also compared with the

standardized results of the ITU-R models for validation purposes.

II. The Ka/Q Band Beacon Receiver

The beacon receiver is located at the premises of BME-HVT. It is installed 120m on top of the main BME-HVT building at N47.48 latitude and E19.06 longitude, with no interference from any object. One of objectives was to build a relatively low cost, high quality, reliable equipment with long term stability. The apparent in-orbit movement of the satellite is predicted not higher than ±3°, therefore the receiver has an independent tracking system to follow the inclined orbit of the Alphasat. Fig. 1 below is an overview of the complete system, based on separate building blocks:

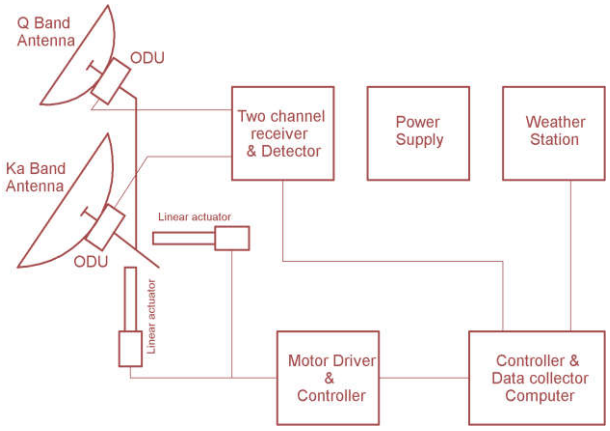

Fig. 1. Block scheme of the Alphasat two channel Beacon receiver station

The beacon receiver station is split into outdoor (ODU) and indoor units (IDU) respectively and includes High Performance Antennas (HPAs) [13]. HPAs Family offer high interference protections, and excellent radiation characteristics which is appropriate for the both Ka/Q-band Alphasat beacon frequencies. These antennas are Cassegrain types including the outdoor units (ODU) located on the back of the reflector dishes.

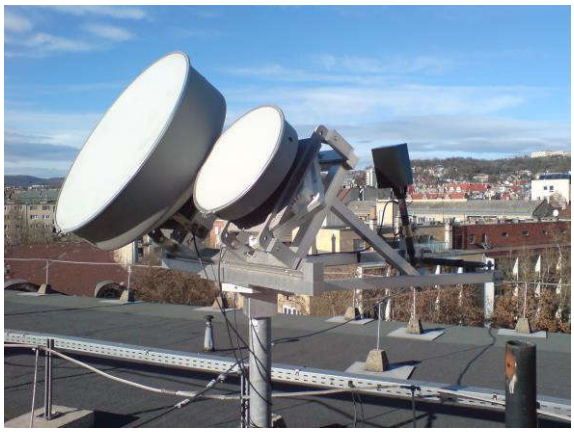

Fig. 2. High performance antennas and the tracking system

The beacon receiver station is equipped with the following antennas:

TABLE I. Technical parameters of the antennas

	Ka-band	**Q-band**
Type (Cassegrain)	HPA 0.6 S 180230 FR	HPA 0.3 S 380 SR
Frequency range	17.7-23.6GHz	37-39.5GHz
Diameter	0.6m	0.3m
Mid band gain	39.5dBi	39.2dBi
Polarization	Linear simplex (V/ H)	Linear simplex (V/H)
Half-power beam width	1.6°	1.7°

The building blocks of the receiver station are modified terrestrial microwave radio equipment with several hardware and firmware modifications. Both the Ka and the Q-band receivers are based on identical ODU construction; the difference is only the frequency of the locally synthesized signals to provide an identical 140MHz IF frequency. The ODU is a double conversion heterodyne receiver with synthesized local signal sources.

One of the main improvements of the original ODU is the reduction of the noise figure to 3dB. In order to generate a stable and jitter-free down-converted intermediate frequency (IF) signal, the oscillator in the ODU was also changed to a low phase noise OCXO with less than ± 1.0 ppb/day stability. The down-converted, filtered (bandwidth=100kHz) and amplified IF signal is connected with a low attenuation coaxial cable to the indoor unit (IDU). The calibrated gain of the ODU is 100dB and the interconnecting cable between the IDU and ODU provides the supply voltage for the outdoor unit. The downlink IF transfers the modulated subcarriers of a duplex control/telemetry channel. The telemetry informs about the current status of the system and contains also temperature information to allow the IDU to compensate the temperature-caused variations of the ODU's gain.

The IDU is based on a modified I-Q demodulator that processes the incoming IF signal. The 140 MHz IF signal is under sampled with an 80MHz analog/digital converter unit. The further functions are implemented by digital signal processing. The role of the quadrature digital down converter (QDDC) module is to convert down the sampled signal into baseband quadrature component signals. The baseband signals (I, Q) are decimated (512) and filtered by CIC and FIR filters.

Moreover, the ODU contains an internal temperature sensor with 1°C accuracy. This information is used for the temperature-compensation of the ODU's amplifier circuits. The temperature-dependency of the receiver chain is determined during the calibration of the ODU in a thermal-chamber. The firmware has a built-in compensation table, resulting in a temperature-independent, high accuracy level measurement. The temperature-compensated values are averaged and fed to a fine gain control unit that ensures the nominal 100dB ODU gain.

The filtered and decimated signal is processed by an 8192 point FFT where the beacon signal can be detected as the spectral component with highest amplitude. The carrier amplitude measurement is performed within 1 second and the final data is forwarded after a logarithmic conversion to the data collecting system. The resolution of the received power is 0.2dBm. By taking into account the speed of A/D conversion, the decimation and the FFT buffer size, the system bandwidth is 80MHz/512/8192=19.07Hz.

The noise figure and bandwidth of the receiver is able to detect signals in the range of -100 to -150 dBm. In addition, several status bits and the ODU temperature are also available for further processing purposes. A computer with RS232 serial interface is connected with 1/sec rate to the data acquisition and storage system. Two independent processing units are performing a simultaneous Ka and Q-band beacons processing.

The technical parameters are detailed in [5] and it was used to estimate the clear-sky received power at the receiving location. Link budget was calculated from the following equations below. Equation (1) is related to the free space attenuation where d is the distance and λ is the wavelength:

$$A_{fs} = 20\log\left(\frac{4\pi d}{\lambda}\right)\left[dB\right] \quad (1)$$

With (2) one can calculate the noise temperature of the Low Noise Amplifier (LNA), where T_0 is the temperature (generally 290°K is considered), NF is the Noise Factor of the receiver's amplifier:

$$T_{\ln a} = T_0\left(10^{NF/10}\right) - 1\left[K\right] \quad (2)$$

The system noise temperature (3) is the sum of the LNA's and the antenna's noise temperature. k denotes the Bolzmann-constant (-226.6 dBW/Hz/K), and B is the bandwidth.

$$T_{sys} = T_{ant} + T_{\ln a}\left[K\right] \quad (3)$$

$$N_{pd} = 10\log(k) + 10\log(T_{sys})\left[dBW/Hz\right] \quad (4)$$

$$N_p = 10\log(k) + 10\log(T_{sys}) + 10\log(B)\left[dBW\right] \quad (5)$$

In (6) G/T qualifies the system, G_r is the gain of the receiver antenna:

$$\frac{G}{T} = G_r - 10\log(T_{sys})\left[dB/K\right] \quad (6)$$

C_p is the carrier power (7) calculated with Effective Isotropically Radiated Power (EIRP), free space loss A_{fs}, receiver antenna gain G_r, and other attenuation factors (A_{nr}-non rain):

$$C_p = EIRP - A_{fs} - A_{nr} + G_r\left[dBW\right] \quad (7)$$

The carrier/noise ratio (8) is the difference of the carrier and noise power:

$$\frac{C}{N} = C_p - N_p\left[dBW\right] \quad (8)$$

Finally, to calculate the rain margin (9) C/N_{min} is the minimal C/N where the carrier is still detectable:

$$R_m = C_p - N_p - \frac{C}{N_{\min}}\left[dB\right] \quad (9)$$

III. Implementation Of ITU-R Rain Attenuation Model

In the ITU-R P.618 recommendation a model is provided for the satellite-Earth propagation channel and it allows to validate real measured time series [8]. Other ITU-R recommendations are also required for these calculations as ITU-R P.837 [9], P.838 [10], P.839 [11], and P.678 [12]. The ITU-R model estimates annual statistics of path attenuation at specified geographical locations for frequencies up to 55 GHz. This model will be applied in this study to comparatively validate the performance of the Ka and Q-band received data in Budapest over a one year period.

The model has the following main input parameters:

R_{001}: point rainfall rate for the location for 0.01% of an average year (mm/h)

h_s: height above mean sea level of the earth station (km)

θ: elevation angle (degrees)

φ: latitude of the Earth station (degrees)

f: frequency (GHz)

R_e: effective radius of the Earth (8500 km).

When local data for the station height above mean sea level is not available, an estimate can be obtained from the maps of topographic altitude given in Recommendation ITU-R P.1511 [1]. These procedures are provided here, with the line-by-line model presented first, followed by the approximation to the models.

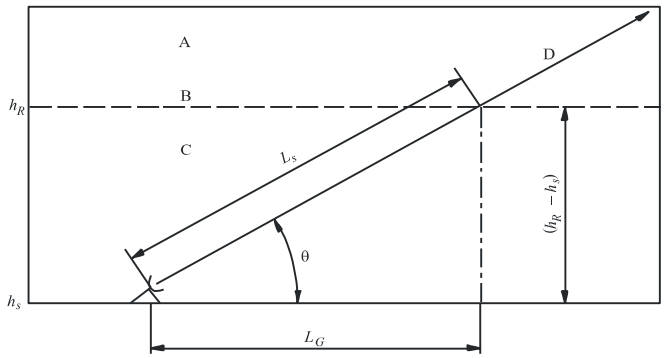

Fig. 3. Parameters for rain height calculations [11]

Step 1: Determine the rain height, h_R, as given in Recommendation ITU-R P.839 [11].

Step 2: For θ ≥ 5° compute the slant-path length, L_s, from:

$$L_s = \frac{(h_R - h_s)}{\sin\theta} \quad [\text{km}] \tag{10}$$

For $\theta < 5°$, the following formula is used:

$$L_s = \frac{2(h_R - h_s)}{\left(\sin^2\theta + \frac{2(h_R - h_s)}{R_e}\right)^{1/2} + \sin\theta} \quad [\text{km}] \tag{11}$$

If $h_R - h_s$ is less than or equal to zero, the predicted rain attenuation for any time percentage is zero and the following steps are not required.

Step 3: Calculate the horizontal projection, L_G, of the slant-path length from:

$$L_G = L_S \cos\theta \quad [\text{km}] \tag{12}$$

Step 4: Obtain the rainfall rate, R_{001}, exceeded for 0.01% of an average year (with an integration time of 1 min). If this long term statistic cannot be obtained from local data sources, an estimate can be obtained from the maps of rainfall rate given in Recommendation ITU-R P.837. If R_{001} is equal to zero, the predicted rain attenuation is zero for any time percentage and the following steps are not required.

Step 5: Obtain the specific attenuation, γ_R, using the frequency-dependent coefficients given in Recommendation ITU-R P.838 and the rainfall rate, R_{001}, determined from Step 4, by using:

$$\gamma_R = k(R_{001})^{\alpha} \quad [\text{dB/km}] \tag{13}$$

Step 6: Calculate the horizontal reduction factor, r_{001}, for 0.01% of the time:

$$r_{0.01} = \frac{1}{1 + 0.78\sqrt{\frac{L_G\,\gamma_R}{f}} - 0.38\left(1 - e^{-2L_G}\right)} \tag{14}$$

Step 7: Calculate the vertical adjustment factor, v_{001}, for 0.01% of the time:

$$\zeta = \tan^{-1}\left(\frac{h_R - h_s}{L_G\, r_{0.01}}\right) \quad [\text{deg}] \tag{15}$$

For $\zeta > \theta$,

$$L_R = \frac{L_G\, r_{0.01}}{\cos\theta} [\text{km}] \tag{16}$$

Else,

$$L_R = \frac{(h_R - h_s)}{\sin\theta} [\text{km}] \tag{17}$$

If $|\varphi| < 36°$, $\chi = 36 - |\varphi|$ degrees

Else, $\chi = 0$ degrees

Step 8: The effective path length is:

$$L_E = L_R v_{001} \quad [\text{km}] \tag{18}$$

where:

$$v_{0.01} = \frac{1}{1 + \sqrt{\sin\theta}\left(31\left(1 - e^{-(\theta/(1+\chi))}\right)\frac{\sqrt{L_R\,\gamma_R}}{f^2} - 0.45\right)} \tag{19}$$

Step 9: The predicted attenuation exceeded for 0.01% of an average year is obtained from:

$$A_{001} = \gamma_R L_E \quad [\text{dB}] \tag{20}$$

Step 10: The estimated attenuation to be exceeded for other percentages of an average year, in the range 0.001% to 5%, is determined from the attenuation to be exceeded for 0.01% for an average year:

If $p \geq 1\%$ or $|\varphi| \geq 36°$: $\beta = 0$

If $p < 1\%$ and $|\varphi| < 36°$ and $\theta \geq 25°$: $\beta = -0.005(|\varphi| - 36)$

Otherwise: $\beta = -0.005(|\varphi| - 36) + 1.8 - 4.25 \sin\theta$

$$A_p = A_{001}\left(\frac{P}{0.01}\right)^{-(0.655 + 0.033\ln(P) - 0.045\ln(A_{001}) - \beta(1-P)\sin\theta)} \quad [\text{dB}] \tag{21}$$

This method provides an estimate of the long term statistics of attenuation due to rain. When comparing measured statistics with the prediction, allowance should be given for the rather large year-to-year variability in rainfall rate statistics (see Recommendation ITU-R P.678).

IV. Measurements and Analysis

The results presented in the following correspond to a complete year from August 2015 to July 2016. The receiver station collects the received power with 1/sec rate, while the meteorological data with 1/min period. The following figure depicts the received power time series for both beacons together with the rainfall rate.

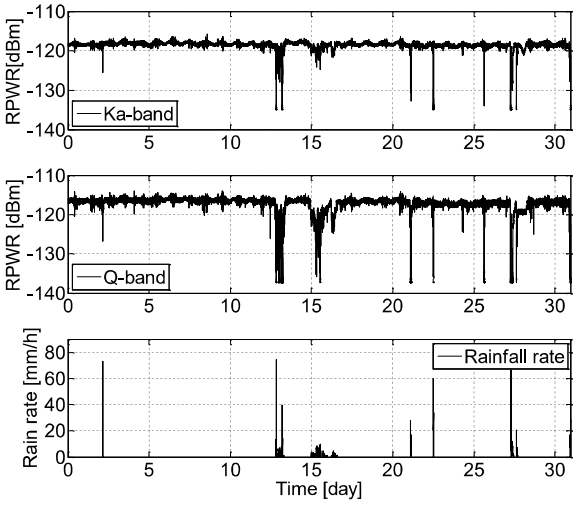

Fig. 4. Attenuation and rainfall rate (July, 2016)

The month of July 2016 was a rainy period and that can be observed in the figure 4, where rain events with 50mm/h or higher were also observed. As the higher frequencies are more intensively affected by the rain, the attenuation on Q-band is always higher than on the Ka-band.

For propagation modelling and statistics, the time series of attenuation provides the most relevant information. In order to convert the received power to attenuation we subtract the measured values from the median (clear sky) level. The attenuation time series for the whole investigated period (08.2015-07.2016) is depicted in Fig. 5.

We can observe several attenuation events in this figure, mainly caused by the rainy periods during this year. The Complementary Cumulative Distribution Function (CCDF) of the attenuation informs us about the probability conditions of different attenuation levels, as it can see in Fig. 6.

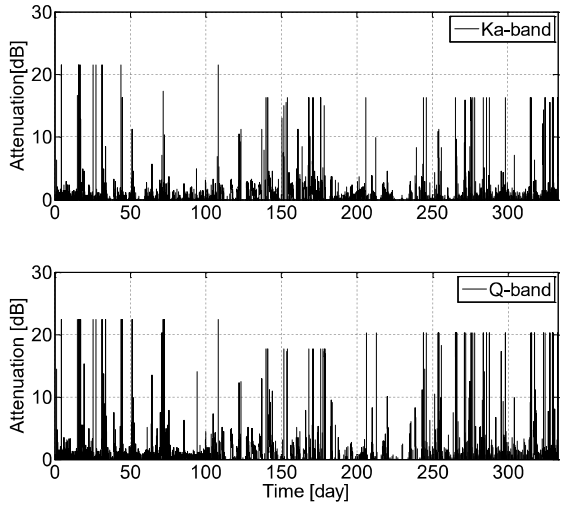

Fig. 5. Ka and Q-band attenuation time series (August 2015-July 2016)

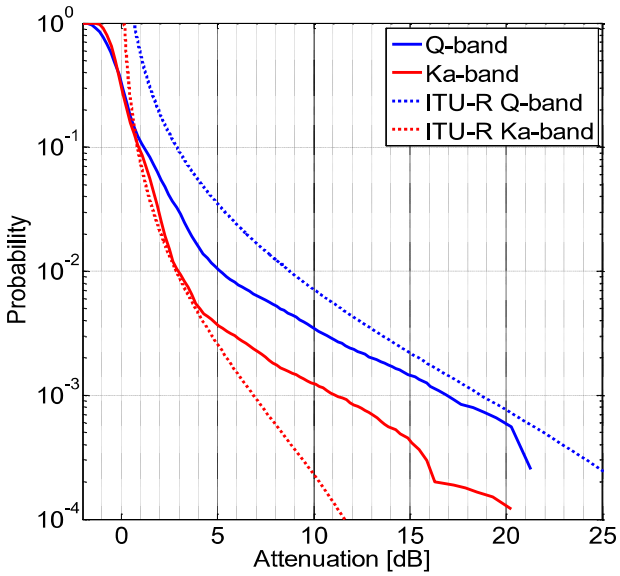

Fig. 6. CCDF of Ka and Q-band annual attenuation

The recommendation ITU-R P.618 was introduced in the previous section. It is a method to calculate the distribution of attenuation for an Earth-space radio link for any desired geographical location. In Fig. 6 both the measured and the modelled CCDF's are presented. There is some deviation between the real measurement and the model, that could be explained with several circumstanced. One important parameter is the R_{001} value that characterizes the given geographical location. According to the ITU regulations its value is 42mm/h for Budapest location. Nevertheless, this value may change during different years according to the local weather conditions. This could be one of the reasons why the measured and modelled curves are not exactly covering each other. Nevertheless, this issue should be studied deeper in the future data processing work.

ACKNOWLEDGMENT

This research work is funded by the Government of Hungary through the ESA Contract 4000109841/13/NL/KML under the PECS (Plan for European Cooperating States).

REFERENCES

[1] Teschl F. et al., "The Ka/Q-band Alphasat Ground Propagation Terminal – First Months of Operation", In Proc. 8th European Conference on Antennas and Propagation, Hague, The Netherlands, 6-11 April 2014.

[2] Machado F. et. al., "The Ka- and Q-band AlphaSat ground station in Vigo", In Proc. 9th European Conference on Antennas and Propagation, Lisbon, Portugal, 12-17 April 2015.

[3] Riera J.M. et. al.," Alphasat Propagation Experiment in Madrid: Quality Assessment of the Measurements", In Proc. 9th European Conference on Antennas and Propagation, Lisbon, Portugal, 12-17 April 2015.

[4] Rocha A. et. al., "Alphasat Q/V-band Propagation Campaign Preparation in Aveiro", In Proc. 9th European Conference on Antennas and Propagation, Lisbon, Portugal, 12-17 April 2015.

[5] Csurgai-Horváth L. et. al., "The Aldo Paraboni Scientific Experiment: Ka/Q Band Receiver Station in Hungary", In Proc. 9th European Conference on Antennas and Propagation, Lisbon, Portugal, 12-17 April 2015.

[6] Nessel J. et. al., "Preliminary Statistics from the NASA Alphasat Beacon Receiver in Milan", Italy, In Proc. 9th European Conference on Antennas and Propagation, Lisbon, Portugal, 12-17 April 2015.

[7] Marziani A. et. al., "AlphaSat Ka-band and Q-band Receiving Station in Rome: development, status and measurements", 9th European Conference on Antennas and Propagation, Lisbon, Portugal, 12-17 April 2015.

[8] Recommendation ITU-R P.618-12, Propagation data and prediction methods required for the design of Earth-space telecommunication systems, ITU, 2015.

[9] Recommendation ITU-R P.837-4, Characteristics of precipitation for propagation modelling, ITU, 2003.

[10] Recommendation ITU-R P.838-3,Specific attenuation model for rain for use in prediction methods, ITU, 2005

[11] Recommendation ITU-R P.839-4, Rain height model for prediction methods, ITU, 2013.

[12] Recommendation ITU-R P.678-3, Characterization of the variability of propagation phenomena and estimation of the risk associated with propagation margin, ITU, 2015.

[13] GRANTE Antenna Development and Production Corporation, HPA…380 Series Antenna Specifications, http://grante.hu

[14] Recommendation ITU-R P.1511-1, Topography for Earth-space propagation modelling, ITU, 2015.

Időjárás és annak előrejelzése a Földön kívül

Egy középiskolai fizikatanár szemszögéből

Komáromi Annamária
Fizika Doktori Iskola Fizika Tanítása Program
ELTE TTK
Budapest, Magyarország
annamaria1015@gmail.com

***Absztract* — A huszonegyedik században a földi időjárás mellett egyre gyakrabban esik szó egy viszonylag új fogalomról, az űridőjárásról. Ez természetes, hiszen egyre több esetben igazolódik, hogy az űridőjárás a földfelszíni folyamatokat is befolyásolja. Például az űridőjárás sokszor hatással lehet a műholdak, illetve bármely űreszköz elektronikai rendszerére, így közvetve a mi mindennapi életünkre is, hiszen a műholdak által szolgáltatott információk mindennapi életünk egyre nagyobb részével kerülnek kapcsolatba. Ezért a középiskolai fizika tanításába is be kell, hogy kerüljön a műholdakra vonatkozó fizikai ismeretek tanítása mellett, az űridőjárás fogalmának tisztázása. Meg kell beszélnünk a diákokkal, mit értünk pontosan űridőjárás alatt, milyen tényezők alakítanak ki egy esetleges kedvezőlen űridőjárást. Rá kell mutatnunk, hogy mi a különbség napvihar és űrvihar között. Ehhez természetesen először meg kell ismerkedni a diákoknak a különböző naptevékenységekkel. Napjainban a technikai fejlődés, és az űrkutatás térhódítása következtében ugrásszerűen gyarapodnak az űridőjárással kapcsolatos információink, melyek meg kell hogy jelenjenek valamilyen szinten a középiskolai fizikaórán is. A téma kiválóan alkalmas arra, hogy alkalmazzuk az úgy nevezett "kutatás alapú tanítás" módszerét, hiszen rendkívül széles skálán juthatnak információhoz a különböző űrkutatási, illetve csillagászati portálokon. Kutatási téma lehet például a kedvezőtlen űridőjárás kevésbé ismert hatásainak a vizsgálata, többek között a költöző madarak vándorlását manipuláló hatása, vagy akár befolyása a csőhálózatok korrózióvédelmére. Ismerjék meg a diákok a legnagyobb űridőjárásjelző központok honlapjait, melyeken valós időben nyomon lehet követni az űridőjárást. Tudjanak arról is, hogy milyen űreszközökkel történik napjainkban az űridőjárás figyelése. Találhatunk grafikonokat az űridőjárás jelző központok honlapjain, melyek kitűnően alkalmasak arra, hogy elemezzék őket a diákok. Ennek a témakörnek a mélyebb tanítása révén is kialakíthatjuk a diákokban az intenzívebb "űrtudatosságot", melynek folytán fel lehet kelteni bennük az űrkutatás iránti érdeklődést, hiszen századunkban jelentősége miatt nagyon fontos, hogy vonzó legyen a fiatalok számára az űrkutatás.**

Kulcsszavak — középiskolai fizika tanítás, űridőjárás, kutatás-alapú tanítás, űrkutatás

I. Bevezetés

A XX. század végére megszoktuk, hogy az időjárás előrejelzésében egyre nagyobb szerep jut a mesterséges holdaknak. Mára mindennapjaink részévé váltak az előrejelzések kapcsán a különböző mesterséges holdak által készített felvételek. Szabadtéri programok, mint például kerti parti, hangversenyek, kirándulások, tervezésekor is természetes, hogy megnézzük a földi meteorológiai radarral készült radarképet, illetve a meteorológiai mesterséges holdak segítségével látható, vagy infravörös tartományban készült radartérképet, és ennek alapján tervezzük programunkat. De ehhez elengedhetetlenül szükséges, hogy megfelelően működjenek ezek az űreszközök. Ezért egyre növekvő jelentősége van az űridőjárás figyelésének, előrejelzésének is, hiszen a kedvezőtlen űrbéli körülmények megzavarhatják a mesterséges holdak működését.

A középiskolai fizika oktatásunkból sem maradhat ki ez a fogalom a fontossága miatt, valamint azért, mert emellett a híradásokban is egyre gyakrabban találkozhatunk vele.

II. Űridőjárás

Az űridőjárás alatt elsősorban a naptevékenységet, illetve az abból származó bolygónkhoz elérkező különböző hatásokat értjük [1]. A kedvezőtlen űridőjárásnak beláthatatlan következménye lehet az emberi társadalmakra nézve, hiszen egy-egy erősebb plazmakitörés megbéníthatja az űreszközök elektronikus rendszerét és ez többek között komoly közlekedési problémákat jelenthet, vagy például az információáramlás akadozása akár pénzügyi tőzsdekrachhoz is vezethet. Az 1. ábrán megfigyelhetjük az űridőjárás hatásait egy egyszerűsített változatban.

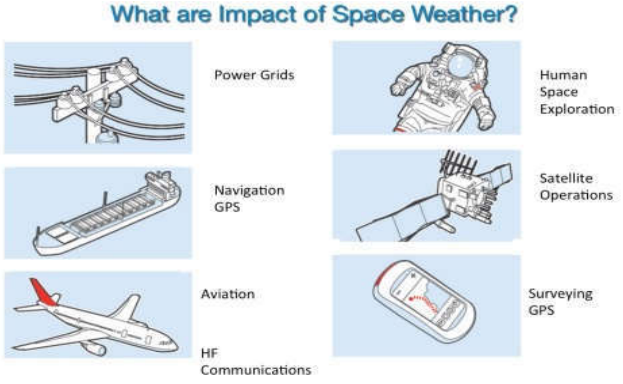

1.ábra: Az űridőjárás hatásai (forrás: [2])

Az űrkutatók, napfizikával foglalkozók körében ez a téma – kiemelkedő jelentősége miatt - az elmúlt években fokozatosan vált az egyik legfontosabb kutatási területté. A hétköznapokban olyankor hallunk csak az űridőjárásról, amikor egy-egy komoly napkitörésnek figyelemre méltó hatása van mindennapjainkra. Ez valószínűleg így is marad annak ellenére, hogy léteznek honlapok, ahol bárki megnézheti a Nap pillanatnyi állapotát, de valójában az esetleges lehetséges védekezés egy-egy mágneses viharral szemben továbbra sem az egyén feladata lesz.

Ezeknek a honlapoknak az adatai ugyanakkor iskolai kutatómunkákhoz is nagyon jól használhatók.

A. Hogyan alakul ki a kedvezőtlen űridőjárás?

Időnként meg lehet figyelni a Nap felszínén hirtelen fényesedéseket, illetve a felszínből kinyúló fényes alakzatokat, melyeket flereknek neveztek el. Ezek tulajdonképpen több milliónyi atombomba energiájának megfelelő robbanások a Nap felszínén. Kialakulásuk oka, hogy a Nap nem minden része forog ugyanakkora szögsebességgel, így a Nap mágneses erővonalai keresztezhetik egymást, és ezek az összecsavarodott erővonalak okozzák ezeket az óriási robbanásokat.

A flereket a 70-es évektől kezdve figyelik meg a GOES (Geostationary Operational Environmental Satellite) műholdak. Ezeket a robbanásokat többnyire a Nap koronájából anyag kidobódás követi, melyet napkitörésként emlegetünk (2. ábra). A nemzetközi szakirodalomban CMS-ként rövidítik a jelenséget (Coronal Mass Ejections CME).

Az iskolai fizika tanításban csak elvétve említjük meg ezeket a viszonylag új fogalmakat, melyek az űrkutatás és csillagászat fejlődésének köszönhetően mára mindennapossá váltak a szakmai körökben.

Egy-egy jelentősebb napkitörés során töltött részecskék sokasága érheti el bolygónkat. Ezek főként nagy energiájú elektronok, protonok és más nehézionok, melyek elérve a Föld mágneses mezejét (magnetoszféra) mágneses viharokat okoznak, melyek megzavarják az űreszközök elektronikus rendszerét, de sokszor a földi elektromos rendszerekre is hatással vannak. Galilei az 1600-as évek elején megfigyelt a Nap felszínén sötétebb területeket, melyeket napfoltoknak hívunk.

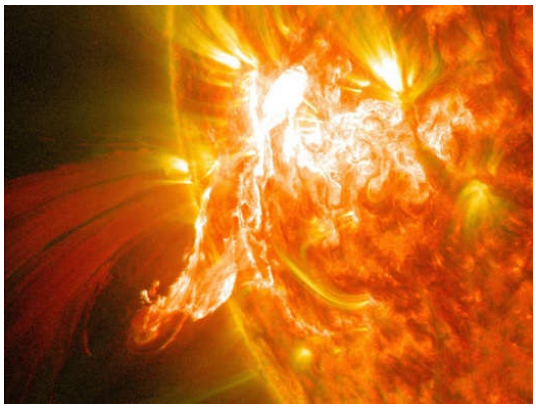

2.ábra: Flerek (forrás: [3])

A flerekben a napfoltok mágneses terében felhalmozódott energia szabadul fel. 1859 szeptember 1-én Richard Carrington angol csillagász felfigyelt egy kiterjedt napfolt csoportra, itt kialakultak flerek, majd az ezt követő koronakitörés 17 óra alatt elérte a Földet, melynek következtében olyan erős mágneses vihar alakult ki, hogy még az egyenlítőhöz közeli részeken is éjszaka lehetett olvasni a sarki fénynél. Az akkori Morse-féle távíróberendezéseket is megzavarta ez a jelentős napkitörés, de ekkor ennek a jelenségnek még nem ismerték az okát.[4]. A töltött részecskéknek ezt az áramlatát először Scott E. Forbush amerikai csillagász, fizikus es geofizikus észlelte 1946-ban, és ő még a Napból érkező kozmikus sugárként értelmezte.

Fontos megjegyezni, hogy ezek a töltött részecskék rendkívül nagy sebességgel, időnként a fénysebesség nagyságrendjébe eső sebességgel, körülbelül a fénysebesség 14%-ával akár 1 óra alatt is elérhetik a Föld magnetoszféráját. Szokás ezt az áramlatot napszélnek is emlegetni, de fontos megjegyezni, hogy a napszél többféle lehet. Forrása mindenképpen a Nap koronája, melynek hőmérséklete olyan magas (6000 K), hogy a részecskék egy részének a sebessége meghaladja a Nap gravitációja által meghatározott szökési sebességet, így el tudja hagyni a Nap felszínét. Közepes erősségű napszél eseten ezeknek a sebessége 400 km/s" [5]. A napszélnek egy további fajtája a korona lyukakból kiáramló töltött részecskék sokasága. Extrém ultraibolya és röntgen sugárzás tartományába eső hullámhosszon lehet megfigyelni a Nap koronáján sötétebb részeket, ezeket nevezzük korona lyukaknak. Az innen kiáramlott részecskék sebessége elérheti akár a 900 km/s –mos sebességet is. A korona lyukak állandóan változnak mind méretüket, mind alakjukat tekintve. A különböző típusú napszeleket a Földön is lehet érzékelni. A Stanford Egyetemen található például a Wilcox Nap megfigyelő obszervatórium, ahol a Napon helytől függően határozzak meg a mágneses tér paramétereit.

B. Napvihar, űrvihar

Különböző portálokat megnézve tapasztalhatjuk, hogy mind hazai, mind nemzetközi szinten keverik a híradásokban a két fogalmat. Fizika tanításunk során érdemes tisztázni a köztük lévő különbséget. Napvihar alatt a Nap felszínéről való anyag és energia kitöréseket értjük. Ez nem feltétlenül okoz űrvihart. Az űrvihar alatt a kedvezőtlen űridőjárás megnyilvánulását értjük, mely a fentebb említett számos fizikai hatással van a Föld környezetére [6].

III. HOGYAN TÖRTÉNIK AZ ŰRIDŐJÁRÁS FIGYELÉSE?

Napjainkban igen sokrétűen történik az űridőjárás megfigyelése. A sokrétűség alatt értem a megfigyelő állomás helyszínét, földi és űrbéli megfigyelőállomások, illetve az érzékelő eszközök is ennek megfelelően rendkívül széles skálán mozognak. Talán ez is az oka, hogy iskolai keretek között normál tanórán erről a témáról nemigen esik szó. A projekt alapú tanításban ezzel szemben érdemes figyelmet szentelnünk ezeknek az eszközöknek, hiszen működési elvük sokszor a fizika különböző területein megtanult törvények megértését segíthetik, illetve a törvények gyakorlati életben történő alkalmazásának mutatják szép példáját.

A DSCOVR (Deep Space Climate Observatory) műhold az első olyan műhold, melyet kifejezetten az űridőjárás megfigyelésére és előrejelzésére állítottak pályára (3.ábra). Az űreszköz a Föld-Nap-űrszonda háromtest-probléma L1 Lagrange pontja környékén kering, azaz ebben a pontban a Nap és a Föld gravitációs vonzása kiegyenlíti egymást. Az űreszköz elsődleges érzékelője az úgynevezett Faraday Cup plazmaszenzor, mely működésének elve, hogy a töltött részecskék hatására az áramkörben elektromos áram jön létre, és ennek erősségéből lehet következtetni a töltött részecskék intenzitására. A Faraday Cup szenzor tudja mérni a kőmérsékletet, illetve a részecskék sebességét. A mért adatok valós időben bárki számára elérhetők a http://www.swpc.noaa.gov/products/real-time-solar-wind%20 honlapon, így iskolai elemzésre is alkalmas. Az eszköz kapcsán lehetőség nyílik arra, hogy világossá tegyük a hőmérsékleti sebesség fogalmát. A fizika tanítása közben először beszélünk hőmérsékletről, melyet fenomenológiai alapon vezetünk be, majd értelmezzük a testek belső energiáját. A kinetikus gázmodellben teremtünk kapcsolatot elméleti úton a makroszkopikus világban értelmezett hőmérséklet fogalom és a mikroszkopikus világban megjelenő részecskék mozgási energiája, ezáltal sebessége között. Ez az összekapcsolás, illetve átmenet az egyik értelmezésből a másikba a diákoknak nem könnyű. Emiatt szerencsés bevezetni a légüres térben a hőmérsékleti sebesség fogalmát, mely könnyebben megérthetővé teszi a hőmérséklet fizikai mennyiségét. A DSCOVR mesterséges hold másik alapvető műszere egy magnetométer, mely mérni tudja a napszél mágneses mezejének erősségét és irányát, ezáltal előre lehet jelezni egy közelgő nagyobb erősségű mágneses vihart.

Felmerülhet a kérdés, hogy a fizika tanítása során mikor célszerű az űridőjárást megemlíteni. Erre több lehetőség is kínálkozik. Akár a magnetométer tanításánál, de például a Lorentz erő említésénél a sarki fény kapcsán is kiváló alkalom van a fogalom megismertetésére. Talán a legszerencsésebb többször visszatérni ehhez a fogalomhoz.

A normál légköri időjárás előrejelzések különböző modellek alapján történő számítások révén jönnek létre. A DSCOVR műhold műszerei által mért adatok segítségével megszülethet a geospace modell, mely alapjául szolgálhat az eddiginél sokkal fejlettebb űridőjárás előrejelzésnek.

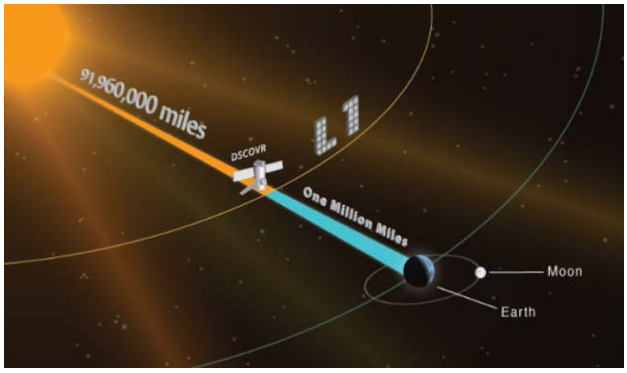

3.ábra: A DSCOVR műhold pályája (forrás: [7])

A. Egy kevésbé ismert hatása a kedvezőtlen űridőjárásnak

A kedvezőtlen űridőjárás hatásai között szerepel egy első hallásra talán meglepő jelenség is, a csővezetékek korróziója. Gondoljunk itt a kőolaj, gáz, de akár a vizet szállító hatalmas csőhálózatokra. Ezek a csövek, ahhoz, hogy a megfelelő nyomást elbírják, acélból készülnek. Emiatt azonban nagy figyelmet kell fordítani a korrózióvédelemre. Kívülről szigetelik őket, illetve sokszor elektrokémiai eljárás alkalmazásával is igyekeznek lassítani a korróziót. Az eljárást katódvédelemnek nevezik, lényege, hogy a védendő csővezeték tölti be a katód szerepét és a környező talajba helyezett megfelelő eszköz (a csővezeték anyagánál nagyobb elektron negativitású anyag, például magnézium) az anódét. Egy egyenáramú áramforrásra kötve létrejön az elektronok megfelelő irányú áramlása, így a védendő csővezeték nem korrodál. A folyamatra jellemző egy -0,85V és -1,35V közötti biztonságos feszültségtartomány. Erősebb naptevékenység hatására kialakuló geomágneses viharok idején a rendszerben lévő feszültségérték kikerülhet ebből a biztonsági tartományból, veszélyeztetve ezáltal a katódvédelem megfelelő működését.

A 4. ábrán egy ilyen feszültség ingadozást figyelhetünk meg 2000 áprilisában. Jól lehet látni, hogy a katódvédelem feszültségét hogyan befolyásolta a mágneses vihar. Az adatokat Ottawában a Gemagnetic Laboratory-ban rögzítették.

B. A kedvezőtlen űridőjárás biológiai hatásai

Már több évtizede, hogy az ember megjelent a világűrben. Az űrhajósok számára komoly veszélyt jelent a napszél. Többek között a Mars-programok megvalósításánál is még a megoldandó problémák között szerepel az űrhajósok részecskesugárzás elleni védelme, ugyanis a világűrben az űrhajósoknál a fokozott sugárterhelés miatt megnövekszik a daganatos betegségek kockázata, emellett a központi idegrendszer is könnyebben károsodhat, valamint az érrendszerre is kihatással lehet az extrém részecskesugárzás.

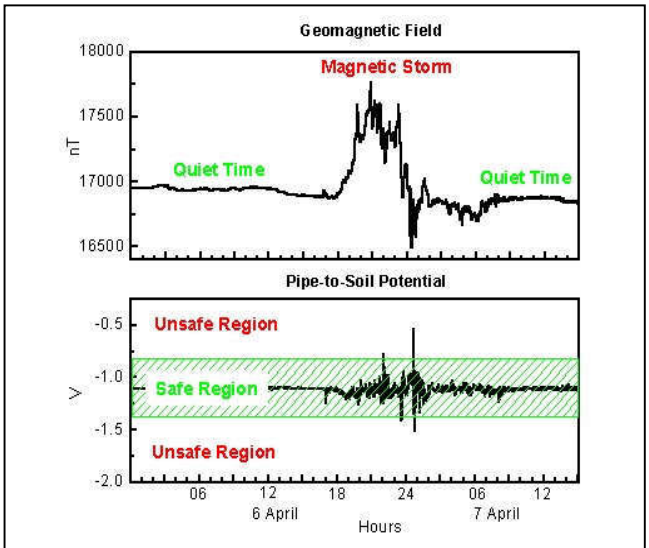

4.ábra: Geomágneses vihar hatása akatódvédelemre (forrás: [8])

C. *A világűrből érkező töltött részecskék detektálása*

A világűrből érkező töltött részecskéket különböző eszközök segítségével érzékelik. Ezeknek működési alapelve sokszor szintén a középiskolában is tanult fizikai törvényeken alapul. Egyik ilyen eszköz a PAMELA (Payload for Antimatter Matter Exploration and Light-nuclei Astrophysics), mely egy orosz távérzékelő műholdon teljesít szolgálatot (5. ábra). A proton antirészecskéjét, az antiprotont is sikerült detektálni nagy számban az olasz PAMELA fedélzeti űreszköznek 2011-ben.

Az antiprotonokat a Föld mágneses tere ejti csapdába a belső Van Allen övben. A PAMELA űreszköznek fontos eleme egy mágneses spektrométer, melynek összetevői egy neodymion-vas-bór állandó mágnes és egy precíziós nyomkövető rendszer. A töltött részecskék beérkezve az eszköz nyílásán eltérülnek a mágneses mezőben. A kialakult pályagörbe alapján következtethetünk a részecske elektromos és mágneses tulajdonságaira.

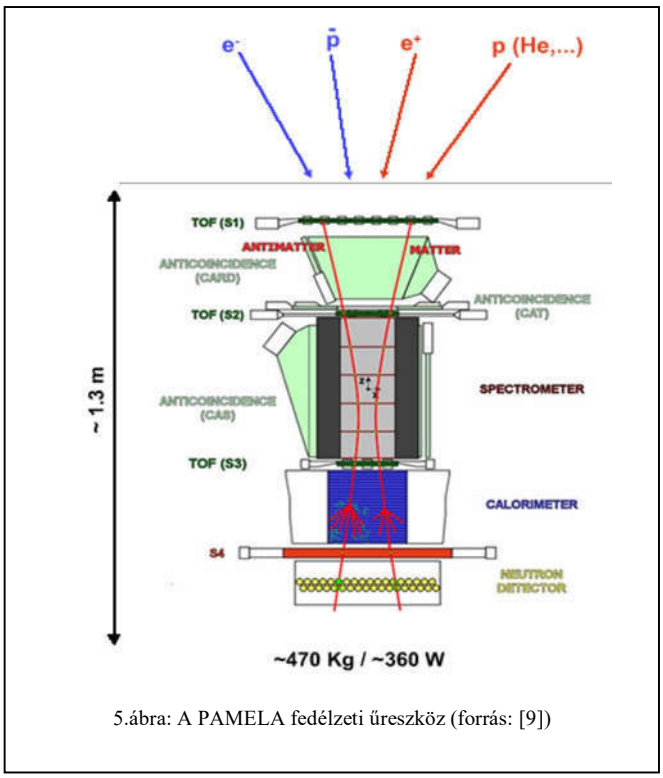

5.ábra: A PAMELA fedélzeti űreszköz (forrás: [9])

A mintavételt egy kaloriméterben képezik le oly módon, hogy vékony szilícium érzékelő lapokat helyeznek be merőlegesen a wolfram érzékelő lemezek közé. A kölcsönható részecske felszabaduló energiáját mérik. A részecskék megsemmisülésekor extra nagy energia szabadul fel, ami részecsketípustól függően, különböző mintát rajzol a kaloriméterbe. A megfigyelt energiamintából következtethetünk az antiproton jelenlétére [9].

IV. Összefoglalás

A leírtak alapján érzékelhető, hogy az űridőjárás kutatása egy szerteágazó és nagyon jelentős kutatási terület, így a témával való részletesebb foglalkozás a középiskolában kiválóan alkalmas akár pályaorientáció kialakítására is.

A cikk anyaga az ELTE Fizika Doktori Iskola Fizika Tanítása program keretében, az űrkutatás nagyobb mértékű bevonása a fizika oktatásába kutatási téma keretében született. A szerző a cikk anyagával megegyező témában előadást tartott 2016-ban az olasz fizikatanárok nemzeti konferenciáján [10], illetve a témához kapcsolódó kísérletét beválasztották a 2017-ben Debrecenben megrendezésre kerülő Science on Stage Nemzetközi Fesztivál Magyarországot képviselő kísérletei közé.

Köszönetnyilvánítás

A tanulmány elkészítését a Magyar Tudományos Akadémia Tantárgy-pedagógiai Kutatási Programja támogatta.

Hivatkozások

[1] Ludmány A., “Naptevékenység és űridőjárás”, Fizikai Szemle 2016/06, pp. 181-184

[2] http://ccmc.gsfc.nasa.gov/support/ILWS/MATERIALS/All_School_Materials/Tutorials_Sunday/Introduction_Domains_Kuznetsova/Inroduction_Domains_Masha_Kuznetsova_without_j2s.pdf

[3] http://www.space.com/24544-solar-flare-partial-eclipse-nasa-sdo.html

[4] http://ccmc.gsfc.nasa.gov/support//ILWS/MATERIALS/All_School_Materials/Tutorials_Sunday/CMEs_Flares_Taktakishvili/CMEs_Flares_Sandro_Taktakishvili.pdf

[5] http://solarscience.msfc.nasa.gov/SolarWind.shtml

[6] http://www.springer.com/us/book/9781402000300

[7] http://www.noaa.gov/its-all-systems-go-noaas-first-space-weather-satellite

[8] http://www.spaceweather.gc.ca/tech/se-pip-en.php

[9] http://pamela.roma2.infn.it/index.php?option=com_content&task=view&id=28&Itemid=264

[10] Komaromi A., “Lo Space Weather nel Liceo”, 55 Congresso Nazionale A.I.F., 12-15 Oct 2016, Gran Sasso, Italy

Philae's landing and autonomous operation control on a comet

challenges, achievements and lessons learnt

A.Balázs[1], A.Baksa[2], H.Bitterlich[3], I.Hernyes[1], O.Küchemann[5], Z.Pálos[1], J.Rustenbach[3], W.Schmidt[4], P.Spányi[1], J.Sulyán[2], S.Szalai[2], K.Szegő[1], P.Vizi[1], L.Várhalmi[1]

[1] Wigner Research Centre for Physics, Budapest, Hungary
[2] SGF Co. Ltd., Budapest, Hungary
[3] Max-Planck Institute for Solar System Research (MPS), Göttingen, Germany
[4] Finnish Meteorological Institute (FMI), Helsinki, Finland
[5] Zentrum für Deutsche Luft- und Raumfahrt (DLR), Cologne, Germany
Contacts via email: balazs.andras@wigner.mta.hu

***Abstract* —** The Rosetta-Philae mission was an ambitious cornerstone project of the European Space Agency. It was of Europe-wide significance in terms of technological and research organisation, and of worldwide significance in scientific and public outreach terms. A brief historical summary of the highlights of the Philae mission in the introductory section creates the framework for discussing the aim of this paper. As basis for reasoning, the major hardware, software and mission operational design aspects of Philae's central on-board computer are also roughly outlined. The second part of the paper is more future-oriented; it is devoted to "lessons learnt". The intention is to scrutinize what the team did or missed to do to make Philae project protected against faults, and yet when faults arose, what the team did or missed to do to overcome them.

***Keywords* —** *critical systems, fault tolerance and graceful degradation, autonomous operation, operational flexibility, mission operational approaches, lessons learnt*

I. A BRIEF, HISTORICAL SUMMARY OF THE PHILAE MISSION

After a ten-year journey across the Solar System and many complicated manoeuvres, the Rosetta spacecraft – carrying the Philae lander, a scientific mini-laboratory – smoothly approached a small celestial body, comet CG/67P. Furthermore, the Rosetta spacecraft executed additional manoeuvres to fly a multitude of low and high altitude orbits around the comet, mapping its shape and surface in detail never seen before. The ballistic delivery of the Philae lander onto the surface of the comet 500 million km away from Earth was also a remarkable technical achievement. The Philae lander [1] had the complexity of a spacecraft; in addition to traditional and some Philae specific subsystems it was equipped with numerous scientific instruments (see Fig. 1a/b).

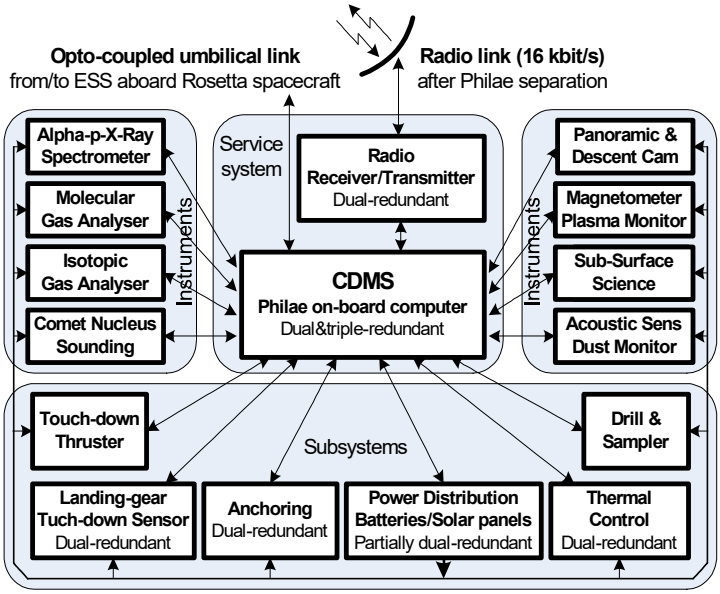

Fig. 1a/b. a/ Service system, subsystems and scientific instruments aboard b/ Philae lander

The Philae maintenance and in-flight calibration activities throughout the ten-year cruise phase and the comet science operations were partitioned into 1+3 mission phases:

Mission Phase	Duration	Energy Sources
Cruise	~10 years	Max. 53W by Rosetta spacecraft
Separation-Descent-Landing (SDL)	~7 hours	Solar generators and ~1300+100 Wh by primary and rechargeable battery
First Comet Science Sequences (FSS)	~60 hours	Solar generators and ~1300+100 Wh by primary and rechargeable battery
Long Terms Science Operations (LTS)	open-ended	Solar generators and ~100 Wh by rechargeable battery

Having completed with the selection of scientifically promising, flight-dynamically [2] safely accessible and environmentally acceptable (temperature, solar illumination, local geography/geology and surface characteristics) landing site of Philae on the comet (see Fig. 2a), the flight-dynamics team of the European Space Operation Centre (ESOC) specified a safe course of the Rosetta spacecraft to deliver Philae to the target landing site on the comet.

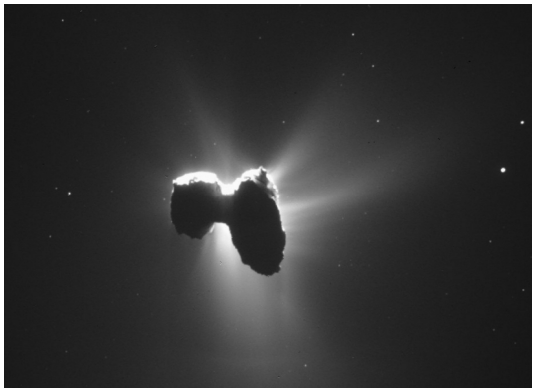

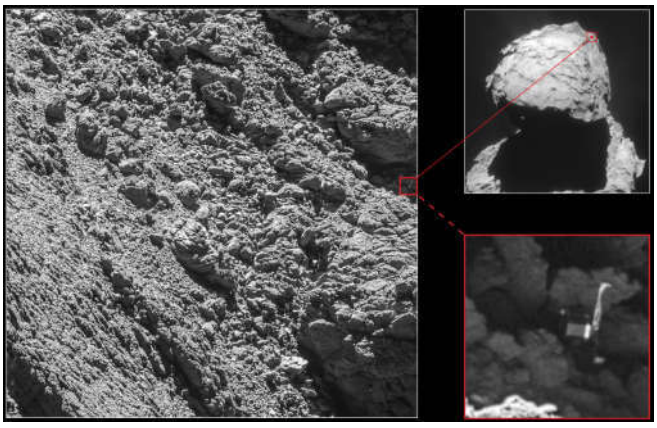

Fig. 2a/b. a/ Comet CG67/P; b/ Philae; Images by Rosetta's NAVCAM and Osiris camera

The landing of Philae on the comet nucleus was initiated by the Rosetta spacecraft ~500 million km away from Earth, at a distance of 22.5 km from the comet on 12 November 2014. Upon touching down after a ballistic descent phase of ~7 hours, the lander could not attach itself to the comet due to an unexpected systematic failure in the dual redundant anchoring subsystem and a malfunction of the non-redundant hold-down thruster. The landing gear [1] absorbed enough energy to prevent complete escape from the weak gravitational field of the comet but the first touchdown was followed by several hours of uncontrolled tumbling motion until Philae reached its final parking position (see Fig. 2b) roughly ~1.2 km away from the original target point. The lander remained functionally intact both over its bouncing motion and afterwards. It also kept radio contact alive with the Rosetta spacecraft, which served as a relay station between Philae and the ground station on Earth. Though some of the scientific objectives of Philae could not be fulfilled, even so it has provided a wealth of new scientific knowledge about the comet nucleus, including spectacular close-up images of the comet's surface.

The probe's primary energy sources supplied energy for doing science on the surface for roughly 60 hours on first run. Thereafter Philae fell into a state of hibernation due to the disadvantageous environmental conditions at its final parking site ~3 Astronomical Units (AU) away from the Sun. Philae woke up after about six months of hibernation at the end of April 2015 at ~1.8 AU distance from the Sun, and its central on-board computer autonomously entered the Long Term Science mode, driven by solar power and the rechargeable battery.

II. Major design aspects of PHILAE's operation control

Once landed, the starting times and durations of the radio visibility windows between the Philae lander and Rosetta spacecraft depended on such factors as the flight track executed by the Rosetta spacecraft, the 12.4 hours rotation period of the comet, the landing site and the orientation of Philae on the comet. Although these time windows were nominally calculable, Philae – in particular its CDMS on-board computer – had to be prepared for deviations from the predictions. We clearly anticipated that the operators might have limited, sporadic and time-restricted opportunities for intervention. Besides, the long 2-way signal travel time (in the range of 2*20 min) between the ground station and the Rosetta spacecraft excluded any on-line control and immediate intervention.

The energy available for the science programmes from the primary- and rechargeable battery was rather limited. Therefore, *CDMS had to be equipped with the capability of minimising the necessity of falling back into stand-by mode and waiting for operator's instructions, and so wasting battery energy without doing any scientific measurements*. In order meet this requirement the capability of on-board autonomous operation control was a primary requirement.

CDMS also had to cope with the extreme environmental and operational conditions throughout the Long Term Science phase, driven solely by solar power and the rechargeable battery, requiring comprehensive power flow management between battery charging and thermal control, operation of scientific experiments as well as radio communication.

Software reprogrammability and hardware reconfigurability were also important design aspects.

A. On-board computer makes itself and other subsystems of Philae fault tolerant

Fault tolerance and graceful degradation capability of vital subsystems, in particular that of the on-board computer (CDMS) of Philae [5] was a primary design goal. Fault tolerance requires fault detection, isolation and system recovery (FDIR) functions implemented in hardware structures (see Fig. 3a/b) and, most importantly, specific software algorithms and mechanisms. If a limited region, in particular the intelligent core (i.e. Digital Processing Units, DPUs) of a complex system can be built to be fault tolerant with self-repairing capabilities, the extension of fault tolerance towards the entire system is constrained only by the time and cost of developing and validating the required additional software. In contrast to the intelligent core, the rest of the system does not necessarily need to be provided with self-repairing capabilities, especially where there are no critical real-time requirements to be met and dynamic recovery is allowed. The self-repairing and intelligent core can reliably test, select and finally activate any other intact functional subunit, provided it has its embedded spare counterpart. This concept was the basic design guideline for the central on-board computer of Philae.

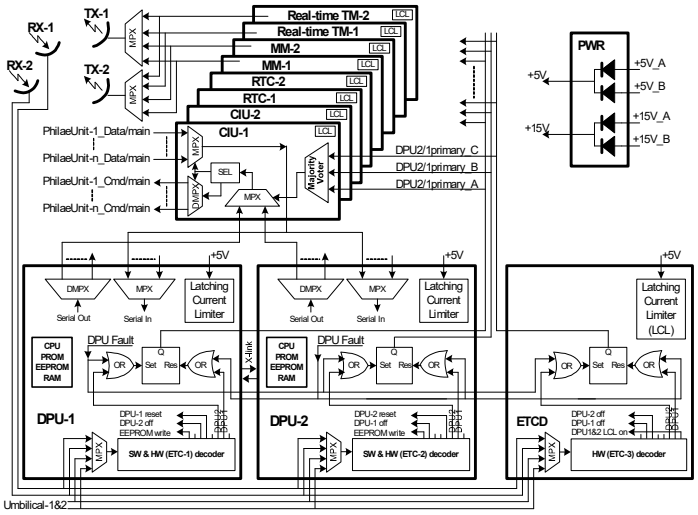

Fig. 3a/b. a/ redundancy control scheme and b/ stack of CDMS boards

Extending tolerance against single-point failures towards some critical parts of the entire Philae system [1] was also a design requirement. These were: power distribution and battery state monitoring, thermal control, touch-down detection and anchoring, radio receivers and transmitters, Philae internal communication channels, treatment of overload caused by any Philae unit, operation control of the instrument complex around the carousel of the drill-sampler unit.

A common command and data exchange protocol for all Philae units had to cope with both intelligent (instruments) and non-intelligent units (mostly subsystems with no processor and software). It enabled CDMS to provide services such as

- on-board time and Philae/CDMS system status distribution to Philae units
- individual or broadcasted, "waterfall-like" (direct or time-tagged) or buffered commanding of Philae units
- individual or grouped housekeeping parameter access from all Philae units
- request-service based science data collection from Philae instruments
- support of data exchange and event flagging between Philae units via CDMS
- notification message of operation completed by any instruments

Numerous fault recognition, isolation and system recovery schemes were implemented in CDMS, as described in [5].

B. On-board autonomy and operational flexibility [5]

CDMS had to be made capable of performing on-board autonomous control of on-comet Philae operations and supporting operational flexibility, particularly during the course of comet science phases. This requirement was implemented by a three-level scheme (see Fig. 4) for facilitating autonomous operation and sequencing of scientific measurements, executing system level nominal activities, and handling nominal and off-nominal events.

We defined specific linked data structures and code execution mechanisms that can be interpreted as an object oriented model for mission sequencing. The three levels were as follows:

1. *Elementary sequencing items* with
   - individual attributes and member variables, including the active lander units to be powered on, selectable power converters, unit priorities, data collection rates, data quotas, and a pointer attribute to the list of relative time-tagged telecommands (TCs) to be executed in conjunction with this item, with zero reference time determined by the start of this item. Further attributes defined the conditions under which a particular elementary sequencing item should be deactivated (i.e. terminated upon time-out, occurrence of nominal or off-nominal events, or upon initiation of a particular lander unit after its operation has been completed), and the means of carrying on the sequencing (e.g. step to the next item or conditional vs. unconditional jump to another item).
   - nominal and off-nominal event handler routines
   - methods covered such jobs as housekeeping and science data collection and execution of system relevant nominal activities. A special feature was provided by a set of stored commands addressed to the processor called "method constructor TC primitives" (see below). This feature allowed new methods to be added during runtime, even during flight (in-flight methods).

2. *Mission sequencing objects*, mostly – but not necessarily – as series of elementary sequencing items.
3. *Mission timeline* is composed of parallel-running mission sequencing objects.

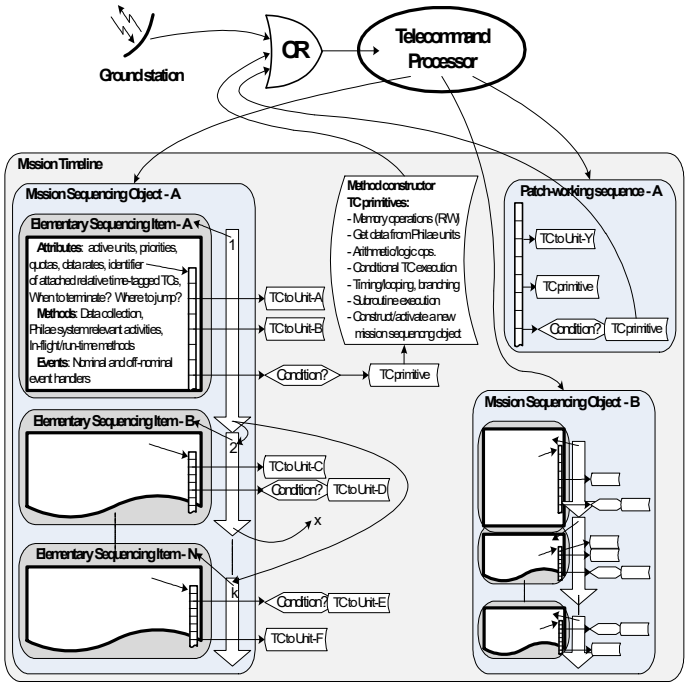

Fig. 4. Mission sequencing scheme

The elementary sequencing items, the mission sequencing objects, and the list and contents of relative time-tagged commands – including method constructor TC primitives addressed to the processor – were all changeable and pre-stored in the EEPROM memory of the on-board computer by means of arbitrarily structured, checksum protected tables. These tables were linked together by appropriate pointers, actually identifiers of their elements.

The list of relative time-tagged TCs contained commands addressed to either the Philae lander units or the CDMS processor unit itself. The latter feature allowed the user to create in-flight methods during run-time in any elementary sequencing item, at any points of the sequences.

A specific set of method constructor TC primitives were defined to realise such in-flight methods by providing functions for

- memory read/write,
- obtaining data from any Philae unit,
- executing arithmetic and logical operations on local variables,
- condition checking and conditional TC execution,
- timing, branching, looping,
- code overlaying to make more efficient use of the limited code memory space,
- subroutine execution ("this" TC itself serves as a container of the executable code), start a patch-working sequence.

C. A patch-working technique for on-board autonomy and operational flexibility

When the various functions of all method constructor TC primitives are looked at together, they strikingly resemble primitives – i.e. fundamental instructions – of a programming language. Method constructor TC primitives were suitable *for introducing additional software and sequencing layer on top of the CDMS core software*.

A particular patch-working timeline had its own unique identifier and was composed of a series of pre-stored, relative time-tagged TCs to execute. These could be any kind of TCs, addressed either to Philae units or to the CDMS processor alone, including any method constructor TC primitives. Besides user-defined patch-working sequences, numerous hard-coded ones were inserted in the CDMS core software at many points. These had the form of either single-shot or regular-launch sequences, but were merely place-holders to be filled up with relative time-tagged TCs by the user. Eventually, a user-defined *master patch-working timeline could manage conditional – event and/or time-out driven – start and termination of any pre-stored sequences, sub-sequences and also further patch-working timelines, all running serially or in parallel*. The scheme has provided a very high degree of flexibility and the ability to establish on-board autonomy in terms of operational organisation and reorganisation, scheduling and rescheduling both in the software development phase and after landing on the comet.

III. CONFLICTING MISSION OPERATIONAL APPROACHES – FACETS OF DECISION MAKING IN THE NET OF DEPENDENCIES

After landing of Philae, the unexpected situation of a non-anchored lander at unknown location with unknown attitude necessitated fundamental reshuffling – and to a large extent discarding – of the originally planned, over many years prepared, in many steps in many respects optimised timeline of pre-stored science sequences. The nominal mission plans including pre-calculated schedules of time-windows for radio contacts came suddenly to nothing, and the prospects for achieving all scientific objectives became significantly restrained. Because of the limited amount of available energy and relatively rare and time-limited radio contacts with Philae, improvisation was required. Series of ad hoc decisions had to be taken on the spot and under time pressure prior to each radio link sessions, by assessing scientific objectives and risks before each steps, and at first run by giving priority to experiments which did not imply mechanical movement. The team of scientists, engineers and mission operators in the control centre mastered the emergency situation; what under

the given circumstances could be, was rather more than less performed, *however, at the cost of being obliged to insert lengthy stand-by periods between subsequent commanding sessions in every 12.6 hours period, and so losing battery energy without doing any scientific measurements.*

Extensive analysis of potential failure sources and a lengthy FDIR document including recovery procedures were prepared prior to the comet phases of Philae. The on-board computer was really prepared to treat some of the potential failure cases and to recover from them by making use of its autonomous capabilities. After the active phase of the mission, several papers have been published on the impact of failed anchoring on Philae, by modelling it as a mechanical system. The question might be raised, *why not beforehand*? It was doubtful already well before Philae separation if it's anchoring would succeed. More importantly, the chance of that Philae would come to rest sideward tilted, instead of being firmly fixed on its feet, appeared to be not negligible. *And yet*, the team did not take measures to systematically prepare both the operational ground segment and in particular Philae for such a trivial emergency scenario.

With due precaution, more might have been performed by an alternative operational approach, by relying more on the on-board autonomous capabilities of Philae's on-board computer. This could have been realised by delegating some elements of operational decision taking steps from the ground segment to the level of autonomous on-board decision mechanisms, as described above in chapter 2.4: A patch-working technique for operational flexibility and on-board autonomy. On the whole, the available energy in the batteries – and thus time of about 3 days – could have been exploited more efficiently. For example, all what was commanded "manually" could have been completed in an autonomous mode during half of the available time period without lengthy stand-by periods. In the rest of the time further rational science experiments could have been executed, in the last resort involving even risk-taking actions, e.g. attempts to change Philae's attitude and/or orientation for better solar illumination conditions and also to take further images from other surface elements of the comet.

After wake-up of Philae from hibernation, the team was obliged to mainly concentrate on the problematic of unstable radio link between the Rosetta spacecraft and Philae. Rather long time (~2.5 months) was invested into these efforts first in nominal then in the "blind" fall-back commanding mode of Philae, while CDMS stayed permanently in stand-by mode. After several short successful communication sessions among many other unsuccessful ones the team decided to command CDMS to execute some science sequences as heritage from the First Comet Science phase after Philae landing. Except a single attempt which was acknowledged and responded by a few amount of telemetry data from the one Philae instrument, these failed too. The Long Term Science mission phase ended up without having done any comet science.

In retrospect, throughout the First Comet Science phase the team was fully occupied with mastering the unexpected situation of Philae and did not take the opportunity to uplink science sequences into Philae-CDMS, specifically for the long term science phase. Thereafter, in the 6 months of Philae's hibernation period the team hoped for a Philae wake-up. Indeed, the first telemetry data after wake-up reported that Philae was in good health condition, and no one calculated on a stepwise degrading hardware status of its vital subsystems. On top of that, *whilst the risk of completely losing Philae due to relatively rapidly declining hardware status of Philae's radio communication units became increasingly high, the team pursued a classic conservative strategy of small steps*. The team continued to contemplate on whether or not the risk of this or that minor steps and alternative ways of commanding CDMS to adapt itself to the degrading status of the telecommunication units would be "too high". Being close to the sun at that time, the thermal and solar power conditions were excellent and the control software for quick battery recharging was obviously operable, yet the team had concerns also about that any temporary discharging of the battery might have led to an "irreparable deficit". *Paradoxically*, the agenda was dominated by the intention to figure out in the first place, why and in what way the telecommunication units were about to degrade, one after another. Despite several displays of hardware related troubles the team missed to realize that exceptional urgency was required to do comet science measurements from the very first sign of problems with the radio telecommunication units, before it was too late, and a fundamental change of the pursued operational strategy might have been more purposeful. In the end, all telecommunication units must have broken down before the team might have come to action, including a tiger-team of experts which was recruited to master the situation, too late however.

With somewhat more foresight, more might have been accomplished by picking up some science, and the collected science data – or at least some part of them – might have been downlinked to the ground station during one or more of the sporadic link sessions after Philae wake-up. Instead of having stayed in stand-by mode all the time, CDMS – since its software had been prepared to do so – might have autonomously executed a default sequence of scientific measurements involving various instruments of Philae, without the necessity of any intervention from ground.

IV. SUMMARY OF LESSONS LEARNT

In contrast to hardware design and implementation, the software – i.e. that of the CDMS on-board computer – does not necessarily need to be completed prior to launch in projects like Philae was. Software reprogrammibility was of essential importance for two reasons.

- Like some of the other subsystems of Philae, the on-board computer, including its software had no elaborated requirements document at the beginning.

The requirements and their conversion into elaborated software algorithms and control processes and finally executable software code have been organically developing with the project over many years, mostly followed by software upgrades, occasionally even with some dead-ends and U-turns. The number of temporary software versions up to the final one was enormous, including not only those for the Philae test-bed on ground, but also numerous flight software versions. This was not unusual or surprising, for Philae was not an off-shelf product from the mass production with a detailed user guide.

- In addition to keeping up with the permanently developing nominal software requirements, software reprogrammability proved to be an effective mean also to overcome hidden hardware problems when the flight hardware was not directly accessible any more.

As for the First Comet Science phase, in lack of pre-acting in terms of being prepared for some trivial failure cases like a sideward tilted Philae, the fortune gave the team an additional chance for re-acting, though with strongly reduced chances to fulfill all mission objectives. What then the Philae team under severe time pressure performed to do comet science even after the anomalous landing was very impressing. This made a first hand experience of manifest graceful degradation of a system in its full complexity, intensively involving the "human component" like scientists, engineers and mission operators.

What after Philae hibernation happened, was not a sudden fatal break-down of the Philae system either. It was a relatively slow hardware degradation process which did have the potential of getting turned into a graceful one also from scientific point of view, yet the team could not manage to exploit this potential.

Even if hard work was invested into the design and implementation of the long term science doing capabilities of Philae, it was actually a mission with not negligible chance to become a short term, still more or less successful mission. Indeed, it did become a short term one, essentially due to a peculiar combination of three circumstances: available energy, non-anchored sideward tilted Philae, degrading subsystems. In fact, roughly twenty years of efforts had to be squeezed into the first several days of an active phase of the mission. This is why a specific accent was devoted in this paper to the point if delegating some of the decisional authorities from ground segment to the autonomous capabilities of the on-board computer might have resulted in more efficient use of the limited resources.

Good identification of fault containment regions in a space mission of high complexity is very important. It goes without saying that struggle for implementing fault tolerance and graceful degradation supporting capabilities shall cover possibly all areas of a space mission. It is a specific attitude, a sort of constructive mistrust that shall not make a stop at the edge of subsystems, nor at that of a system, not even at that of a spacecraft; the ground segment needs also to be involved, including mission planning, operation evaluation tools and also the "human component".

REFERENCES

[1] Bibring J.-P., Rosenbauer H., Boehnhardt H., et al.: Rosetta Lander Philae: System overview, Space Science Reviews (2007) 128:1–21, DOI: 10.1007/s11214-006-913-8-2.0

[2] K.H. Glassmeier, H. Boehnhardt, D. Koschny, E. Kührt, I. Richter: Rosetta Mission: Flying towards the origin of the Solar System, Space Science Reviews (2007) 128: 1-21, DOI: 10.1007/s11214-006-9140-8

[3] A.Baksa, A. Balázs, Z. Pálos, S. Szalai, L. Várhalmi: Embedded Computer System on the Rosetta Lander, DASIA 2003 Data Systems In Aerospace, SP-532, p.250-256, Prague, 2-6 June 2000

[4] A.Balázs, A.Baksa, et al.: The central on-board computer of the Philae lander in the context of the Rosetta space mission, Proceedings of conference on Reliable Software Technologies – Ada-Europe 2015, Madrid, LNCS 9111, pp. 18–30, 2015. DOI: 10.1007/978-3-319-19584-1_2

[5] A.Balázs, A.Baksa, et al.: Command and Data Management System (CDMS) of the Philae lander, Acta Astronautica 210: p. AiP. (2016) DOI:10.1016/j.actaastro.2015.12.013

Simulated Mars Rover Model Competition More Than a Decade as a Research Area

Pal Gabor VIZI
Space Physics and Space Technology
MTA Wigner RCP
BUDAPEST, Hungary
vizi.pal.gabor@wigner.mta.hu

Attila SIPOS
Competition of Applied Engineering Sciences
magyarokamarson.hu
KISKUNHALAS, Hungary
siposattila@ magyarokamarson.hu

***Abstract*— A serial of competition is a proper field and can speed up this process together with competitors from many educational centers and can proof the students and young experts in one time. Results can be realized as mission concepts in integrated space systems when solutions are emerging from serials of tasks during year by year of the contest.**

Keywords — evolution competition space model engineering education

I. INTRODUCTION

Competition is the base of the evolution. Possibilities are increasing in the field of space research and industry according to evolution of the industrial progression worldwide both in science and in the available technology. New demonstration and standardized methods can arise virtually from nothing, but the background of the new successful solutions is the several independent attempts. A serial of competition is a proper field and can speed up this process together with competitors from many educational centers and can proof the students and young experts in one time. Results can be realized as mission concepts in integrated space systems when solutions are emerging from serials of tasks during year by year of the contest.

The Competition of Applied Engineering Sciences, working name is Magyarok a Marson (Hungarians on Mars) is in process more than a decade. Founder of the contest is Attila Sipos. We presented our previous works (Sipos, Vizi 2009-2015) [1,2,3,4,5,6] at the 40th-47th LPSC and at several conferences in Hungary, e.g. at H-SPACE 2016 where we described shortly the ten years of the Competition [7].

II. COMPETTITIONS YEAR BYYEAR

Simulation and Realization: Organizers and authors of this article prepared CGI and physical simulations of the dashboard, robots and race and presented them before the date of competitions. Importance for researching and developing is to reach the capability to supply a good emulation environment before any mission, first at our competition and next in a wide spectrum of space and planetary environments. The style of appearance is entertaining-educational to reach the attention of the possible younger competitors also and similar to a sci-fi trailer.

Missions: In all year the most important task is to command the robots with automatism. To become a winner can be reached only by an automatic device.

2006-2009: The actual goal of the competition can be achieved by building a moving device (usually a rover) with manipulators. The track is an 8x8 square meter sized field of special material and tracks, different during years. Controlling of rovers was necessary behind of a folding screen and using a delay to simulate the distances between planets.

2006 Competitors have to build a rover which starts from either corner of the field to reach the target crater at the opposite other corner and to collect debris or soil of the crater.

2007 Competitors have to search power cubes to collect energy across of field.

2008 Competitors had to collect liquid material. Those students have won the race this year, who later designed the successful first Hungarian satellite Masat-1 and they can be seen in the picture standing in dark blue T-shorts. They rover is at the top right corner of the picture of 2008.

2009 The goal of this year could be achieved by building an amphibian rover with sensors, manipulators and advanced communication.

2010 To reach the target place and to read and send back to base a DNA sequence represented by a 16 character display and to collect soil, and to carry and put the specimen into the harbor where a space-elevator model is. The end of mission is to reach the top of the space-elevator.

2011-2015 *More than one rover was on the stage* from this year on due to the increased and large number of competitors and full mission time was not enough to complete the contest one by one.

2011 More than one rover was on the stage from this year due to the increased and large number of competitors and full mission time was not enough to complete the contest one by one. The mission was to reach and occupy marked places on one's own field and to try to occupy other marked places on the fields of other competitors, thus some robots had to be substituted by other robot.

2012 Spider like robots occupied pyramid like targets by "eggs" and pushed down other's eggs.

2013 Doubled wheel robots in a 8mx8m labyrinth putting magnet own eggs and collect from others.

2014 All skills just before but with hovercraft to simulate the micro gravitation in 2D.

2015 All skills just before, in addition robots were necessary to build in situ at the place and during the time of the competition from locally available materials.

2016- The following section tells the events which have not been published yet.

2016 The task of the year 2016 was a blind remote and self-controlled contest to reach several places, to position a small target in different highs of tower shaped targets, to take a sensing/measuring process, to compete others by catching high score targets form each other. It was similar to a job to clean up a contaminated target field only from dangerous pieces of space debris repeatedly as the frame story described.

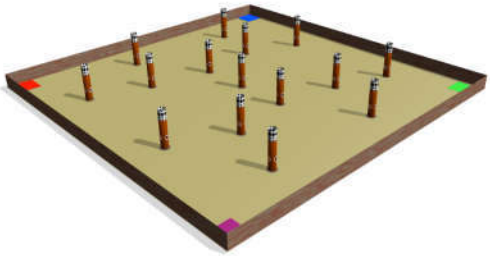

Plotting board of 2016

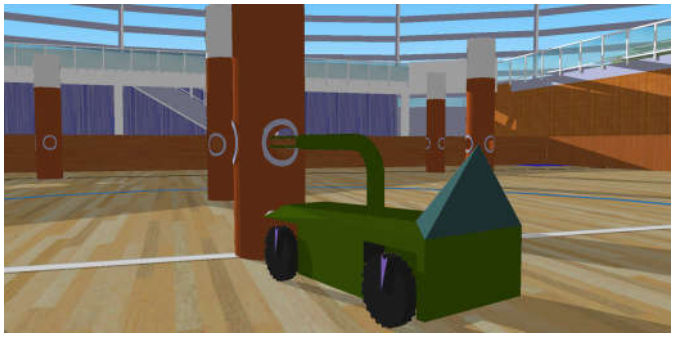

Pre-simulated full controllable robot and field of competition 2016 (any target can be simulated e.g. a sports hall which is was the place of the contest in this case).

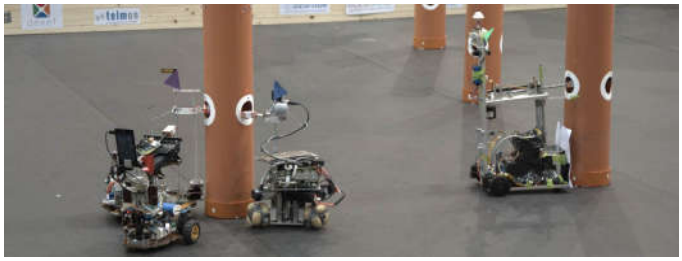

Robots are in action to solve the task to win.

Teams and solutions are on the stage in the year 2016.

Plotting board of 2017:

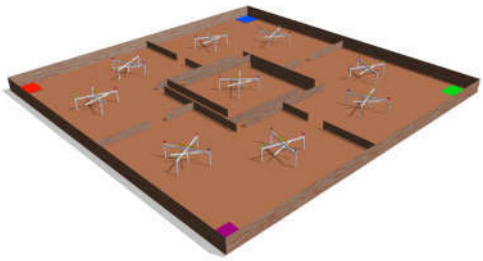

2017 The tasks for the 2017 year will a remote (‘hand moving follower’ sensors) and self-controlled contest to deploy ball shaped, meteor ball like small robots, to reach several different high positions, to pass rotating gates, to set they own color marks as a sign that the measurement made by the team. Competitors have to invent and apply several smart tricks when crossing the plotting board. They not only have to build a proper hardware but they have to know the target place and to estimate the complex moving on the obstacle course and in addition they must have an optimization for crossing each other.

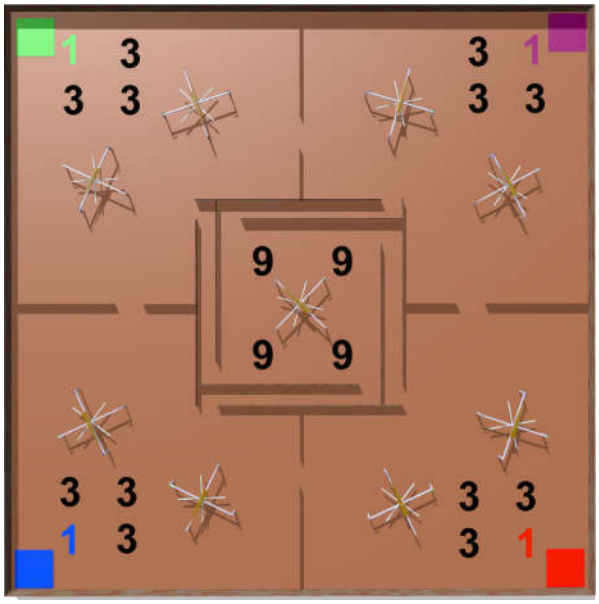

The score table of 2017 on the dashboard

Competitors score is 1 in self-part, 3 points in others part and 9 points at the center portion. Positions and points can be captured from each other to increase the score. In point of view of researching the best contestant team can became a good robot builder expert to reach the more places for the more significant measurement data Estimated type of robots will be balance transfer pendulum driven, inside of the sphere two wheels driven robots, four tetrahedron wheels driven or some other tricky driving solution, who knows?

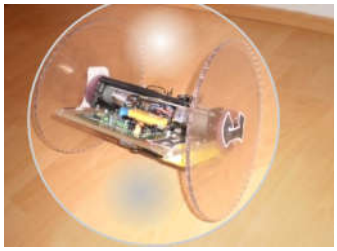

Potential transferable, already have built robot in a plastic ball

III. Conclusion

Competitors have to be capable of designing, developing and constructing complex autonomous robots, and moving them by driving in order from wheel and caterpillar, through amphibians, elevator climbers, legs, balanced double wheels and air cushion.

The emerging skills during our competitions are giving an excellent self-developing process not only for participant students and young engineers but also for their teachers. The most important outcomes of the races are the realized and mainly solved problematic remote controlling situations on a mainly unknown “detached” terrain for a researcher who is involved in remote distant space missions, because several successful and reliable solutions are born during contests.

References

[1] SIPOS,A., VIZI,P.G.: LPSC40 #2519 ; http://www.lpi.usra.edu/meetings/lpsc2009/pdf/2519.pdf

[2] LPSC41 #2649 ; http://www.lpi.usra.edu/meetings/lpsc2010/pdf/2649.pdf

[3] LPSC42 #2014 ; http://www.lpi.usra.edu/meetings/lpsc2011/pdf/2014.pdf

[4] LPSC 44 #2850 ; http://www.lpi.usra.edu/meetings/lpsc2013/eposter/2850.pdf

[5] LPSC 46 #2602 http://www.hou.usra.edu/meetings/lpsc2015/eposter/2602.pdf

[6] LPSC 47 #2098 http://www.hou.usra.edu/meetings/lpsc2016/eposter/2098.pdf

[7] A. Sipos, P.G. Vizi: Ten Years of the Simulated Mars Rover Model Competition, p 61/62 in H-SPACE 2016 - 2nd International Conference on Research, Technology and Education of Space, 2016., http://space.bme.hu/sites/default/files/sima_lap/Proceedings_H-SPACE2016.pdf

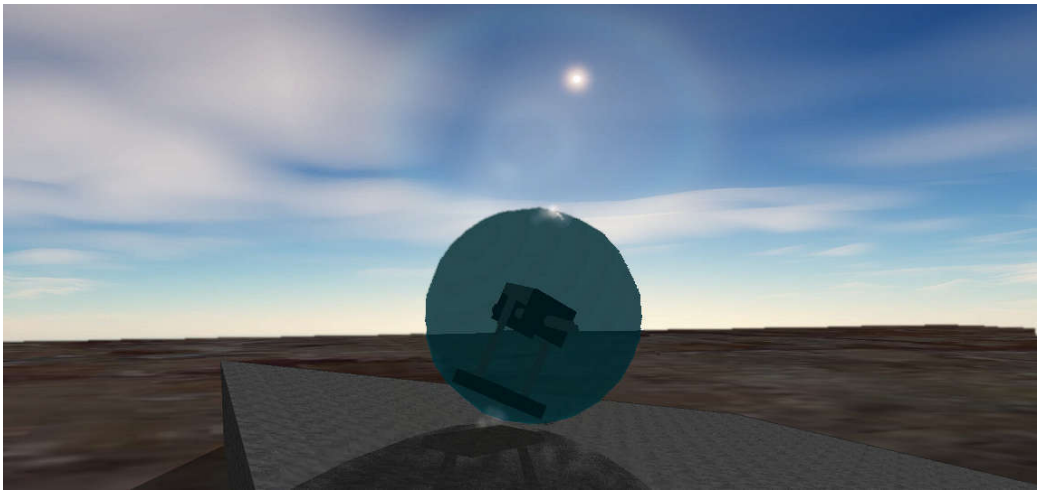

Pre-simulated Spherical Robot with balance transfer driving

Hexavalent Chromium Free Coatings for Satellite Metallic Hardware's

Kalaivanan Thirupathi
Department of Polymer Engineering
University of Miskolc
Kalaivanan01@gmail.com

Pál Bárczy
MATMOD Limited
Miskolc, Hungary
pal.barczy@admatis.com

Márton Béla Somosvári
Admatis Limited.
Miskolc, Hungary
Somosvari.bela@admatis.hu

Tamás Bárczy
Admatis Limited
Miskolc, Hungary
Tamas.barczy@admatis.com

Considering aviation and space sectors, aluminium alloys are commonly used due to its excellent mechanical and physical properties. Though satellite hardware is confined to controlled environment. It requires a highly protective anticorrosive treatment followed by a systematic coating scheme (Primers and paints). Chromate conversion process using hexavalent chromium is the most traditional method for protecting surface of aluminium alloys from corrosion. Due to toxic and carcinogenic nature of hex chrome it has been prohibited with mandates and regulation by various directives from European Union. This paper will address an environmentally friendly and cost efficient trivalent chromate conversion coating, which is qualified for space application by this research work. The overall objective of this innovative work by MATMOD Limited under supervision of ESA is to test if trivalent chromate coating system that includes pre-treatment, primers and paints over various aluminium alloys is suitable for replacing hexavalent chromium coating in space industrial application

Keywords- Space qualification test , Trivalent chromate conversion coating, Aluminium alloys

I. INTRODUCTION

Aluminium and its alloys are widely used as manufacturing material for space vehicles and hardware's [1]. In general, most satellite components will be handled in a controlled environment before launching phase. However, are cases when metals are exposed to normal atmospheric conditions. The protection of material against degradation is prime importance for NASA and ESA for space operation capabilities. Hexavalent chromium (Hex chrome or Cr(VI) based chromate conversion coating has been in use till date for protecting substrate because of its high corrosion resistance and self-healing properties [2]. The replacement of Cr(VI) coating becomes inevitable because of its toxicity, carcinogenic and hazardous nature to human health [3]. In addition to this, European Space Agency (ESA) faces stringent regulations from Registration, Evaluation, Authorisation and Restriction of Chemical substances (REACH) and Restriction of Hazardous Substance Directive (RoHS) that have set a mid-2017 as sunset date for hex chrome hardware's. In this regard, the aerospace community takes huge effort to find and qualify alternatives for hexavalent chromium.

A study has been conducted at initial phase of this Eco-friendly Coating Development (ECD) project by MATMOD Ltd. about previous efforts taken by other space oriented companies. The assessments report of alternate chemical from ESA revealed that chromium based conversion coting is most suitable for space oriented application due to high vacuum and thermal cyclic requirement [1]. NASA itself tested three alternative pre-treatments such as Alodine 5700, Okemcoat 4500 and Chemidize 727ND most of chemical was dropped intermediate due to poor performance. The reports from 2013 under NASA, TEEREM projects showed that trivalent chromium based chromate conversion coating can perform as good as hexavalent chromium containing pre-treatments. Based on these results, a recent report "Pre-treatments Only Interim Test Report July 20, 2015" form collaborative efforts between NASA and ESA signified that pre-treatments from SURTEC industries provides excellent results under salt spray testing that meets requirement of MIL-DTL-5521. Considering these previous effort, MATMOD Ltd. took a part and continues its work in qualification of SURTEC based trivalent chromium containing products in partnership with the European Space Agency (ESA) through ECD project [5].

The objective of this collaborative effort by ESA and MATMOD Ltd. is to test and evaluate coating system including pre-treatments, pre-treatment with primers and pre-treatment without primers as a replacement for traditional coating system in aerospace application. The main aim of this work is to understand any unexpected interaction failure between the pre-treatments, primers and topcoats that does meet set of predefined requirements for space application. In addition to this, SURTEC based Cr(III) coating is expected to possess good corrosion resistance, electrical properties, thermal and adhesion characteristics over various substrates of Al alloys.

II. EXPERTIMENTAL PHASE

A. MATERIALS:

Most commonly used aluminium alloys have been selected in this project such as AA6063-T651, AA6082-T651 and AA7075-T651 with chemical composition mentioned Table 1 below [5]. The specimens received as 100 x 200 mm was cleaned with detergent to remove oils, grease, contamination and wiped with isopropyl alcohol for degreasing.

AW7075-T651	Fe	Si	Cu	Mg	Mn	Cr	Ti	Zn	Ni	V	Ga	Al
	0,150	0,095	1,48	2,43	0,05	0,19	0,034	5,78	0,003	0,013	0,009	Bal.
AW6082-T651	**Fe**	**Si**	**Cu**	**Mg**	**Mn**	**Cr**	**Ti**	**Zn**	**Ni**	**V**	**Ga**	**Al**
	0,20	1,100	0,053	0,99	0,7	0,028	0,011	0,062	0,004	0,012	0,009	Bal.

AW6063-T651		Fe	Si	Cu	Mn	Mg	Cr	Ti	Zn	Ni	Al
	Min	-	0.20	-	-	0.45	-	-	-	-	-
	Max	0.35	0.6	0.10	0.10	0.9	0.10	0.10	0.10	0.05	Bal.

Table 1: Elemental composition of alloy (wt. %)

B. Sample preparation

The samples are prepared as per recommendation from SURTEC and ADMATIS Ltd with review of previous works related to development of Cr(III) conversion coating for space application. The following procedure was also recommended by various scientific community as mentioned in most of journals related to trivalent based chromate conversion coating [5].

1 Solvent cleaning (detergent and Isopropyl alcohol)
2 Alkaline etching (SurTec 181, by 5- 10 % volume at 20° - 60° C for few minutes)
3 DI water rinsing
4 De smutting (SurTec 495, by 17 % volume at room temperature for few minutes)
5 Rinsing thoroughly using DI water for few minutes
6 Conversion coating (SurTec 650, by 20- 50 % volume at 30° - 40° C for few minutes)
7 Final rinsing with DI water with conductivity less than 20µm
8 Ageing
9 Certain sample are painted using space qualified paints

This type treatment produces a thin (50-90 nm) coating layer over the metallic surface. The coated layer consists of Cr, Zr, Al and O atoms (see Fig.1) being in amorphous gelatinous state. The structure of freshly coated film is composed by a mixture of Al, Cr and Zr hydroxide-oxide and water. During room temperature aging, the hydroxide transforms to oxide with water loss and volume shrinkage resulting in a change from hydrophilic to hydrophobic behaviour. In addition to this, under vacuum the layer shows further transformations so applicability of such layer in space seemed very questionable. Therefore, the following test sequences were concluded and executed.

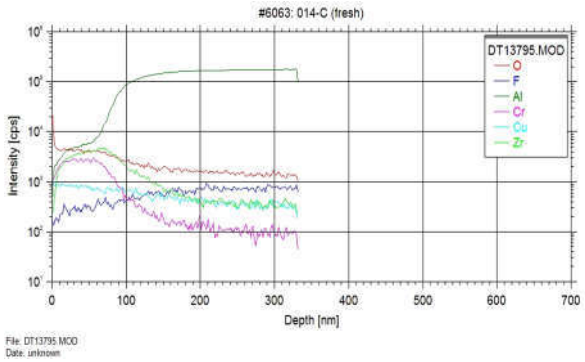

Fig.1. Typical element distribution in a chromated coating

III. EVALUATION OF THE ALUMINIUM ALLOY SAMPLES

Test	Test Method	Evaluation Criteria	Performing Entity and No of samples
Visual Inspection test	N/A	No evidence of contamination or cracks on coating	60 Admatis Ltd.
Wet wipe test	N/A	No evidence removal of coating from substrate	60 Admatis Ltd
Neutral Salt Spray Test (NSS)	ASTM B 117	No evidence of corrosion, before and after exposure of corrosive environment	15 University of Miskolc
Contact Electrical Resistance (CER)	MIL-DTL-81706	Resistance value should not exceed 5000 microohms psi before NSS test and 10000 microohms psi after NSS test	9 University of Miskolc
Bake Out Test	ECSS-Q-ST-70-01C	No evidence of adhesion loss after exposure	28 Admatis Ltd.
Humidity Test	ECSS-E-ST-10-03 C	No evidence of adhesion loss after exposure	28 Admatis Ltd
Thermal Cycling Test (TC) and Thermal Vacuum Cycling (TVC) Test	ECSS-E-ST-10-04 C	No evidence of adhesion loss	14 AAC Austria
Cross cut test	ASTM D 3359	ASTM D 3359, Method B classification of Adhesion test	40 Admatis Ltd.

Table 2: Standards for testing space oriented products

IV. RESULTS AND DISCUSSION

A. Visual Inspection and wet wipe test

Initially all chromated samples had been inspected visually for any changes in colour of coating. The panels that has clear visible tan blue layer without any defects visually had been selected as a reference for further test like wet wipe test and salt spray test. Certain samples exhibit slight inhomogeneous in colour possibly due to its drying condition or human error. In addition to this, wet wipe test is one of the standard testing procedure to measure adhesive behaviour of coating. The coated sample with defects in coating will exhibit some contamination on the cloth during test procedure. The isopropyl alcohol wetted cloth will remove loose parts of chromate layers.

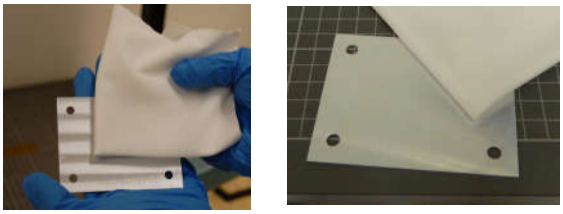

Figure 2: An example of a successful wet wipe test. No residues can be found on the cloth (left: AA 6082; right AA 6063)

B. *Salt spray resistance*

Salt spray test is standardized testing method used for testing corrosion resistance of materials and surface coating [6]. It is usually operated by placing samples of various size and shape inside the chamber that are exposed to saline fog or spray that is even distributed among the samples inside B117 testing chamber. The chamber is checked daily for pH and temperature during test. Results are usually examined visually or with magnifying glass to measure the integrity of alloy coating. For aluminium alloy, if the test panels exhibit any kinds of pits under visual inspection then panel are considered as a failed as per standard mentioned above. Mostly aluminium and its alloy based substrates are subjected to neutral salt spray test which reflects, fact that the NaCl test solution is prepared to a neutral pH of 6.5 to 7.2.

Alloy	Batch	24 Hrs	48 Hrs	72 Hrs	168Hrs
6063	1	Pass	Pass	Pass	Pass
	2	Pass	Pass	Pass	Pass
	3	Pass	Pass	Pass	Pass
	4	Pass	Pass	Pass	Pass
6082	1	Pass	Pass	Pass	Pass
	2	Pass	Pass	Pass	Pass
	3	Pass	Pass	Pass	Pass
	4	Pass	Pass	Pass	Pass
7075	1	Pass	Pass	Fail	Fail
	2	Pass	Pass	Fail	Fail
	3	Pass	Fail	Fail	Fail
	4	Pass	Fail	Fail	Fail

Table 3: Evaluation – ASTM B 117, 168 hours of exposure

C. *Contact Electrical resistance test*

The purpose of this test is to determine electrical resistance property of coating material [6]. The test was conducted as per MIL-DTL-81706 B standard [8]. Nine samples were tested before and after exposure in to salt spray chamber. The electrical resistance was measured using kelvin bridge circuit experimental setup. This setup includes two copper electrodes of various diameter with surface polished to a mirror finish fixed to compression tester. The test was carried out by placing test panels on top of copper electrode with a larger diameter (25 mm), then the constant force of 200 Psi was applied over panels by electrode of smaller diameter using mechanical load. The probe from the circuit was integrated to copper electrode for taking resistance reading. Once galvanometer shows null then ten set electrical resistance was noted down on each panel by changing position [7].

These results exhibit value much lower than the maximum acceptable recommended values.

Condition	Alloy	CER (Micro ohms)
Before NSS	6082-T651	794
	7075-T651	1580
	6063-T651	1537
After NSS	6082-T651	2299
	7075-T651	3862
	6063-T651	1736

Table 4: CER values of Cr(III) coated Al- alloy.

D. *Thermal cyclic test:*

Thermal cyclic test is conducted to evaluate fatigue or adhesion failure of coatings under various temperature cycles. The samples were subjected to extreme temperature, that are held constant for certain amount of time. The changes in temperature was performed at constant rate with set of specified number of cycles. During test procedure, the test panels tend to expand or contract in accordance to heating up and cooling down state of chamber. These internal changes may possibly cause the trivalent chromate to loss its adhesive nature toward paint or substrate [1].

The thermal cyclic test was performed under ambient air using thermal chamber at Aerospace and Advance Composite GmbH Austria. The thermal profile was setup from +100° C to -100°C for 90 cycle at ambient pressure. In addition to this, another set of thermal cyclic test was carried out under vacuum condition with thermal profile correspondence to +100° C and -100°C for 10 cycle at pressure less than 10-5mbar.Over all fourteen panels was test with paints, with and without primers only one side of test panels.

Alloy	Condition	Adhesion Failure	Visible cracks or changes
7075	Only coating	Nil	Nil
	Paint with Primers	Nil	Nil
	Paint without primers	Nil	Nil
6082	Only coating	Nil	Nil
	Paint with Primers	Nil	Nil
	Paint without primers	Nil	Nil
6063	Only coating	Nil	Nil
	Paint with Primers	Nil	Nil
	Paint without primers	Nil	Nil

Table 5: Evaluation of coating technology under thermal cycling test.

E. Cross Cut Test

The cross-cut test is most commonly used in coating industry to evaluate adherence property of coatings films to substrate in which they are applied. This test is carried out by applying and removing pressure sensitive tape over cuts made in the films. Among three-different type of test available cross/cut tape, scrape adhesion and pull off test. The cross-cut test is frequently used by several industries to evaluate coatings, as per recommendation by ESA in this ECD project MATMOD Ltd. used cross cut test to evaluate adhesion of paints that is applied to aluminium alloy substrate with and without primers.

The panels were tested in accordance with ISO 2409 under classification of test method B, cross cut tape test. Which is the standard method for measuring adhesion of films by tape method. The test panels were painted with dry film thickness of 0.00006 inches. The test panels are paints using space qualified polyurethane and silicon paint. As per the standard mentioned above a lattice pattern was made in each direction on the paints to substrate. Then pressure sensitive tape was applied over the lattice and removed, depending upon the damage in paints adhesion of paints was evaluated in percentage

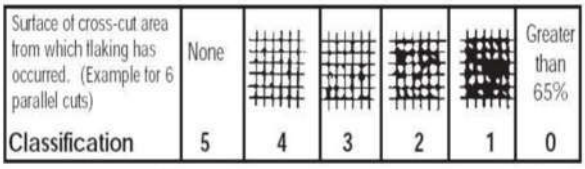

Figure 3: Classification of cross cut test

Alloy	Paints	Results	Prototype
7075	Polyurethane	5B	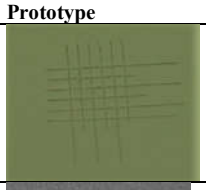
	Silicon	5B	
6063	Polyurethane	5B	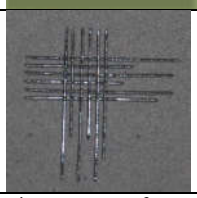
	Silicon	5B	
6082	Polyurethane	5B	
	Silicon	5B	

Table 6 : Result of cross cut test with and with primers over surface

F. Bake out test.

The bake out is process in which coatings is condition for space application process. It is typical requirements for all the products to be launched in space. In addition to this, it is also used for evaluating outgassing property of the hardware. The out gassing is critical problems that is faced by most of the industries to maintain high vacuum environments. NASA and ESA has a list of low outgassing materials that is to be used as spacecraft materials [9]. The major problems in most of the previously launched satellites are from outgassing for example, NASA'S stardust space probe suffered reduced image quality due to an unknown contamination that had condensed on the CCD sensor of navigation camera. The probable reason is due to an outgassing product, that can condense on to optical elements, thermal radiators or solar cells and obscure them.

Alloy	Condition	Visual Inspection	Wet wipe test	Cross cut test	Out gassing
7075	Only coating	Pass	Pass	n/a	nil
	Paint with Primers	Pass	n/a	5B	low
	Paint without primers	Pass	n/a	5B	low
6082	Only coating	Pass	Pass	n/a	nil
	Paint with Primers	Pass	n/a	5B	low
	Paint without primers	Pass	n/a	5B	low
6063	Only coating	Pass	Pass	n/a	nil
	Paint with Primers	Pass	n/a	5B	low
	Paint without primers	Pass	n/a	5B	low

Table 7: Evaluation of Cr(III) under bake out test

G. Humidity test

In general, most of launches are in humidity environment. For Europe's its spaceport is situated at South America in French Guiana an overseas department of France [11]. This is root cause for testing the behaviour of coating in high humid condition to avoid failure before launch. The humidity test determines how components and its subsystem behave in severe environments that involves elevated temperature and high or fluctuating relative humidity. In ECD project MATMOD Ltd. evaluated changes in coating by testing it for ten days at 50^{o} C around 95 % of relative humidity.

Alloy	Condition	Visual Inspection	Wet wipe test	Cross cut test
7075	Only coating	Pass	Pass	n/a
	Paint with Primers	Pass	n/a	5B
	Paint without primers	Pass	n/a	5B
6082	Only coating	Pass	Pass	n/a
	Paint with Primers	Pass	n/a	5B
	Paint without primers	Pass	n/a	5B
6063	Only coating	Pass	Pass	n/a
	Paint with Primers	Pass	n/a	5B
	Paint without primers	Pass	n/a	5B

Table 8: Result analysis of Humidity test

V. CONCLUSION

- The environment friend trivalent Chromium base MATMOD technology provides protective coatings resulting in suitable corrosion resistance for each experimental alloy.
- The samples of MATMOD coating technology survived all stringent space qualification tests.
- The main message of ECD project of MATMOD Ltd. is to ESA and its costumers that traditional hexavalent chromium based conversion coating can be replaced by our new trivalent chromate coating for spacecraft components.
- This is a real example how transformed a R+D work on effect of PECS support to space qualified technology for general application of European space industry.

ACKNOWLEDGMENT

The authors are thankful for valuable collaboration of F.Tranta, G.Lassu and G.Zsoldos (Miskolc University), A.Csik (ATOMKI), furthermore V.Liedtke (AAC Gmbh).. The project was financed by ESA, Contract No.4000114580/15/NL/ND.

REFERENCES

[1] A.M Pereira and G. Pimenta, "Assessment of chemical conversion coating for the protection of aluminium alloys," European Space Agency, 2008.

[2] G. Artur and H.-j. Streitberger, Basics of Coating Technology, Germany, 2003.

[3] Technology Evaluation for Environmental Risk Mitigation Principal Center., "Hexavalent chromium free coating for electronic applications," NASA, 2012.

[4] Matmod and ESA, "Environmental friendly conversion coating development (PECS contract)," ESA Contract No.4000114580/15/NL/NDe, Matmod Ltd., Miskolc, Hungary, 2016.

[5] J.Qi, T.Hashimoto, G.E.Thompson and J.Carr, "Influence of water immersion post-treatment parameter on trivalent chromium conversion coating formed on AA2024-T351 alloy," *Journal of Electrochemical society,* pp. C131-C138, 2016.

[6] ASTM International, "Standard Practice for operating salt spary for apparatus," Department of Defence, United states.

[7] M. William, U. Toshio and N. Maciej, "Surface resistivity and surface resistance measurement using a concentric ring probe techinque," Terkinc, 2013.

[8] MIL-DTL-81706 B, *chemical conversion materials for coating aluminium and aluminium alloys,* Naval Air Warefare Centre Aircraft divison, 2002.

[9] "Outgassing Data for Selecting Spacecraft Materials.," NASA, 12 01 2016. [Online]. Available: https://outgassing.nasa.gov/.

[10] "Europe's spaceport launchers," 12 May 2004. [Online]. Available: www.esa.int/Our_Activites/Launchers/Europe_s_Spaceport/CENS_at_Europe_s_Spaceport. [Accessed 12 11 2015].

[11] ALFUN, "Certificate of Conformance," Miskolc, 2011.

High speed integrated space streaming swarms as mission concepts

Pal Gabor VIZI
Space Physics and Space Technology
MTA Wigner RCP
BUDAPEST, Hungary
vizi.pal.gabor@wigner.mta.hu

***Abstract*—The idea described hereby is the Streaming Swarm of Nano Space Probes (SNP) as mission, instruments and payload concept.**

Keywords— mission concept swarm fleet stream system

I. Introduction

Recent technologies allegedly promise fast speed space devices - probes - accelerated by a launch base until to some percent of the speed of light. Some new reports talk about big plans to reach really distant targets [1]. Several hard challenges are standing before those plans and let we try to show some of them with potential and promising concepts.

The idea described hereby is the Streaming Swarm of Nano Space Probes (SNP) as mission, instruments and payload concept. However well-known it isn't possible to complete the mission described here nowadays, maybe it is interesting to thinking about it.

Author's earlier works described the Nano, Pico Space Devices and Robots (NPSDR) [2-4] and the fleet of Micro Sized Space-Motherships (MSSM) [5] which type or similar devices maybe can fulfil the requirements incidentally.

II. Hard Troubles

Let we show some trouble affecting a swarm and elements in case of high speed.

A. Accelerating

How can we accelerating up to order of magnitude of speed of light? In the vicinity of Earth it is maybe solvable to accelerate some type of space probes.

B. Decelerating

How can we decelerate down the probes from the 'near speed of light'? *No how, no way*. Is any solution to use them without decelerating? Let we try to thinking about it (see below).

C. Relativistic view and communications

According to different rates of Doppler effects new telecommunication systems needed.

Can we measure any characteristic at the target for example outgassing, magnetic fields and spectrums on a high speed?

D. Radiation

Extreme radiation affects the devices.

III. Concepts and possible solutions

Let we look some advantageous solutions if we assume that they are feasible.

In case of big abundances of elements of the swarm we can command a special part of the swarm to do a specific job inside a space interval. Let we divide the space into sectors near the target – a moon, planet or star. Particular space intervals demand definite activities. One classical probe is orbiting the target and makes measurements in circulating or near rounding orbit. A high speed streaming swarm couldn't orbit the target. *But we can command the part of them at just the target area to make the same measurements at the same position where classical probe made.* Behaviors of the prepared elements of the flowing swarm are turning into the position dependent program branch and collecting the data. When the element leaves the position turning the behavior to the next program branch, makes new measures and finally transmit all the collected data to a backward to the relay transmitter.

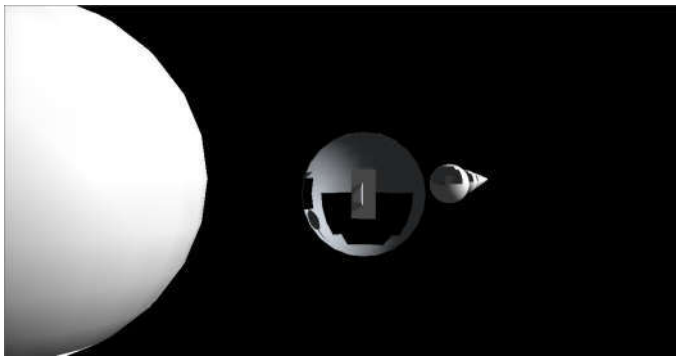

Fig. 1. Simulated view of SPN to the direction of streaming at the target

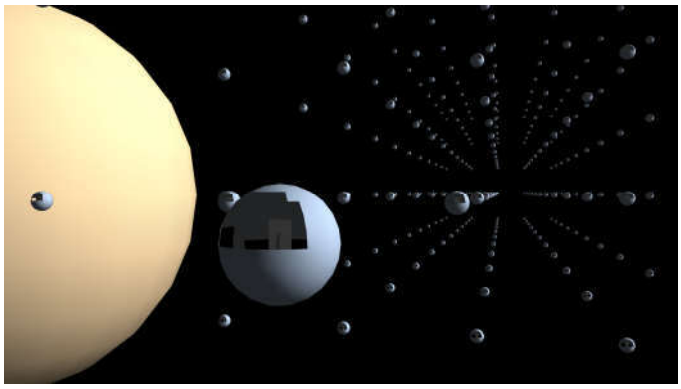

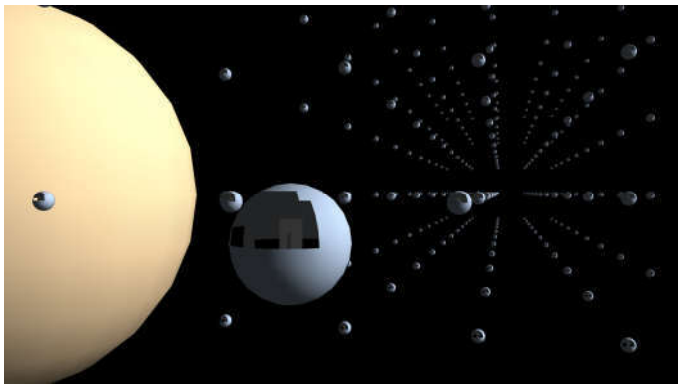

Fig. 2. Simulated view of SPN fleet. (The picture pair is a cross eyed stereo image, the left image to the right eye and the right image for the left eye.

IV. Communication in Swarm

It is necessary to communicate each other inside of the swarm. First parts of the stream collect measurements, start to preprocess data and send back to the next part of the stream relevant information as a negative feedback for better settings to help to collect data more precisely

A. *Negative feedback to next part of Swarm*

It is a key opportunity to modify, to correct and to involve the behavior of the next part of the stream according to results of the first part of the stream. The k^{th} parts of the stream make measurements and start to process the data. According to the results, the k^{th} part of the stream could send feedback to the $k+1^{th}$ part of the stream and so on step by step. It is a theoretical possibility to pinpoint the next new specific measuring according to the preprocessed data. Swarm can send back the whole collected data in one time together to the Earth with the united power of the Stream at cornerstones of mission.

V. Detailing

During any sensing process in the life, in industry or in research the serial of results are involving the next steps. Streaming NPSDRs have ability to focus some factors which are become important until then and they can emphasize more significant point of view and able to weight out the tasks. For example if we have some useful information about a planet which planet's atmosphere could be clear or cloudy just exactly at that time then the elements of the stream which have arrived earlier can inform the next elements of the stream to set up they sensors to getting ready to use a fitted settings of parameters for the specific measuring. The result must be the same like in case of a single space probe which can turn on and off experiments and they measuring sensors in accordance with the conditions expected. Usually conditions are so rigorous to find the best balance between the available time and electrical power and the importance of significant measuring to achieve the best results for the knowledge.

A. *Considerations*

- More independent manufacturers: more independent manufacturers giving benefits during test and demonstration phase and finally the standardization for the best manufacturer.
- Telecommunications e.g. slow and fast; laser or quantum telemetry. Long term and low power consumption for swarm chain communications.
- Single or multi purposes - Combined from one task oriented elements of swarm to multi featured sur-face with different sensors on one element of swarm.
- Task specific altered devices are necessary at different planetary target places.

B. *Communication*

Let we try to estimate some communication features. The parallel neighborhood of the swarm – are in a perpendicular planar to the streaming lines - can communicate with short distance radio communication, e.g. with a rod antenna. Farther elements can reach each other, the telecommunication relay station or the Earth with focused telecommunication. The example version element of the stream is a sphere like doubled paraboloids, (middle in Fig 1.) which can serve as the parabolic antenna and in addition a relay antenna system. The doubled paraboloids can be set to opposite side alternatively; may face each other and in opposite directions. Several considerations, developing and test is necessary to get a working model of this concept.

C. *Power sources*

Batteries for operation for long term slow consumption and for short term high energy demand. Space qualified small battery cells for long term slow consumption operations. In case of high energy demand for example during transmission of collected scientific data power can be earned from two component power sources, shortly like a spark. Two components usually means one solid and one liquid component, according to pressure, mainly independently if we keep them in a closed space in a vessel, which can hold enough pressure until activating the liquid, without sublimation.

D. *Environment friendly*

Environment friendly small probes can be contained similar elements like in meteorites according to cosmic abundance of elements. We can call them ‘meteorite-like probes’.

Fig. 3. The two meteorite examples are demonstrating the chance to survive an invasive arriving into a rocky planet atmosphere and to reaching the surface. Inner structure of meteorites in cm size array is can completely survives the insults of impact into an rocky planet through the atmosphere e.g. in case of Earth. Usual impact speeds are 17km/s – 60km/s in case of Solar System according to local planetary speeds usual here.

E. Analytical methods

Analytical methods can be noninvasive and invasive. Noninvasive method is when during measuring in first step the target can be examined only in the original state without interaction, e.g. light, mechanical spectral analyses of target, e.g. dust or gas.

- **Noninvasive method** when mechanical membranes can hit or collect dust or gas elements and can measure them with chirp - ing vibration and can get spectral results Next step can be the invasive measuring method when a chemical reagent can be distributed or a mechanical interaction can be executed, e.g. hitting, drilling and carving. Noninvasive mode all of the light based measuring e.g. spectral analysis. This is an absolutely new field of the researching to develop, to make and to test experiments and equipment to measure chemical knowledges at relativistic speeds.

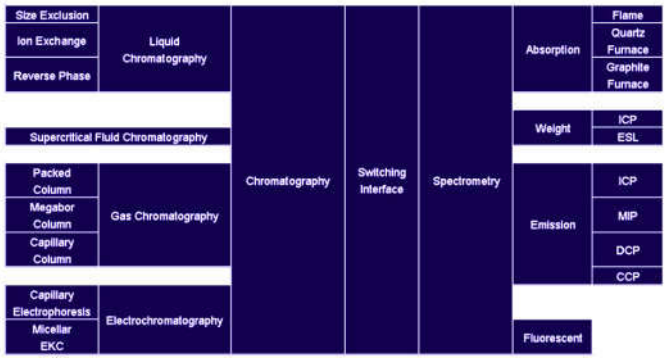

Fig. 4. Usual analytical methods suitable in the Earth. Which can be implementable in Space furthermore?

- **Invasive method** is to touch the thermo-, meso-, or stratosphere - just swept the planet's air – or reach deeper inner regions of the atmosphere or the surfaces (In some cases maybe we can deploy long-shaped bullet like NPSDRs). It is applicable ammunition or rocket like drive in case of reaching the surface to shot itself deeply, according to kinetic conditions. In case of relativistic speed some part of the fleet of swarm can be developed and ordered to reach the target invasive and in this time the other, logically connected part of the swarm can look the events and to make spectral analysis, e.g. optical or radio. The invasive part of the fleet can send measuring data until they can. This is a forced invasive measuring, which must be well-founded and reasonable because of environmental friendly reasons which are important. (See the environmental part) Million tons of "natural invasive" meteorites and dust arriving to the Earth.

- **Measuring experiments:** Experimental devices for measurement may be as follows: Sensors in radio, microwave and optical spectrum. The photosensitive spectral sensors with lens or telescopic lens together with prisms. Dust impact monitors on the measuring surface of SNPs which are orthogonal to the direction of travel, because the relative speed between the local area space and those orthogonal surfaces is just only the same as in case of usual space probe.

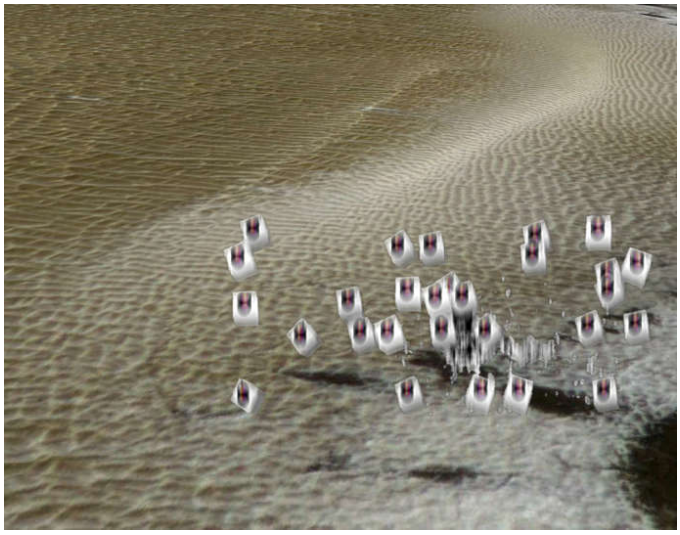

Fig. 5. Simulation of Planerary Type SNP fleet at south pole of Mars

- **3D modelling** is for interesting site selection, GIS Geographical Information Systems (GIS) useable in geoinformatics, e.g. cartography, geodesy, geographic information, photogrammetry, remote sensing, spatial analysis and deployable in planetary sciences. Spatial analysis includes a variety of techniques, many still in their early development, using different analytic approaches and applied in fields as diverse as astronomy, with its studies of the placement of planets, moons, comets and asteroids in the cosmos, i.e. in Earth and planetary sciences. To reconstruct surface in 3D from a few available images of a distant object, to increase the well estimation of the places of interests from more viewing angles on an unknown surface. It is very important to earn good results of analytical methods to choose a perfect landing or deploying site. The surface reconstructed from images gives an

opportunity to estimate a better result during searching for the best landing surface.

- **3D modelling problem** is the high-demand computing. Distributed computation can be realized in a part of the swarm.

F. *Target objects*

- *Planets with magnetic field:* Possible target objects in point of view of space physics are magnetic planets, non-magnetic planets.
- *Planetary object size:* Requirements are also different in point of view of size, ranging from asteroids, comets to rocky planets through to the gas giant sized planets.
- *Dusty fields:* Dusty places e.g. comets or rings of planets which are around of gas giants usually.
- *Combined:* Gaseous big planets according to our knowledge significantly have moons, magnetosphere, dusty halo with particle shower together with huge particle streams and massive amount of individual seemly random particles may come from even may come even long distances e.g. the distance of Kuiper Belt or Oort Cloud or high radiation galactic particles.

G. *Self-Regenerating*

According to last few considerations, some self-regeneration is necessary which is possible in electrical parts of devices according to research of Center for Nanotechnology, NASA Ames Research Center [6] By applying voltage to the gate electrode, the gate dielectric and isolation dielectric are annealed by the high temperature generated by Joule heat, and the damaged device can be recovered to a fresh state.

VI. Conclusion

Special philosophy is necessary to choose the HW and SW plans depending on the abundant enough or restricted availability of resources. In case of smarter but more expensive elements measuring and transmitting can be turned really efficient. The redundancy is also coming from the large amount of abundance of the Streaming Swarm of Nano Space Probes (SNP). In case of a realistic streaming swarm mission a weighted distribution of tasks necessary to elaborate during developing and *the whole streaming fleet necessary to behave like one big organization* as one big integrated space system and perhaps can be realized as a planetary mission solution with ***stream type*** *instruments and payloads*. (Fig. 6)

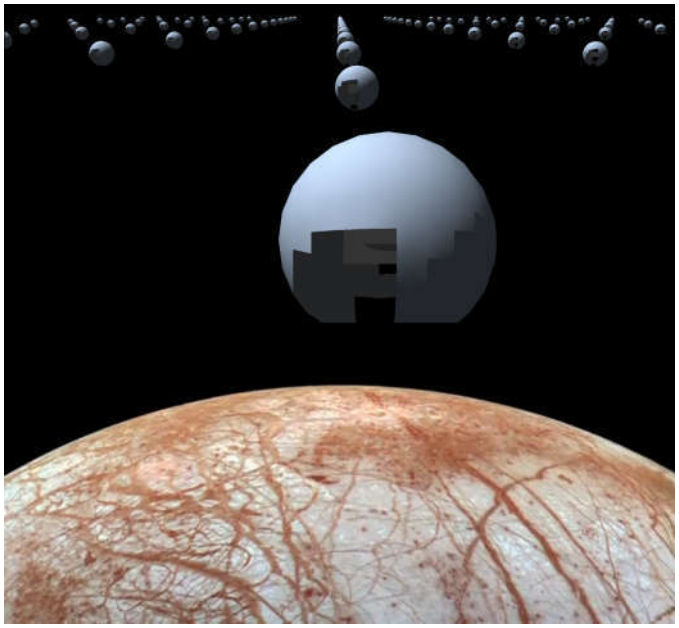

Fig. 6. Sheet of a conceptual Flat Fleet of SPN at Europa Moon of Jupiter for surface and environmental monitoring

References

[1] Malcolm Ritter: Stephen Hawking joins futuristic bid to explore outer space, phys.org, April 12 2016, http://phys.org/news/2016-04-stephen-hawking-life-tiny-spacecraft.html

[2] Vizi P G, Horváth A, Hudoba Gy, Bérczi Sz, Sík A.: 'Lump Sugar and Salt Shaker'-Like Nano and Pico Space Devices and Robots, IPM International Workshop on Instrumentation for Planetary Missions. Greenbelt (MD), 2012. http://www.lpi.usra.edu/meetings/ipm2012/pdf/1122.pdf http://ssed.gsfc.nasa.gov/IPM/IPM2012/PDF/Posters/Vizi-1122.pdf

[3] Vizi PG, et al.: Possible Identification Method for Martian Surface Organism by Using a New Strategy of Nano-Robots, 44th LPSC#2281 2013 http://www.lpi.usra.edu/meetings/lpsc2013/pdf/2281.pdf http://www.lpi.usra.edu/meetings/lpsc2013/eposter/2281.pdf

[4] Vizi et al. Modern Analytical Methods Applied to Earth and Planetary Sciences for Micro, Nano and Pico Space Devices and Robots in Landing Site Selection and Surface Investigation, Workshop on The Modern Analytical Methods Applied to Earth and Planetary Science, Sopron, Magyarország, 2014. LPI#4007http://www.hou.usra.edu/meetings/methods2014/pdf/4007.pdf

[5] P. G. Vizi: Application of the Fleet of Micro Sized Space-Motherships (MSSM) Deploying Nano, Pico Space Devices and Robots (NPSDR) in Space p. 43-44 of H-SPACE2016, http://space.bme.hu/sites/default/files/sima_lap/Proceedings_H-SPACE2016.pdf

[6] Sustainable Electronics for Nano-Spacecraft in Deep Space Missions Center for Nanotechnology, NASA Ames Research Center, Moffett Field, CA, USA, 2016 IEEE http://nobent.kaist.ac.kr/nobel/data/paper/2016/FC_DIM_sustainable%20electronics

Simulation of Earth-satellite Quantum Key Distribution

Ákos Korsós
Department of Networked Systems and Services
Budapest University of Technology and Economics
Budapest, Hungary
korsosa@mcl.hu

László Bacsárdi
Institute of Informatics and Economics
University of West Hungary
Sopron, Hungary
bacsardi@inf.nyme.hu

Zsolt Kis
Wigner Research Centre for Physics
Hungarian Academy of Sciences
Budapest, Hungary
kis.zsolt@wigner.mta.hu

***Abstract*—In this paper the properties of the Earth-satellite quantum communication is analyzed by simulating a global, satellite based quantum key distribution (QKD) network. The results are evaluated and a solution is proposed to correct some of the effects that distort the polarization measurement of the photons.**

Keywords—cryptography, quantum key distribution, satellite

I. Introduction

Currently we live in an era, where public key cryptosystems like RSA can guarantee computationally secure communication. Yet, the quantum computers are evolving and with Shor's quantum algorithm we will be able to crack RSA in just a few seconds. This would make RSA based protocols like SSH and SSL/TLS obsolete [1]. Thus, we need new methods for key distribution that can withstand attacks from quantum computers. Quantum key distribution may be a solution, that could take cryptography to the next level.

Using quantum key distribution (QKD), which is probably the most advanced practical branch of quantum communication, two communicating parties can establish an information theoretically secure, secret cryptographic key [2]. Since the security is based on the fundamental properties of quantum mechanics, in principle information-theoretic security can be achieved [3]. The secret key, established with QKD can be used to encrypt further classical communication to provide information-theoretically secure encryption and a mobile QKD network could deliver an unparalleled level of security to wireless users. In the future, even the one-time pad could be used in conjunction with QKD protocols.

Although commercial applications of QKD technology are already available, currently direct QKD links on the ground cannot reach distances beyond a few hundred kilometers due to optical losses [4]. With quantum repeaters, long-distance QKD networks may be feasible, but such devices are not ready for operational integration yet [5].

Alternatively, satellites could be used as relays to provide a global free-space QKD network. An orbiting satellite could act as an untrusted node, connecting two ground stations and facilitating key distribution without knowing the key, or as a trusted node by exchanging individual keys with each ground station and broadcasting the combination of the keys [6]. Then the two ground stations can extract the key of the other station from the broadcasted combination, giving both stations a shared key [7]. This way no other party than the satellite can intercept the shared key. By requiring only one link at a time the trusted node satellite has a simpler design and allows key distribution between two parties located anywhere on Earth, with a suitable orbit [8].

II. Global QKD Network

Let's assume that Alice and Bob are two communicating parties, who wish to establish a secret key with entangled pairs of photons using a global satellite network. In this case, the satellites could be used in several different ways to provide a secure quantum key distribution [9].

For example, Alice can generate the entangled pairs of photons and send one photon from each pair to Bob, using a satellite as a relay (Fig. 1). In this scenario, the satellite is an untrusted node with the sole task to forward the photon without disturbing the quantum state. During the communication, the path of the photons is very long and contains both uplink and downlink, which significantly distorts the photon polarization.

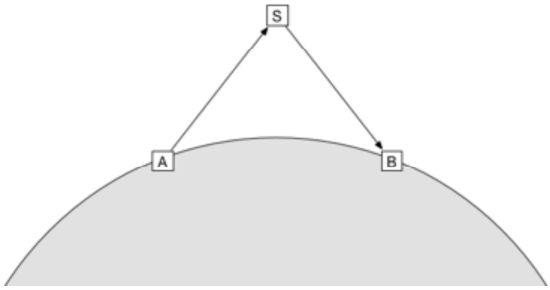

Fig. 1. The S satellite acts as an untrusted relay and forwards the photons received from A ground station to B ground station without disturbing the quantum state.

The satellite could also be used as a trusted node, when it independently establishes individual keys with Alice and Bob (Fig. 2). Then the satellite broadcasts a combination of the two keys, from which Alice and Bob can extract each other's key. In this case, the path of the photons is much shorter. Also, since this setup requires only one link at a time, this allows key distribution between two parties located anywhere on Earth, however, it still contains both uplink and downlink paths.

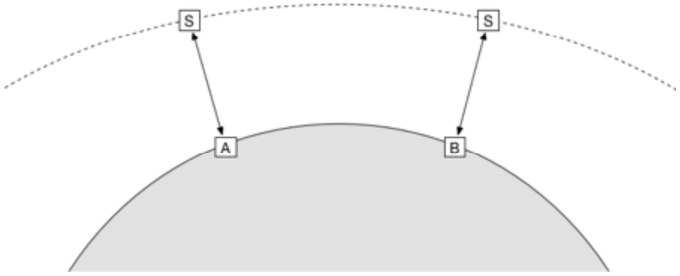

Fig. 2. The S satellite acts as a trusted node and first it establishes a key with A station, then later with B station. This solution does not require simultaneous line of sight between the stations and the satellite, so a larger area can be covered, however the B station has to wait for the satellite to arrive.

The solution proposed in this paper utilizes the satellite as a trusted node. In this scenario, the satellite is used to generate entangled pairs of photons, then sends one-one photon of each pair to Alice and Bob, respectively. The range covered by the satellite can be extended by using other satellites with plane mirrors.

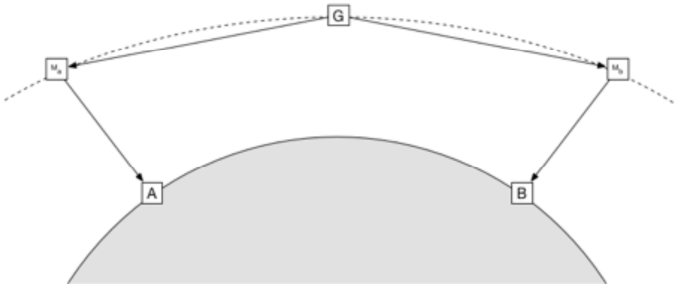

Fig. 3. The *G* satellite generates the entangled pairs and sends one photon of each pair to *A* and *B* ground stations. The range is extended with M_A and M_B mirrors. If the links between the generator and the mirrors are above the atmosphere, a significant amount of distortion can be avoided.

To simplify the calculations, I have assumed that the generator and the two mirrors are on the same orbit. And as stated before, the orbital plane is equivalent to the plane of the equator.

III. Rotation of Quantum Basis States

While the moving satellites generate and reflect the entangled pairs of photons, the basis states of the received qubits may be rotated in reference to what the basis states were on the generating satellite. The angular velocity of this rotation depends on the location of the ground station, the attributes of the mirror and the generator. The aim is that, we want to be able to calculate the received qubit's angle of rotation knowing the attributes of the ground station and the satellites.

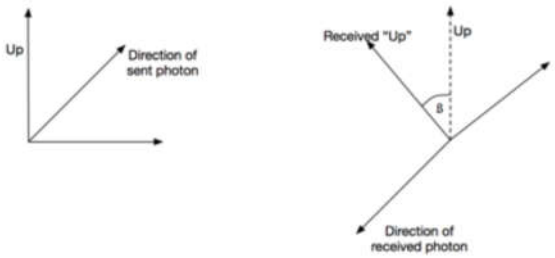

Fig. 4. The left figure shows the basis states when they are generated. The G generator chose the "up" base which points to the North, sends the photon to the mirror and the third base is the cross product of these two. The right figure shows the received photon from the perspective of the ground station (after reflection). The received "up" vector has been rotated during the reflection and the angle of the rotation depends on the velocity of the generator and the mirror and the position of the ground station as well. We have to calculate the β angle in order to correct the rotated "up" vector

I have used a Cartesian coordinate system during these calculations with the center of Earth as the origin. I have also assumed that the equatorial plane is the orbital plane and the vernal point is where the prime meridian passes the orbital plane.

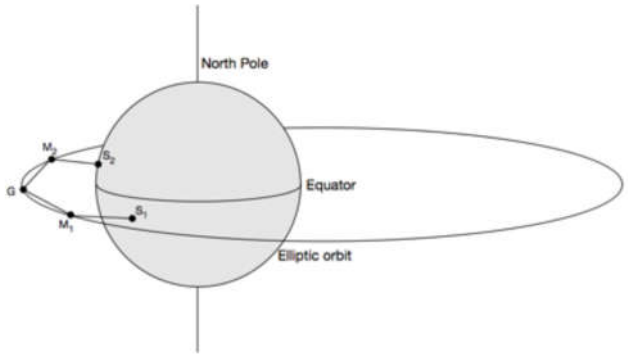

Fig. 5. G is the generator satellite, M1 and M2 are the mirror satellites, S1 and S2 are the ground stations on the surface of Earth. The perigee is equal to the vernal point which is at the prime meridian (the 0 longitude on Earth)

First we have to calculate the normal to the surface of the mirror satellites which will be used to reflect the qubits. Since we would like to reflect the photon beam from the generator to the stations on Earth, we can calculate the normal to the surface of the mirrors from the positions of the ground stations, the generator and the mirrors. According to the law of reflection, the incident ray, the reflected ray and the normal to the surface of the mirror all lie on the same plane. Also, the angle of reflection is equal to the angle of incidence.

I have used a Cartesian coordinate system during these calculations with the center of Earth as the origin.

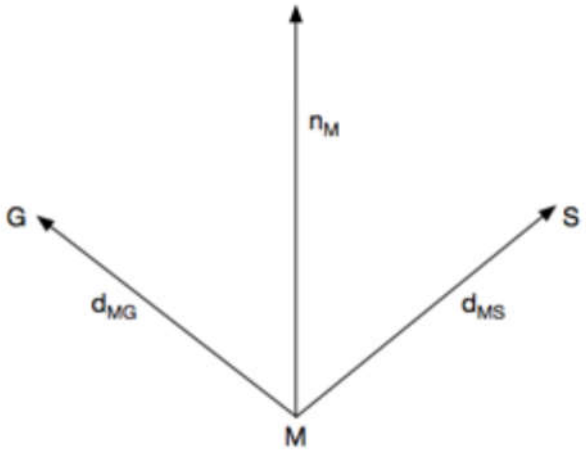

Fig. 6. $\bar{n}_m$ is the normal to the surface of M mirror which can be calculated from the directional vectors pointing from the mirror toward G generator (d_{MG}) and the S ground station (d_{MS}). The directional vectors and the normal vector have to be normalized.

Assuming that all of the vectors are normalized and have a length of 1, we can write the following equations:

$$\bar{n}_{M_1} = \bar{d}_{M_1G} + \bar{d}_{M_1S} \tag{1}$$

$$\bar{n}_{M_2} = \bar{d}_{M_2G} + \bar{d}_{M_2S} \tag{2}$$

where $\bar{d}_{M_1G}$ and $\bar{d}_{M_2G}$ are the normalized direction vectors pointing from the mirrors towards the generator, $\bar{d}_{M_1S}$ and $\bar{d}_{M_2S}$ are the normalized direction vectors pointing from the mirrors towards the ground stations, $\bar{n}_{M_1}$ and $\bar{n}_{M_2}$ are the normals to the surfaces of the mirrors, which have to be normalized.

When the normals of the mirrors' surfaces are known, we have to decide the basis of the quantum states. I have assumed that the basis states includes an "up" vector which points to the North, the travel direction of the photon *(which is the generator-mirror direction)* and the cross product of these two. However, these bases can be arbitrary vectors which are perpendicular to each other.

After we have chosen our basis, these basis can be represented as 3 perpendicular vectors which have to be reflected on the mirrors using the law of reflection. This gives us the reflected basis vectors

$$\bar{b}'_x = \bar{b}_x - 2(\bar{b}_x \cdot \bar{n}_m)\bar{n}_m \,, \tag{3}$$

where $\bar{b}'_x$ is a reflected basis state *(x stands for one of the three vectors)*, $\bar{b}_x$ is the original basis state and $\bar{n}_m$ is the normal of the mirror where the reflection occurs.

When the reflected basis states (which will be received by the ground stations) are known, we have to determine the direction of the original "up" vector which is visible from the ground station looking towards the mirror. This is a simple vector pointing to the North Pole and have the same inclination and right angle as the incoming photon's direction vector.

If both the original "up" vector of the ground station and the received "up" vector are known, we can easily calculate the angle between the two vectors using the equation

$$\cos\theta = \frac{\bar{a}\cdot\bar{b}}{|\bar{a}|\cdot|\bar{b}|} \,, \tag{4}$$

where the two "up" vectors are $\bar{a}$ and $\bar{b}$ and is the magnitude of the vector. Using the inverse cosine function we can determine the θ angle which is the angle of rotation of the quantum basis states.

The equations 1,2,3 and 4 give us the angle of rotation at given satellites positions. Using numerical analysis with very small position changes, we can calculate the angles at different satellite positions. For this we have to introduce a small Δt and calculate the new positions of the satellites at every elapsed Δt time.

As the initial position of the satellites and the parameters of the orbit are assumed to be known, we can calculate the velocity of the satellites. From these we can calculate the position of the satellite after Δt elapsed time

$$S' = S + \bar{v}\cdot\Delta t \,, \tag{5}$$

where S' is the new position of the satellite (originally at position S) after Δt time while travelling with $\bar{v}$ velocity.

At the new position we also have to recalculate the distance between the orbiting bodies and the new direction/magnitude of the velocity.

By choosing a sufficiently small Δt and using the equations 1, 2, 3, 4 and 5 one after another to calculate the positions after every elapsed Δt, we can calculate the angle of rotation for every specific time and position. From the calculated data we can also calculate the difference between two angles at two specific times, which gives us the angular velocity of the rotating quantum state basis and shows how fast the basis are rotating.

IV. Data Analysis and Results

I have developed a custom simulator application in Python language, using OpenGL for 3D visualization. In the application, I have implemented the equations described above and run several simulations with different orbit and base station parameters.

To simulate the rotation of the quantum basis states, I have used $6.677 \cdot 10^{-4}$ as the eccentricity of the orbit and 400km as the altitude of the satellites at the perigee, similar to the attributes of the International Space Station's orbit.

In this scenario (see Fig. 7 and 8), the initial longitude of the generator, as viewed from the Earth is 3° to the east, M_2 mirror is 18° to the east and M_1 mirror is 12° to the west. The satellites are orbiting to the west.

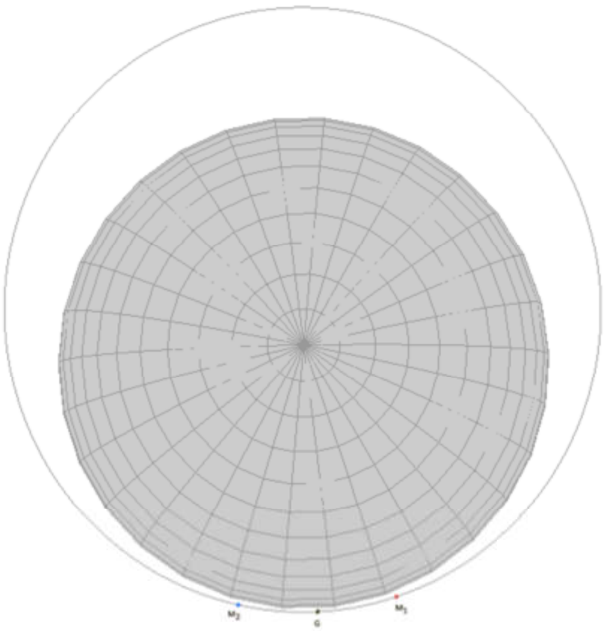

Fig. 7. The simulated orbit viewed from the north. The satellites on the figure from left to right are M_2, G and M_1

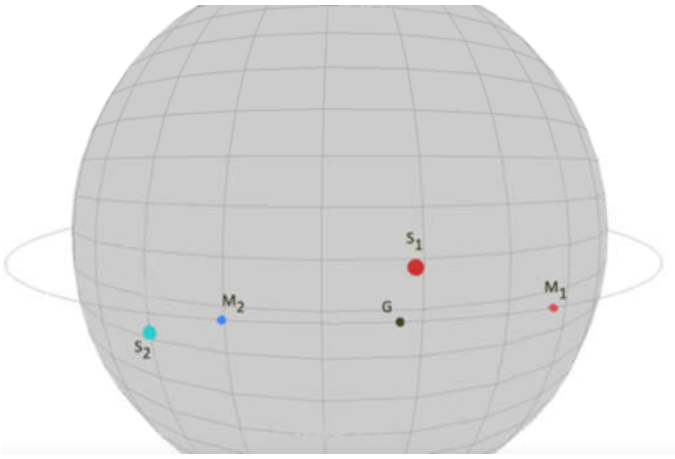

Fig. 8. S1 ground station has been placed on the northern hemisphere at 5° latitude, 5° longitude. S2 ground station is located on the southern hemisphere at -5° latitude, -30° longitude.

The ground stations are configured, so that they can establish a quantum channel with a satellite only if the zenith angle is smaller than 60°. If the zenith angle is larger than 60°, the laser beam would have to travel across much more atmosphere which would cause great distortion.

The calculations mentioned before (moving the satellites, recalculating the velocity and distance from the center of Earth, recalculating the rotation of the basis states) are repeated at very small time intervals.

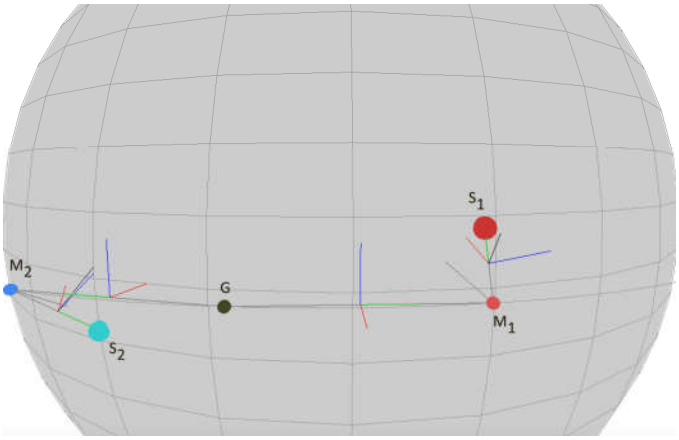

Fig. 9. the satellites are visible from the ground stations under 60° Zenith angle, so an active quantum communication is possible. The lines connecting the satellites and the stations indicate a quantum communication. The three vectors in the middle of these lines indicate the basis states and the blue vector means the "up" vector. On the mirror-ground station connections the black line indicates the true "up" vector which is visible from the ground station's perspective. The difference between this black "up" vector and the received "up" vector is the angle of rotation.

Because of the simulation it is clear, that the basis states are rotated when received by the ground stations. The moving satellites cause this rotation to continuously change during the communication and for this rotation countermeasures should be taken at the ground stations.

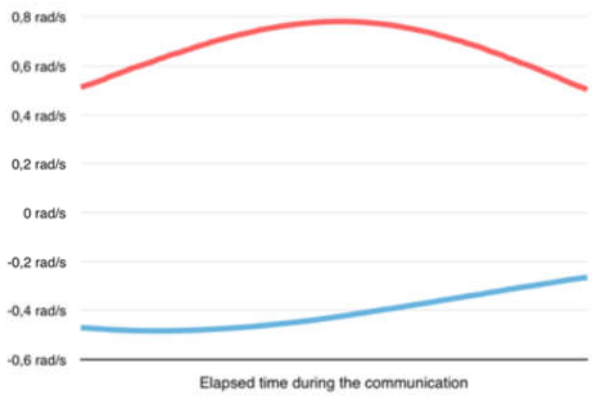

Fig. 10. This line chart shows the required rotation during the simulated quantum communication. The S_2 base station (illustrated by the top, red line) had to rotate the bases at a rate of 0.5 rad/s but the speed of the rotation was the fastest when the M_2 satellite was the closest. The same is visible on the bottom, blue line which shows the speed of basis rotation at S_1 base station.

A negative speed of rotation means that the received "up" base is getting closer to the original "up" direction. On the northern hemisphere, this means a counter clockwise rotation, while on the southern hemisphere it is the opposite.

These results clearly indicate that if the photons are generated or reflected by a moving satellite, the received quantum basis states are possible rotated. That also means that even during a few seconds of communication the speed of this rotation changes in time, which should be actively corrected as the photons are received.

V. Conclusion

It seems increasingly urgent to develop a global QKD network that can provide truly random and information theoretically secure keys between any two nodes on Earth. From previous researches we already know that a satellite based QKD network is indeed feasible.

If satellites are used for quantum communication, we must take several new factors into our calculations to ensure the synchronization of the quantum basis states. These simulation results indicate that if the photons are generated or reflected by a moving satellite, the received quantum basis states are possibly rotated. That also means that during a quantum communication event the angular speed of this rotation changes in time, which should be actively corrected as the photons are received. The calculations in this paper help to compensate this rotation and by extending the simulator application in the future, even other attributes can be calculated.

Acknowledgement

The research was supported by the Hungarian Scientific Research Fund – OTKA PD-112529.

References

[1] Simon Singh, "The Code Book", Anchor Books (2000)

[2] S.Imre, F. Balázs, "Quantum Computing and Communications - An Engineering Approach", Wiley (2004)

[3] S Imre, "Quantum Computing and Communications - Introduction and Challenges", COMPUTERS & ELECTRICAL ENGINEERING 40:(1) pp134-141 (2014).

[4] D.Stucki et al, "High rate, long-distance quantum key distribution over 250km of ultra low loss fibers", New J. Phys. 11 075003 (2009)

[5] N.Sangouard, C. Simon, H. Riedmatten, N. Gisin, "Quantum repeaters based on atomic ensembles and linear optics", Rev.Mod.Phys.83, 33 (2009)

[6] L. Bacsardi. "On the Way to Quantum-Based Satellite Communication", IEEE Comm. Mag.51:(08) pp. 50-55. (2013)

[7] L. Hanzo; H. Haas, S. Imre, D. O'Brien, M. Rupp and L. Gyongyosi, "Wireless Myths, Realities, and Futures: From 3G/4G to Optical and Quantum Wireless", Proceedings of the IEEE, Volume: 100 , Issue: Special Centennial Issue, pp. 1853-1888.

[8] H. Curtis, "Orbital Mechanics for Engineering Students", Elsevier Butterwort-Heinemann (2005)

[9] J-P.Bourgoin et al, "Free-space quantum key distribution to a moving receiver",Opt.Express 23, 33437 (2015)

Space research and mini-satellites in secondary high school

Mária Pető
"Székely Mikó" High School
St. George, Romania
rkollegium@yahoo.com

Abstract— ***Space research, the universe and satellites are three fascinating questions for which students have no possible answers in the regular school curriculum. Therefore, every opportunity to bring these topics into school activities and closer to students' interest is welcomed. Few years ago I found the European Cansat competition held by ESA (European Space Agency), which presented itself as one solution for fulfilling this demand.***
Cansat is a mini-satellite that can be fit into a Coca-Cola soda can (330ml) and it is released from 1km altitude. This mini device is based on Arduino- microcontroller and it performs certain scientific missions like measuring air pressure, temperature, humidity, dust pollution, radiation level, location, telemetry, etc.
This competition and the preparation period are very useful for students as they offer a special opportunity to learn about sensors, microcontrollers, radio communication, space research missions, project management. Furthermore they aid the development of technical skills and applications of the acquired theories.

Keywords: cansat, satellite, Arduino, education

I. WHAT IS A CANSAT?

The CanSats (can-soda-satellite) are mini satellites fit into standard soft-drink cans (330ml, 115mm height and 66mm diameter) which simulate the work of a real scientific satellite. The CanSat is required to have a mass between 300-350grams, it must work continuously for at least 4 hours, and it should have a safe recovery system and an easily accessible power switch, maximum flight time being recommended between 120-190 seconds with a descent rate between 4,6m/s-11 m/s. Also, the unit must be able to withstand an acceleration up to 20G and a pressure of 40atm. During flight, it should be in contact with the ground station permanently, transmitting measuring data. The total budget of the finished CanSat device should not exceed 500€. [3, 4]. The CanSat is released from a rocket (Intruder) or a light plane at an altitude of 1kilometre. During the fall, the mini satellite will perform a certain scientific mission and it is expected to land on ground safely. The primary scientific mission is compulsory for every participating team, and it consists of measuring the air pressure and temperature. The secondary mission is chosen by the participating teams, for instance advanced telemetry, guided landing on a target, radiation level, etc. The European CanSat competitions are held by ESA. ESA member states take turns organizing national competitions and the winners will participate at the international level. The final phase of this contest is organized at Andoya Rocket Range in Norway or Santa Cruz Air Field in Portugal. During the whole competition the students should write technical progress reports and design documents (in English) sending them regularly to the competition board.

The big challenge for the high school students (aged 15-19) is to develop a scientific mission, like designing a real satellite and filling all measuring subsystems, communication and power units into a small space, thus producing innovative scientific, technological and educational value and promoting their activity.

II. OUR CANSATS

My students participate at this fascinating competition since 2012. At the beginning, we were absolute beginners because we did not know anything about satellite-building. So we started from the basics. After a few introductive lessons about satellites and electronic sensors we built a very simple but well-functioning measuring device that includes pressure, temperature and dust sensors, a radio communication unit and a Yagi antenna. The antenna used by our team was similar to a Yagi-Uda array one. This antenna was a tuned one, at a frequency of 433MHz. We designed three parachutes for different weather conditions and we placed the device into an special home-made steel cylinder.

The main idea for the secondary mission was to improve students' knowledge about atmosphere physics by verifying the barometric pressure formula and vertical temperature gradient law, as well as to complete an air pollution chart. We chose to measure dust density since we know that our region is relatively highly polluted, as far as dust density is concerned because of the close factories. Our goal was to form a proper image of the situation and therefore increase public awareness. Firstly, we made a detailed plan of the whole process. Then, we designed and built the measurement device (hardware and shell). In the next phase, every single subsystem of the CanSat (the sensors, the radar, the GPRS module, the RF transmitter and the parachute) was tested separately. Finally, we assembled the CanSat and we tested all of the systems together. This part served as an overall simulation of the Launch Campaign.

Fig.1. The Bolyai CanSat team Andoya Rocket Range, 2012

During the launch campaign at Andoya Rocket Range we have achieved our goals:

- the CanSat worked properly;
- parachute deployed properly;
- good descent rate (7.6 m/s);
- no major damage at landing;
- continuous radio communication between CanSat and ground station;
- two sets of measuring data were collected and saved;
- there were no significant differences between values measured in a defined height interval;

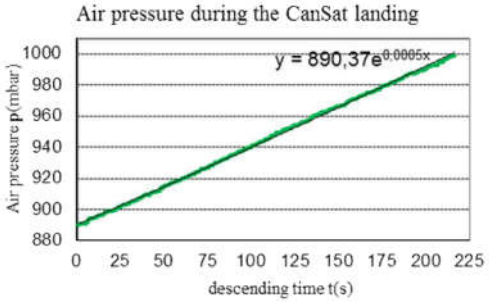

Fig.2. Air pressure during the CanSat landing

The readings from the pressure sensor obey the barometric law, which describes the change of air pressure with altitude. There is an exponential function that helped us to calculate the maximum altitude of the Cansat. According to our calculations, the maximum altitude (z) of the rocket and our Cansat was about 930meters.

$$p = p_0 e^{-z\frac{g\varrho}{RT}} \quad (1)$$

The diagram of the pressure measurements should be an exponential curve, although on our diagram it seems to be linear, the reason for this being that this is just a small part of the whole curve. (the exponential curve could be seen if the measurements took place at an altitude of at least 10 km).

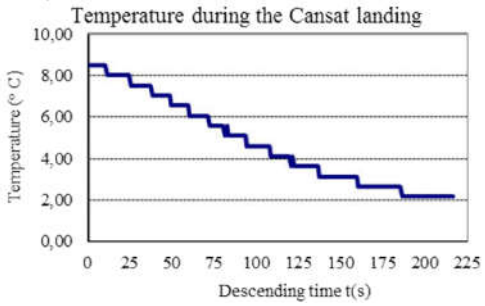

Fig.3. Temperature during the CanSat landing

The diagram (3) presents the temperature data received from the Cansat throughout the descent. Our diagram is linear and shows that the temperature decreased according to the inversed gradient law. Interestingly, the values are higher at high altitudes than near the ground. The explanation for this is the phenomenon of temperature inversion. For this to happen, several factors needed to coincide:

The night before the launch day the sky was clear, the temperature was 1°C. (22nd April, 2012). Due to this, the whole air cooled down, cooling down also the ground and the surrounding sea. In the morning of the launch day (23rd April, 2012) dense clouds appeared at a 1 km altitude which reflected the sunlight and its heat, not allowing the Earth's surface to heat up. However, the low clouds absorbed the heat.

For the 2o15 and 2o16 Cansat contest we designed more complex and complicated devices. These mini satellites complied with all the rules and standards of the CanSat competition and could perform special data analysis, by associating the data received with a 3D map, falling simulation and different dynamic and position measurements. During the descend, the unit sent measuring data to the ground with the help of a radio transmitter and uploaded the received information to a web server with a GPRS module. The collected data were analysed and processed by students and the results were presented at conferences or used at physics classes.

In 2015 for the secondary mission we choose to simulate the exploration of a newly discovered planet like a real satellite. So we divided our mission in two parts. First, we determined the quality of atmosphere measuring the air pressure, temperature, humidity, different gas concentration and dust pollution. The second task proposes to explore the surface of the planet with a small rover after the CanSat landing. This rover then would investigate soil moisture levels. Along with these we will also gather GPS data. From the acquired data we intend to compile a vertical map of humidity, temperature and UV radiation intensity and a horizontal map of soil moisture levels. We set out as a goal to get an accurate picture of the physical properties of the atmosphere and ground in order to determine whether these provide a possibility for life. We wanted to see how accurate data gathered with such measurement methods can be, and then adjust them accordingly. For this task we introduced a mini rover into the Cansat which was deployed after the landing. The rover was a semi-autonomous vehicle which is small enough to fit in our CanSat and it had a soil moisture sensor.

The rover was driven by two electric motors with two gearboxes and tracks. The rover was controlled by an Arduino unit based on the Atmel ATmega 328 microcontroller. All of the rover's components will be held together by the main chassis, which will be made of PLA (PolyLactic Acid). The ground receiver unit was entirely built by our team, based on an Atmel Atmega 328 microcontroller and the transceiver included in the CanSat kit.

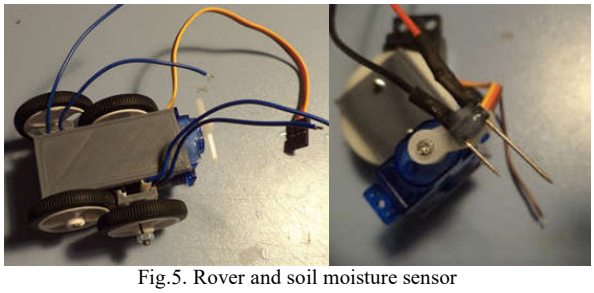
Fig.5. Rover and soil moisture sensor

Cansat15 unit used the SEN-VRM-08 humidity sensor to measure the amount of water vapour in the air. Being an analogue sensor, it measures changes in resistance as the humidity varies, emitting an analogue signal which is then processed and transmitted by the unit. We measured the humidity in a scale of 300-900 (300 indicates dry air and 900 air containing up to 95% vapour).

Being aware of the problem of the global warming, we are studying its special aspects in our region, since our town has an individual microclimate, due to which the general meteorological reports are not valid. Provided we analyse more seriously the aspects of the atmosphere, we hope that we can find signs which can confirm or confute the existence of the global warming. Last year, we designed an Arduino controlled mini meteorological ground station and now we will use the CanSat's geophysical and meteorological sensors for precise measurements at higher altitudes.

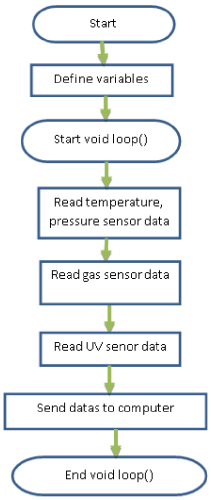

Fig.6. Flowchart for CanSat15 unit

In 2016 our secondary mission was based on different dynamics and position measurements, 3D mapping and data communication. For the dynamic position analysis we measured acceleration along the three axes (x, y, z). We also used a 3-axes compass to determine the momentary position as accurately as possible, combined with real-time GPS data. Our CanSat assigned its location to all the data it measured. This location was completed with the altitude and the tilting data in comparison with the vertical state. These three measurements were processed by a program written in javascript, which creates an animation about the movements of the CanSat. The data are a basis to our educational outreach, which is based on a 3D map of the environment around the CanSat.

One of the objectives of the secondary mission was to successfully log the data obtained from the sensors not only on a ground unit via the RF transmitter, but also on a webserver (in a MySQL database) using a built-in GPRS module. Another objective, closely connected to the latter was to draw a virtual track of the CanSat's descent. Our last technical aim was to back-up all the data on a microSD card (aboard the CanSat) with an OpenLog unit. Data uploading to the webserver was achieved using a small subsystem consisting of an Olimexino Nano Gsm data processing unit combined with a SIM800H quad-band GSM/GPRS module, that works on frequencies GSM850MHz and PCS1900MHz. SIM800H features GPRS multi-slot class 12/class 10 (optional) and supports the GPRS coding schemes CS-1, CS-2, CS-3 and CS-4. Basically, this circuit is the core item of our data processing plan, and it works in the following way: it collects the data received from the sensors and uploads it on a web page provided by us. Since this is a complete subsystem, even in case of failure will not affect other parts of the secondary mission and also it leaves more computing capacity for other tasks.

Nevertheless, during the fall, the measured data were sent with a radio transmitter to the ground, then they were uploaded to a server with the GPRS module. The server saved the received data in a MySQL database, and immediately processed them on a webpage. On the page we illustrated the line of falling in 3D based on information received from GPS, the incidence angle of CanSat from Gyro data, and the rate of fall based on accelerometer data.

We were always amazed by how the professionals at ESA and NASA create wonderful images or maps containing a lot of information from data obtained and transmitted back to a ground station by space telescopes. It still remains very interesting for us how one can map the surface of an unknown space object without having to actually land any kind of equipment on it. An orbiting unit is enough to scan the surface, and even mountains, valleys and rivers can be drawn based on the obtained data. This interest of ours determined our secondary mission to create a 3D map based on the position of the CanSat and pictures from a CMOS camera module with a resolution of 728x488 pixels.

Our data visualization was based on a 3D map of the terrain beneath our flying unit which is created in Autocad 3DSMax. On this map we presented a visualization of the measured atmospheric features as well as our position and movements. Using the data obtained from the sensors we calculated the height of the point compared to sea level. Furthermore, the exact coordinates were determined using the GPS data, the speed of the fall, acceleration of the CanSat and also data measured by the gyro sensors.

The CanSat started to collect data right at beginning of the descent. In this way we were constantly receiving data about pressure and temperature readings. From these measurements, we calculated the parameters of the weather and displayed them on the 3D map. After the CanSat landing these measurements data were processed in Wolfram Mathematica and Mathlab to create falling simulation. Our snapshots taken by a CMOS camera, due to the large quantity of data, were only saved to the SD card and were not transmitted to the ground station via the RF transmitter.

We considered designing an efficient and safe recovery system and outer shell is another part of our secondary mission. Our recovery system mainly consisted of the parachute. We made a lot of tests to define how large the surface the of parachute should be because the multitude of natural unpredictable natural factors. Finally we decided to make three chutes up from 6, 8 and 12 isosceles acute triangles, and choose the most efficient according to the weather conditions. We used a canopy material, which is adequately strong and flexible. To design the parachute the

students used some simple physics principles, which they have learned at Mechanics classes: Newtonians laws, fall in gravitational field, drag, etc.

We used the following formula to determine the diameter of the parachute:

$$D = \sqrt{\frac{8 \cdot m \cdot g}{\pi \cdot \rho \cdot c_d \cdot v^2}} \quad (2)$$

Where:
m- total weight of body and parachute
g- acceleration of gravity, equal to 9.81 m/s^2
ρ- local density of the air (ρ=1.22 kg/m^3).
C_d- the drag coefficient (for the semi-spherical parachute Cd=1,5)
v- descent speed of the CanSat (the maximal speed reached during the fall is v=8m/s)

For the shell of the CanSat we tested two materials. One of our choices was the carbon-fiberglass, since it is a strong material and has a surprisingly good solidity. Moreover, it is flexible, within its breaking elongation limit, at the offload it gets back to the original shape. This feature changes depending on the change of the material's thickness. It does not absorb humidity, it is non-flammable and also heat insulator. Its only disadvantage was the price. Beside the carbon-fiberglass, we tested a PLA (polylactic-acid) plastic as possible raw material for our shell. We decided to use plastic because it is cheaper and more accessible than the carbon-fiberglass, and due to the highly customisable character of plastic we made a proper outer cover that withstands the forces appearing at the moment of impact with the ground. This year our CanSat's protection shell had two scopes. The first one was ordinary, it had to protect the main part of the electric circuits. In addition to this, we suspended on it a set of mini solar panels. We thought a lot about making it strong and light enough. Firstly we had the idea of making two different shells of which one supposed to be made of simple fiberglass and the other of vacuumed plastic. We made a 2-3 mm thick fiberglass shell, and fixed on it 4 rows of solar panels.
First we made a wood moulding which was covered with the fiberglass sheet and epoxy resins. We superpose several fiberglass slab and resins and after dried them. The surface of the template was very smooth, and the outside diameter was 3 millimetres smaller than that of the CanSat's.
The Miko-Cansat16 components:

Weather related data, mean temperature, atmospheric pressure and humidity, were measured by two different sensor units. Temperature and humidity were measured by the same unit, an HTU21D Digital Relative Humidity Sensor with Temperature Output. This sensor provided us calibrated, linearized signals in digital, I^{2}C format. Besides the low power consumption and fast response time another advantage of this sensor was that the resolution (both for RH and T) can be changed by command. Our pressure sensor, the LPS25H, was incorporated into the AltIMU-10 v4 unit. The LPS25H is an ultra-compact absolute piezoresistive pressure sensor. It includes a monolithic sensing element and an IC interface able to take the information from the sensing element and to provide a digital signal to the external world. An added advantage was that it had a high shock survivability of 10000g.

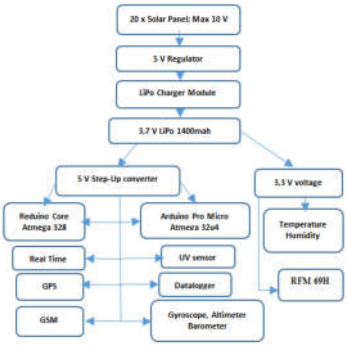

Fig. 7. The Miko-Cansat16 block diagram

The AltIMU-10 v4 unit was also equipped with a three-axis digital output gyroscope and an ultra-compact high performance e-Compass 3D accelerometer and 3D magnetometer module (LSM303D). The L3GD20H gyroscope was a low-power three-axis angular rate sensor. It included a sensing element and an IC interface able to provide the measured angular rate to the external world through digital interface (I2C/SPI). The LSM303D was a system-in-package featuring a 3D digital linear acceleration sensor and a 3D digital magnetic sensor.

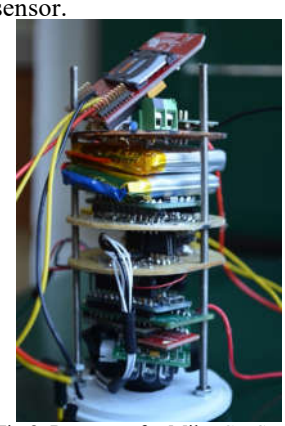
Fig.8. Prototype for Miko CanSat16

The nine independent rotation, acceleration, and magnetic readings provided all the data needed to make an altitude and heading reference system (AHRS), and readings from the absolute pressure sensor can be easily converted to altitudes, giving a total of ten independent measurements (sometimes called 10DOF). With an appropriate algorithm, the microcontroller built in device and our computer was able to use the data to calculate the orientation and height of the AltIMU board.

The device was also equipped with a piezoelectric component to detect the moment when the CanSat lands. At the moment of landing, a small electrical tension was produced in the piezo element. The piezo is an electronic device that generates a voltage when it's physically deformed by a vibration, sound wave, or mechanical strain. If the sensors output is stronger than a certain threshold, the board sends the string "Knock!" to the computer display over the serial port.

GPS data were provided by a ADH-tech sensor. The GP-735 is a slim, ultra-high performance, easy to use GPS smart antenna module designed with u-bloc's latest 7th generation single chip.

Another sensor (ML8511) measured UV intensity, which value is then weighted according to the CIE Erythemal Action Spectrum (a standardized measure of human skin's response to different wavelengths of sunlight from UVB to UVA) giving us the UV index. The UV index is a number on a linear scale from 0 to 11. We currently used the ML8511 sensor, but we were testing several other types of sensors too. Considering the low supply current (300mA in function and 0.1mA in standby mode), the current sensor guarantees a long battery life. In addition, it operates perfectly between -25°C and 75°C, which is in accordance with atmospheric measurements. The whole measuring device was driven by an Arduino microcontroller with an appropriate programme written by the students.

III. CONCLUSION

The students are very interested in this project since it is something new and exciting for them, which could help them discover the fascinating world of space science and technologies. Not only will the acquired knowledge and experiences aid them in their daily student lives (at school) but also in the future in our professional career. These contests offer a very good opportunity to improve the students' knowledge in transcurricular topics, they could combine physics and math knowledge with computer science, programming and engineering.

After every contest I try to use our achievements in the teaching process. So we built a mini meteorological station using the Cansat components and we collect air parameters every day. We created a comparative meteorological (pressure, temperature, UV radiation, wind) map for our town and Launch Campaign site and I use them during physics lessons (regarding topics such as thermodynamics, geography, biology). In the preparation phase of this project we made some 3D charts with data collected while testing at Sugás-Hill, near our town, so these data can also be used.

Our outreach activity is carried out parallel to the planning, building and testing phase of Cansat, this way we could inform the public regarding our most recent accomplishments. We hold presentations on special physics lessons at "Bod Péter" County Library, interactive workshops for primary school students (9-11 years old) during the Science Day or science camp; we keep blogs in three languages (Hungarian, Romanian and English). On these blogs we have the opportunity to publish articles presenting details for all who are interested and to share information about the whole progress of the project. In addition, we do the same on the website of our school. Furthermore, we publish articles in the school and local newspapers.

REFERENCES

[1] M. Pető "Experiments with Cansat"-ICPE-EPEC 2013 Active learning - in a changing world of new technologies; Editors: L. Dvořák, V. Koudelková; Praga, 2014, ISBN 978-80-7378-266-5; pp. 766-774.; http://www.icpe2013.org/uploads/ICPE-EPEC_2013_ConferenceProceedings.pdf

[2] M. Pető "Atmosphere physics in a soda can-CanSat12" (Légkörfizika egy üdítős dobozban avagy CanSat12)- Conference book (in Hungarian language), editors: A. Juhász., T. Tél-A fizika, matematika és a művészet találkozása az oktatásban, kutatásban, Eötvös Loránd University, Budapest, 2013, pp.272-284; ISBN 978-963-284-346-9; e-book: http://fiztan.phd.elte.hu

[3] The CanSat book- ESA, NAROM (Norwegian Centre for Space-related Education) - e-book:
https://www.narom.no/bilder/bilde1_20130826154135.pdf

[4] What is a Cansat?, Cansat webpage,
http://www.esa.int/Education/CanSat/What_is_a_CanSat

[5] R.Pietraru. "10 projects with Arduino" (in Romanian language: 10 proiecte cu Arduino), Techno Media, Sibiu, 2015;

Follow-up Psychological Status Monitoring of the Crew Members of Concordia Research Station at Antarctica Based on their Speech

Gábor Kiss, Klára Vicsi
Department of Telecommunications and Media Informatics
Budapest University of Technology and Economics
Budapest, Hungary
kiss.gabor@tmit.bme.hu, vicsi@tmit.bme.hu

***Abstract*—In this study an automatic prediction system is presented, which can predict the severity of the depression of examined subjects based on their speech signal. This work has been completed under an ESA project, titled the "Psychological Status Monitoring by Computerized Analysis of Language phenomena (COALA-Phonetics)". One aim of this project is to monitor the psychological status of the researchers at the Concordia research station at Antarctica, especially to detect depression based on speech processing. Speech samples were collected from each crew member about twice a month. Two type of tasks were recorded: a short voice diary and reading out loud a standard phonetically balanced folk tale. Separately from this recording, speech data were collected from depressed patients and healthy subjects in normal life and atmospheric conditions as well, and this Reference Depressed Speech Database was used to train our automatic prediction system. Each sample in the database was labelled according to the Beck depression inventory II (BDI-II) scale, which measures the severity level of the given mental state. On the base of this database an automatic method was developed which predict the severity of depression based on speech signal processing. A characteristic feature vector, which describes the severity of depression well was selected from a basic parameter set by Sequential Forward Selection (SFS) method, using the Reference Depressed Speech Database. Support Vector Regression (SVR) model was developed for our automatic prediction system. The severity of depression of each record of each crew member of the Concordia research station was predicted using this automatic depression severity prediction system and thus we have got the severity of depression for each crew member as a function of time.**

Keywords—depression, SVR, speech, follow-up status monitoring

I. INTRODUCTION

In this study, an automatic follow-up status monitoring method is presented, which is able to predict the severity of depression of examined subjects based on their speech.

In our project, titled "Psychological Status Monitoring by Computerized Analysis of Language phenomena (COALA-Phonetics)" one aim is to monitor the psychological status of the researchers at the Concordia research station, especially to detect depression based on speech. The Concordia research station is located in Antarctica, where a group of selected researchers are stationed for a year. Due to the environment of the station, the researchers are almost separated from the outside world, they live and work in a small research station and other circumstances are extreme too, like the outside temperature, and the lack of the sunshine at winter. Speech samples were collected from each crew member about twice a month. Two types of tasks were recorded: a short voice diary and reading out loud a standard phonetically balanced folk tale. In this study we used only the recordings of the short folk tale.

Depression is a psychiatric disorder. Several events can cause depressed state in the life of a person, like stressful events, persistent sadness, and difficulties in the daily duties and so on [1]. The World Health Organization (WHO) Depression - the publication of Global Public Health Concern - stated that there were 350 million people suffering from depression in 2012 [2]. The WHO predicts that by 2030 unipolar depression will be among the top three most serious diseases worldwide, alongside HIV/AIDS and heart disease [3].

Upon the development of depression, the depressed person's quality of life and ability to work are impaired, and there is an increased chance of suicide [4]. This raises a serious problem, both humanly and economically. The problem is aggravated by the depression diagnosis being performed by a limited layer of medicals which is both time-consuming and expensive. For this reason, it is important to develop a depression detection application that could make the process of medical diagnosis easier.

In 1921, Emil Kraeplin published, that the speech of the depressed people is different from the speech of the healthy people. He observed differences mainly in the dynamics of the fundamental frequency, the dynamics of the intensity, the length of pauses [5]. With the development of computer technology and the increasing speech databases, there are now a number of other acoustic phonetic characteristic which were also identified as a good markers of the depressed state, like formant frequencies, jitter, shimmer, spectral components [6]. For these reasons, the speech seems to be a promising indicator as a biomarker of depression.

The research was supported by European Space Agency COALA project: Psychological Status Monitoring by Computerized Analysis of Language phenomena (COALA) (AO-11-Concordia).

Our earlier results proved that automatic classification of depressed and healthy state can be carried out based on speech [7]. In the present study we intended to create an automatic system which can make an automatic prediction of the severity of depression based on speech signal. Thus, in the COALA project, a regression model was trained, which is capable to predict the severity of depression of a speaker based on her/his speech. This automatic depression severity prediction system was used to predict the severity of depression of the crew members based on their recordings.

II. Databases

A. Reference Depressed Speech Database

Speech data were collected from depressed patients and healthy subjects in normal atmospheric and normal everyday life conditions. The automatic prediction method was trained with the Reference Depressed Speech Database.

To measure the severity of depression, the Beck depression inventory II (BDI-II) was used [8], and each sample were labeled with this value. The BDI-II scale differentiates 63 degrees of severity where 0 is the totally healthy and 63 is the most depressed. The following classification is usually given for the range of values of the BDI score: 0-13: minimal depression (healthy); 14-19: mild depression; 20-28: moderate depression; 29-63: severe depression. The Database contains speech samples from 288 subjects (186 females; 102 males), with mean value of BDI score 14,6 (-+12,4; min: 0; max 50).

B. Coala Recordings

Speech samples of five crew members from the Concordia station were collected from 2013 November to 2014 September. This speech database is referenced as Coala Recordings in this paper. All the recordings were checked and those were excluded where the background noise was too high or more than one subject spoked. It was necessary because the speech samples from the Reference Depressed Speech Database were recorded in quiet environment. The speech samples were from four men and from one woman. One subject stopped to participate in our experiment based on his own request. There are overall 42 speech sample from the 5 crew members.

III. Methods for the Constuction of the Depression Severity Prediction System

A. Automatic depression severity prediction system

The dataflow diagram of the automatic depression severity prediction system is presented in Fig. 1. During the development of this system, first the SVR model was trained with the help of the Reference Depressed Speech Database, then the prediction of the severity of the depression of the examined crew members (Coala Recordings) were calculated.

The speech samples were segmented and labelled into phoneme-like units. Each sound file was characterized by a feature vector containing the selected acoustic-phonetic parameters, the selection method is described later in the Feature Vector Selection section. The model was trained with the feature vectors derived from the training dataset. The input of the automatic prediction was the output of the trained model and the feature vectors derived from the predicting dataset. The output of the automatic prediction system was the predicted BDI score. Different models were trained for genders separately. The precision of the training model was evaluated with leave-one-out cross-validation method, mean absolute error (MAE) and root mean square error (RMSE) was calculated and used as the describers of the precision.

B. Speech Segmenter

Every speech sample was segmented and labeled on phone level using SAMPA phonetic alphabet with the help of an automatic language independent phoneme segmenter [9]. Segmentation is necessary to measure accurate segmental acoustic-phonetic parameters.

C. Preprocessing

The measured acoustic-phonetic parameters were selected based on our earlier experiences and in accordance with the literature: fundamental frequency, intensity, mel-band energy values, jitter, shimmer, formants frequencies (first and second), bandwidth of formants (first and second). The parameters were measured with 10 ms step time. The following parameters were measured also in middle of the same vowel “E” (SAMPA): formant frequencies, the jitter, the shimmer and the mel-band energy values [10]. All the parameters were calculated with Praat software [11]. The reason of this two type of measurement was that these parameters are highly sensitive to the location of the measurement, and thus the obtained values may reflect more accurately the influence of the depression to the speech, if they were measured on the middle of the same sound. We selected vowel “E” because it was one of the most frequent vowel in the speech databases.

Derived descriptive features were obtained from the values of the measured acoustic-phonetic parameters with using the following three statistical functions: mean, standard deviation and percentile range. Thus for each speech sample, 178 descriptive features were obtained.

D. Regression Method

Support Vector Regression (SVR) method was used for automatic predicting, which is one type of Support Vector Machine (SVM) designed for regression tasks [12]. The SVR was implemented in LIBSVM [13]. This type of regression was selected because we obtained good results with SVM in our earlier work [7]. Separate models were trained for both sexes, because the values of the measured acoustic-phonetic parameters differ between sexes, and the depression can influence the speech differently between sexes either.

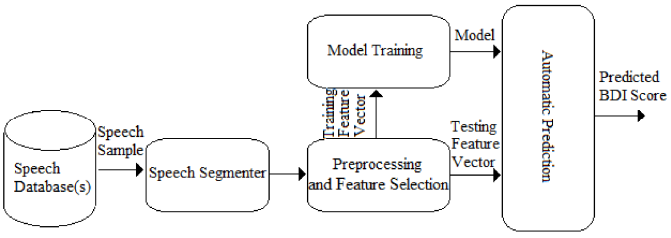

Fig. 1. Dataflow diagram of the depression severity prediction system

E. Feature Vector Selection - SVR model for the prediction of the severity of depression

The precision of the SVR is highly dependent on the good selection of the feature vector, because the unnecessary and noisy features can impair the operation. This is particularly true in the case of a small number of training sample set, such as in our case.

There are several feature selection algorithms to produce a better performing feature vector, we used Sequential Forward Selection (SFS) algorithm.

The essence of SFS is, that it selects a (sub)optimal feature vector from a large feature set. At the beginning of the algorithm, the (sub)optimal feature vector is an empty feature vector. Than at the *i*-th step, the algorithm expands the (sub)optimal *i-1* long feature vector with that unused feature, with which the new *i* long feature vector performs the best. At the end of the algorithm it selects a *k* long feature vector which performed the best. The SVR was used during this algorithm to establish the best performing *i* long feature vector in each step, with leave-one-out cross-validation, and the RMSE indicator was used for the precision.

The parameters in the selected feature vector were the followings: variance of intensity, percentile range of fundamental frequency, mean and variance of first formant frequencies of Vowel "E", mean and variance of the bandwidth of the first formant frequencies of vowel "E", mean and variance of second formant frequencies of vowel "E", mean of jitter of vowel "E", mean of shimmer of vowel "E", mel-band energies of vowel "E" (from 1000 HZ to 3000 Hz).

At the end SVR model was constructed for the prediction of the severity of the depression measuring the optimally selected *k* long feature vector, and using Reference Depressed Speech Database for the training.

IV. Results

A. SVR model validation

The precision of our model was evaluated with leave-one-out cross-validation. The results can be seen in Table I. where some more other results are given too, to compare our model with the results of other researchers, and to validate it. The precision of our model is noted with bold.

The other results are from AVEC-2013 challenge [14] [15], where the task was similar to our work, and the examined database had the similar distribution of BDI scores (mean 14,9; +-11,7) to the Reference Depressed Speech Database.

TABLE I. The precison of Our Model

	RMSE	**MAE**
AVEC-2013 baseline	14,1	10,4
The winner of the AVEC-2013	8,7	7,1
The runner-up of the AVEC-2013	10,1	7,8
Our model	**9,6 (female: 9,7 male: 9,5)**	**7,6 (female: 7,6 male: 7,5)**

It is important to note, that our system was designed for quasi language-independent operation [16], trained and tested for 3 different languages, while the task in the AVEC challenge was monolingual, trained and tested only for German language, and thus the implemented methods were highly language dependent.

After the comparison, it can be stated that the accuracy of our model, which was designed for quasi language-independent operation, is comparable with language dependent methods, thus our model is acceptable and valid, and it can be used for the monitoring system.

The quasi language-independent solution was necessary because in international research station crew members mother tongue can be highly varied.

B. Predicting the severity of depression of the crew members

Using our depression severity prediction system, BDI score has been assigned to each speech record from the Coala Recordings with our regression method, thus we obtained predicted BDI scores for each speech recordings of each crew member. Each crew member is referenced with the following notation: Subject_[f]/[m]_[id], where [f]/[m] indicates the sex of the subject female/male.

First, we examined the predicted BDI scores for each crew member when they arrived to the Concordia research station. It has been established that each crew member's initially predicted BDI score was below 14 (which shows healthy state). The maximum score right after the arrival was 12,8, the minimum was 0, and their mean value was 6,9. These results satisfied our expectations, because at the beginning, when the crew members arrived to the Concordia research station, no one suffered from depression based on the psychological test before departure.

Furthermore, the mean and the maximum value of the predicted BDI scores was calculated and examined for each crew member and these values were compared to their initial scores. The results of this examination can be seen in Table II. From the values of the starting, mean and maximum BDI scores it can be seen, that 2 people from 5 may suffered from depression occasionally during the experiment (subject_m_1 and subject_m_2), because relatively high differences were experienced between their predicted initial BDI score and later predicted scores.

TABLE II. Analysing the Predicted BDI Scores

	Starting BDI Score	**Mean BDI Score**	**Maximum BDI Score**
Subject_m_1	12,8	22,1	27,1
Subject_m_2	0	14,6	20,4
Subject_m_3	2,6	0,3	2,7
Subject_m_4	11,2	11,3	21,2
Subject_f_5	8	8,4	13,5
Avarage	6,9	11,3	17

For further examination, each predicted BDI score of each crew member was shown in Fig 2. as a function of time. Between the recordings, the predicted BDI scores were derived with interpolation, and each function was normalized to the initially predicted BDI score by subtracting it. We did this, because at the beginning everyone was known to be healthy and thus in this way it was possible to eliminate the personal characteristics, and thus the function depicts the change of the depressed state of each subject better.

From the Fig 2. it can be seen that our preliminary analysis was right, since based on this examination the same two subjects seemed to be depressed sometimes during the experiment. One subject's (Subject_m_3) normalized predicted BDI scores were below 1 all the time, so it can be stated this subject was not suffered from depression. Two subjects' (Subject_m_4 and Subject_f_5) normalized BDI scores were fluctuated during the first-two months (around 5-10) than their normalized BDI scores were decreased and were stabilized around 0. Because from 0 to 14 the BDI score doesn't indicate depression (and their not normalized BDI scores were above 14 only for short periods), these subjects weren't suffered from depression either. This phenomenon (the initial fluctuating) can be also observed in other two subjects. One possible explanation of the fluctuation of the initial BDI scores can be that the initial difficulties influenced the subjects cognitive state and thus their speech. However, the method has some own uncertainty, so this phenomenon may be a random coincidence. The predicted normalized scores of Subject_m_1 were above 14 from 2014.05.24 to 2014.06.14 which indicates mild depression. This period corresponds to the onset of winter in Antarctica. The most interesting results were from Subject_m_2, his starting BDI score was zero (without normalization either) after that within three weeks his predicted BDI score increased above 14 and it fluctuated around mild and moderate depression in the rest of the time. Unfortunately, Subject_m_2 is stopped participating in the experiment on his own request. Thus we couldn't monitor his cognitive state further. Probably he suffered from some cognitive disorder, like depression.

V. Conclusions

In this study an automatic status monitoring system was presented which is able to predict the severity of depression of examined subjects based on their speech. The system was used and examined on five crew members from Concordia research station located at Antarctica.

Support Vector Regression (SVR) method was used for the automatic prediction. To train the support vector regression the Reference Depressed Speech Database was used, which contains speech samples from depressed patients and healthy subjects recorded in normal atmospheric conditions. Separate models were trained for both sexes. 178 acoustic-phonetic features were calculated from each speech sample. The final feature vector, which was used for the training, was derived from this feature set with SFS algorithm separately for both gender with leave-one-out cross-validation.

The precision of our prediction method was examined with leave-one-out cross-validation, to measure the precision RMSE and MAE indicators were used. It was found, that the precision of our predicting method is acceptable.

BDI prediction was performed for each speech sample of each crew member, and thus we got the severity of depression for each crew member as function of time.

Our prediction system could follow the cognitive state of the crew members. The initial predicted depression value for each

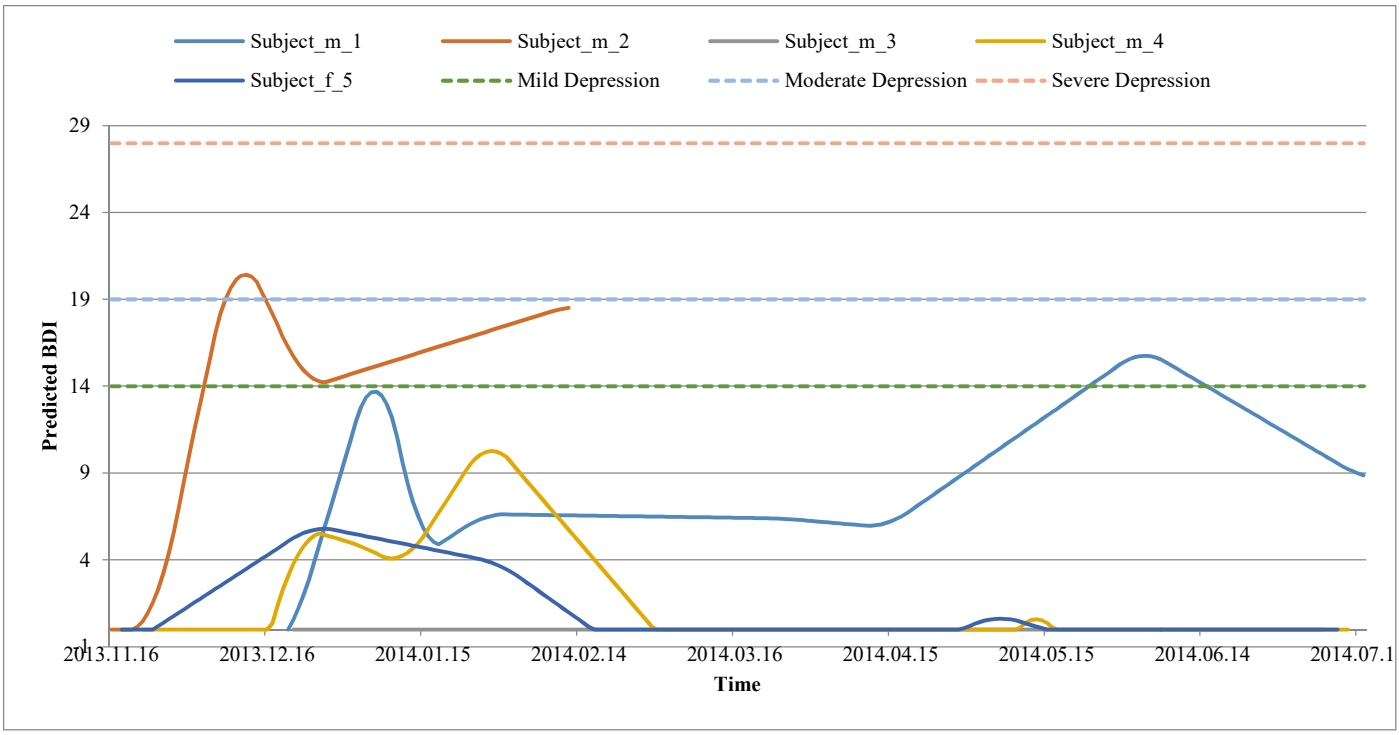

Fig. 2. The normalized predicted BDI functions for each crew member

crew member was low at the beginning of their stay at the research station. Later, in case of one subject from the five the predicted BDI score increased rapidly after some weeks and stopped to participate in our experiment before winter period, three subjects were probably not suffered from depression during the experiment (but their highest predicted BDI score was in the first two months), and only one subject had higher predicted score around at winter period.

In the future, we would like to expand our analysis with speech samples from other crew members, and increase the precision of our predicting method, with expanding our Reference Depressed Speech Database, and finding more acoustic-phonetic features which can indicate depressed state.

ACKNOWLEDGMENT

We would like to thank Björn Schuller and his co-workers Jarek Krajewski and Sonja-Dana Roelena for sharing with us the database of AVEC 2013 for research purposes.

The research was supported by European Space Agency COALA project: Psychological Status Monitoring by Computerized Analysis of Language phenomena (COALA) (AO-11-Concordia).

REFERENCES

[1] Schumann, I., Schneider, A., Kantert, C., Lo¨we, B., Linde, K., 2012. Physicians' attitudes, diagnostic process and barriers regarding depression diagnosis in primary care: a systematic review of qualitative studies. Fam. Pract. 29, 255–263.

[2] Marcus, M., Yasamy, M. T., van Ommeren, M., Chisholm, D., & Saxena, S. (2012). Depression: A global public health concern. WHO Department of Mental Health and Substance Abuse, 1, 6-8.

[3] Alghowinem, S., Goecke, R., Wagner, M., Epps, J., Breakspear, M., & Parker, G. (2013, May). Detecting depression: a comparison between spontaneous and read speech. In 2013 IEEE International Conference on Acoustics, Speech and Signal Processing (pp. 7547-7551). IEEE.

[4] Brendel, R.W., Wei, M., Lagomasino, I.T., Perlis, R.H., Stern, T.A., 2010. Care of the suicidal patient. Massachusetts General Hospital Handbook of General Hospital Psychiatry, 6th ed. W.B. Saunders, Saint Louis, pp. 541–554.

[5] Kraepelin, E., (1921). Manic depressive insanity and paranoia. J. Nerv. Ment. Dis. 53, 350.

[6] Cummins, N., Scherer, S., Krajewski, J., Schnieder, S., Epps, J., & Quatieri, T. F. (2015). A review of depression and suicide risk assessment using speech analysis. Speech Communication, 71, 10-49.

[7] Kiss, G., Tulics, M.G., Sztahó, D., Esposito, A. and Vicsi, K., 2016. Language independent detection possibilities of depression by speech. In Recent Advances in Nonlinear Speech Processing (pp. 103-114). Springer International Publishing.

[8] Beck, A. T., Steer, R. A., Ball, R., & Ranieri, W. F. (1996). Comparison of Beck Depression Inventories-IA and-II in psychiatric outpatients. Journal of personality assessment, 67(3), 588-597.

[9] Kiss, G., Sztahó, D., & Vicsi, K. (2013, December). Language independent automatic speech segmentation into phoneme-like units on the base of acoustic distinctive features. In Cognitive Infocommunications (CogInfoCom), 2013 IEEE 4th International Conference on (pp. 579-582). IEEE.

[10] Kiss, G. and Vicsi, K., 2014, October. Physiological and cognitive status monitoring on the base of acoustic-phonetic speech parameters. In International Conference on Statistical Language and Speech Processing (pp. 120-131). Springer International Publishing.

[11] Boersma, P., (2002). Praat, a system for doing phonetics by computer. Glot international, 5(9/10), pp.341-345.

[12] Smola, A., & Vapnik, V. (1997). Support vector regression machines. Advances in neural information processing systems, 9, 155-161.

[13] Chang, C. C., & Lin, C. J. (2011). LIBSVM: a library for support vector machines. ACM Transactions on Intelligent Systems and Technology (TIST), 2(3), 27.

[14] Valstar, M., Schuller, B., Smith, K., Eyben, F., Jiang, B., Bilakhia, S., Schnieder, S., Cowie, R. and Pantic, M. (2013, October). AVEC 2013: the continuous audio/visual emotion and depression recognition challenge. In Proceedings of the 3rd ACM international workshop on Audio/visual emotion challenge (pp. 3-10). ACM.

[15] Williamson, J. R., Quatieri, T. F., Helfer, B. S., Horwitz, R., Yu, B., & Mehta, D. D. (2013, October). Vocal biomarkers of depression based on motor incoordination. In Proceedings of the 3rd ACM international workshop on Audio/visual emotion challenge (pp. 41-48). ACM.

[16] Kiss, G., Vicsi, K. Mono- and multi-lingual depression prediction based on speech processing. Speech Communication, unpublished (accapted with major revision)

Analyzing the Quantum Efficiency in Satellite-based Quantum Key Distribution Network

Andras Kiss
Institute of Informatics and Economics
University of West Hungary
Sopron, Hungary
kissa@gain.nyme.hu

Laszlo Bacsardi
Institute of Informatics and Economics
University of West Hungary
Sopron, Hungary
bacsardi@inf.nyme.hu

***Abstract*—In the last years, there were several proofs about the feasibility of the satellite-based quantum communications [1]. Nowadays, the satellite-based quantum communication is getting closer to be applied in our everyday life [2]. A typical case of space-based quantum data transmission is basically composed of a satellite, a ground station (or optionally another satellite). The receiver object needs to have a detector to detect and measure the signal [3]. All of the analyzed quantum key distribution (QKD) protocols, including BB82, B92, S09, Gisin take into account the efficiency of the detector to determine the Quantum Bit Error Rate (QBER) of the protocol. That means one of the most important performance property is the quantum efficiency in a quantum-based satellite network. In this paper, our primary goal is to analyze and evaluate the influences of the quantum efficiency of the detector.**

Previously, we developed the Quantum Satellite Communication Simulator software directly to execute simulation scenarios in satellite-based quantum communication applications [4]. It provides opportunity to execute evaluations in the following scenarios: calculation by constant parameters, sensitivity analysis, time driven communication, optimization and channel analysis. In the latest development phase we focused on the opportunities of the detailed examination of the detector properties and as a result we performed several simulations to analyze the efficiency of the detector. In summary, depending on the QKD protocol the efficiency of the detector is as important factor as the link transmittance or the mean photon number of the signal is.

Keywords—quantum communication; satellites communications; quantum efficiency

I. INTRODUCTION

The quantum communication is based on the laws of quantum mechanics, and utilizes different quantum-based algorithms and protocols [1]. Comparing with classical algorithms, which are used in classical computation, the advantages of quantum algorithms are the quickness, the factorization and encryption [2]. The base unit of the quantum computing is the quantum bit (qubit), which can be represented by different polarization states of a photon. The state of a classical bit can be represented by only one of the 0 and 1 values, but the qubit can be an in arbitrary superposition of 0 and 1.

The first quantum cryptographic protocol was published by Bennet and Brassard in 1984 [3] followed by several others like B94 [4] or S09 [5]. The BB84 key distribution protocol was the first which worked on quantum physic principle. It creates random bit sequences which is known only by the two communications parties and it also cover the security of the communication. This property of the BB84 protocol is based on the so-called No Cloning Theorem (NCT). The result of the exchange process is a classical string of bits, which can be further applied in nowadays used symmetrical coding protocols. This means that QKD could enhance the security of our existing systems including satellite networks [6]. This is why Chine has launched the world's first quantum communication satellites in 2016.

In a satellite-based quantum key distribution network, we use quantum bit to transfer data from the sender to the receiver. In the communication channel, there is a point where we have to do a measurement to determine the classical value of a qubit. The measurement results 0 or 1 value. Compared the quantum communication channel to the classic communication channel, in case of an eavesdropping attack, the measurement performed by an attacker changes the quantum state and by this, the opportunity is given to detect the attacker. This is one of the biggest advantage of the quantum communication channel.

For satellite-based quantum communication, we distinguished three types of communication links: satellite–satellite, satellite–ground, ground–satellite.

A complex, satellite-based network could enable a global quantum key exchange service. Due to the nature of quantum-based protocols, the noise of the channels need to be estimated since the errors introduced by an eavesdropper could be masked by the natural noise of the channel. Currently, several research groups are investigating the potential benefits of the quantum-based satellite communication.

Between the communicating parties, including parties like a ground station and a satellite or two satellites, the data is encoded into the polarized states of the photon. It is a critical point to transfer the photon from the sender to the receiver with

as low loss as possible. That is why it is needed to use laser beam (typically 860 nm or 1060 nm) for the data transmission with relatively low scattering. On the receiver side, the photon arrives to the mirror and it reflects into the detector. Here appears the importance of the quantum efficiency of the detector.

In our simulation model, there are three types of communication channels: ground-satellite, satellite-satellite and satellite-ground. These types are enough to model, simulate and determine the performance characteristics even a complex network [4].

We have to take into account several physical parameters and formulas to calculate as accurate results as possible, including the DQE (Detector Quantum Efficiency) and the QBER (Quantum Bit Error Rate). This is the reason we developed the 2.0 version of our former developed Quantum Satellite Communication Simulator software [8-9].

There are two groups of the currently used quantum key distribution (QKD) solutions. The first generation protocols use singe-photon sources, while coherent laser is used and the wave properties of light is exploited in the second generation protocols. This first approach is named as Discrete Variable QKD (DV-QKD), the second one is named as Continuous Variable QKD (CV-QKD). In this paper, we have focuses on DV-QKD solutions.

Fig. 1. Input photon stream and response

II. DETERMINATION OF QUANTUM EFFICIENCY

A. Detector Model

As Fig. 1. shows, the input photon stream X arrives to the detector and Y is the response of the detector.

X is a random variable with a Poisson distribution:

$$P(X=k)=\frac{q^k}{k!}e^{-q}, \quad (1)$$

where $q = \lambda A \tau$.

The response is an event stream Y, by the following formula:

$$Y = h(X) + Z. \quad (2)$$

The aim is to determine the intensity λ of the input photon stream.

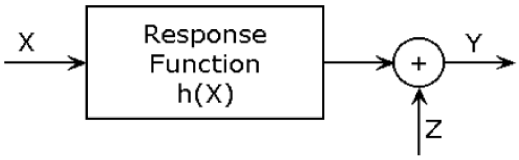

Fig. 2. Detector response function

In Fig. 2., we can see how the $h(X)$ detector response function works, where Z is an independent random variable with a known probability distribution.

Estimator

Estimator is a rule to calculate the value of a quantity of interest from one or more observations of a random variable. Estimate is also a function of a random variable, and is therefore itself a random variable.

Let λ be an estimate of λ. We would like to have $E[\lambda] = \lambda$. This is an unbiased estimator of λ.

We would also like to have var[λ] be as small as possible. The quality of the detector is measured by comparing the quality of the estimate that could be made from X to the quality of the estimate that can be made from Y.

B. Detective Quantum Efficiency

The Detective Quantum Efficiency can be defined in a number of equivalent forms. The basic definition is the following: The Detective Quantum Efficiency for a detector is the ratio of the variance of an estimate of λ based on the detector input X to the variance of an estimate of λ based on the detector output Y. The Detective Quantum Efficiency is always in the range 0 to 1 [10].

C. Determination of the Detective Quantum Efficiency

One of the most important parts of analyzing the quantum efficiency is to determinate the value of DQE. It requires to take into account all necessary physical parameters and formulas. The Table 1. contains the physical parameters what we used during the simulations. All of the factors in Table 1. are implemented as input values in the Quantum Satellite Communication Simulator software.

TABLE I. PARAMETERS FOR DETECTIVE QUANTUM EFFICIENCY

Symbol	Meaning	Unit
T	Expose	minutes
ϕ	Flux	$\gamma/cm^2/s$ (photons/cm^2/sec)
ε	Detector conversion efficiency	counts/photon
A	Detector area	cm^2
σ^2_R	Readout noise variance	counts
σ^2_D	Dark noise variance of photon detector	counts/second

TABLE II - FORMULAS FOR DETECTIVE QUANTUM EFFICIENCY

Formula	Result
$q = \phi AT$	-
$N_{out} = (q\varepsilon + \sigma^2_D T + \sigma^2_R)^{1/2}$	Output noise
$S_{out} = q\varepsilon$	Output signal
$N_{in} = q^{1/2}$	Input noise
$S_{in} = q$	Input signal
$(S/N)_{in} = S_{in} / N_{in}$	Input signal to noise ratio
$(S/N)_{out} = S_{out} / N_{out}$	Output signal to noise ratio
$DQE = [(S/N)_{out} / (S/N)_{in}]^2$	Quantum efficiency of detector

In this project, we developed a functionality into the simulation software to calculate the DQE value. The Table 2. contains the set of formulas, which are necessary to determine the DQE.

III. QUANTUM SATELLITE COMMUNICATION SIMULATOR

The first version of the Quantum Satellite Communication Simulator was developed in 2011. The only functionality of that version was to determine the QBER value of the BB84 protocol. Later several improvements were implemented, including more quantum protocols and the scenario-based architecture of the software. Before the planning of the latest version, we decided the trend of the further versions. It is the fine tune of the calculations, which belongs to the sender, channel, receiver and to the atmosphere. In Fig. 3., the cover of the latest version of the Quantum Satellite Communication Simulator is illustrated.

In this paper, we present results about the analyzation of quantum efficiency of the detector. We have extended the simulation software by the parameters and calculations, which are described in the *Determination of the Detective Quantum Efficiency* section. This type of calculation is also a fine tuned calculation of the QBER value. In Fig. 4., the settings of the calculation of DQE are illustrated.

Fig. 3. The cover of Quantum Satellite Communication Simulator 2.0

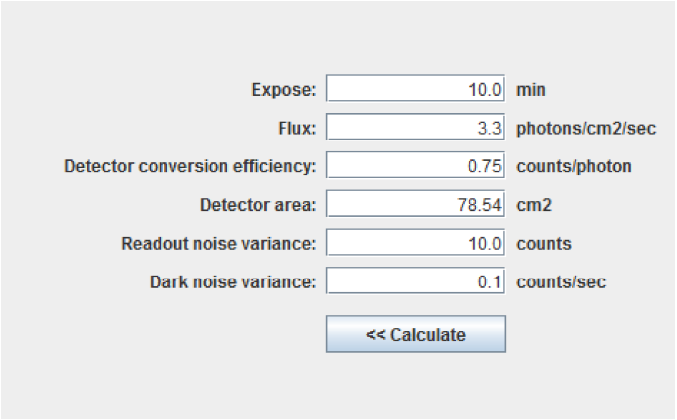

Fig. 4. Settings of calculation of quantum efficiency of the detector

In this version of the application, the scenarios are still the same as in the previous version. The main improvement was the separated settings before starting the scenarios. It resulted the opportunity to simplify the GUI in some cases, e.g., the interface of the Calculating by Constant Parameters scenario as it is illustrated in Fig. 5. As it shows, it only informs the user about the input parameters and the results.

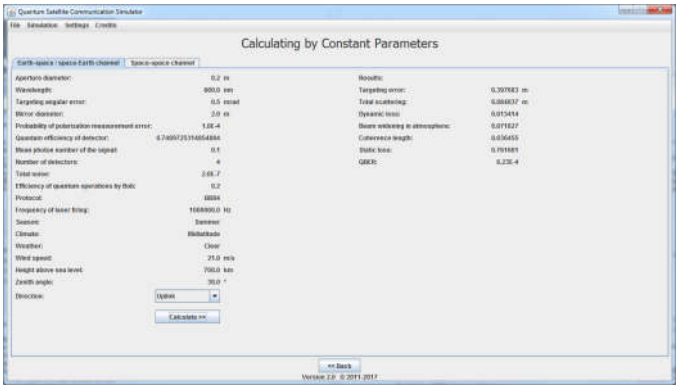

Fig. 5. Calculating by Constant Parameters scenario

IV. SIMULATION RESULTS

We executed examinations for the DQE in function of all of the necessary input parameters. In every simulation, if no other parameter is specified, the default values were the following:

- Expose: 10 minutes
- Flux: 3.3 $\gamma/cm^2/s$
- Detector conversion efficiency: 0.75 counts/photon
- Detector area: 78.54 cm^2
- Readout noise variance: 10 counts
- Dark noise variance: 0.1 count/second

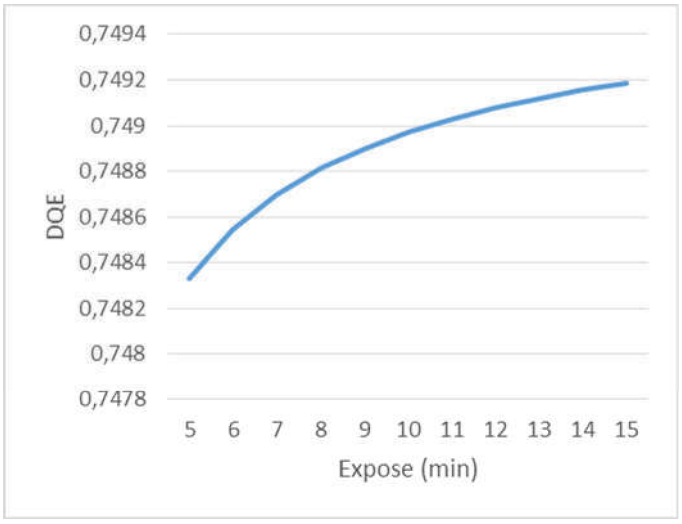

Fig. 6. Values of DQE in function of expose

The values of Detective Quantum Efficiency in function of expose are illustrated in Fig. 6. As the chart shows, the higher expose time results higher DQE value.

In Fig. 7., the values of DQE in function of flux are shown. The results are very similar to the DQE values in function of expose. The difference between the results of the charts is less than 1% in the examined range.

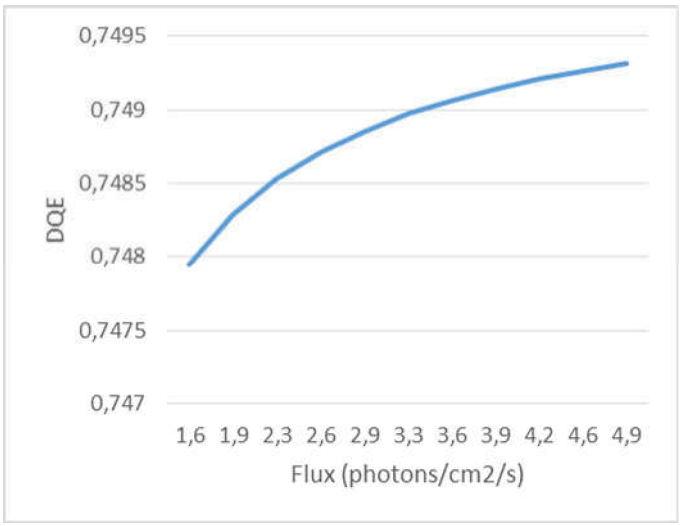

Fig. 7. Values of DQE in function of flux

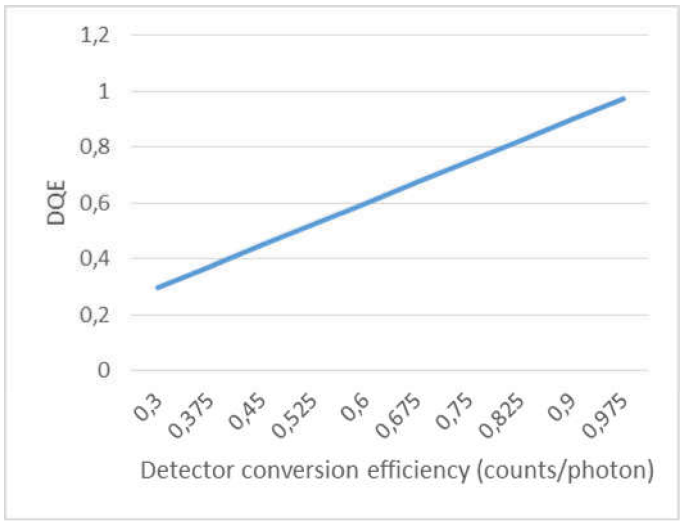

Fig. 8. Values of DQE in function of detector conversion efficiency

In Fig. 8., the values of DQE in function of detector conversion efficiency are illustrated. As the chart shows, the function is very near to the linear relationship and it is an increasing function.

In Fig. 9., the values of DQE in function of detector area are shown. It is also a logarithmic function and its DQE values are totally equals with the DQE values in function of flux.

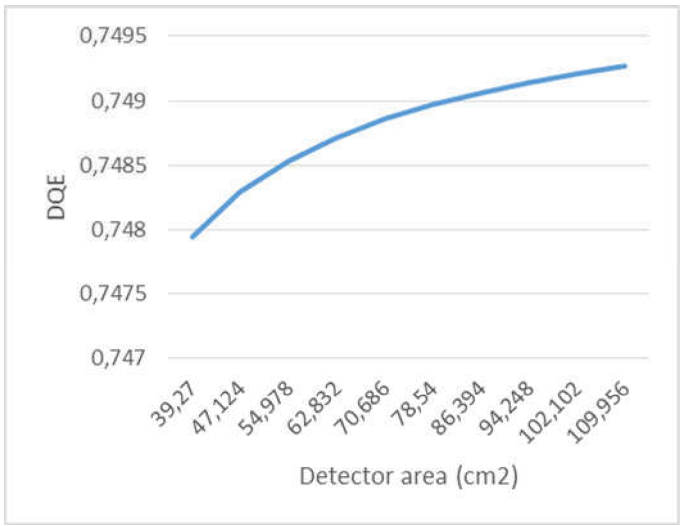

Fig. 9. Values of DQE in function of detector area

Other aspect is the analyzes of DQE in function of readout noise variance as it is shown in Fig 10. It is a negative factor, which means the higher readout noise variance value there is, the lower detective quantum efficiency there is.

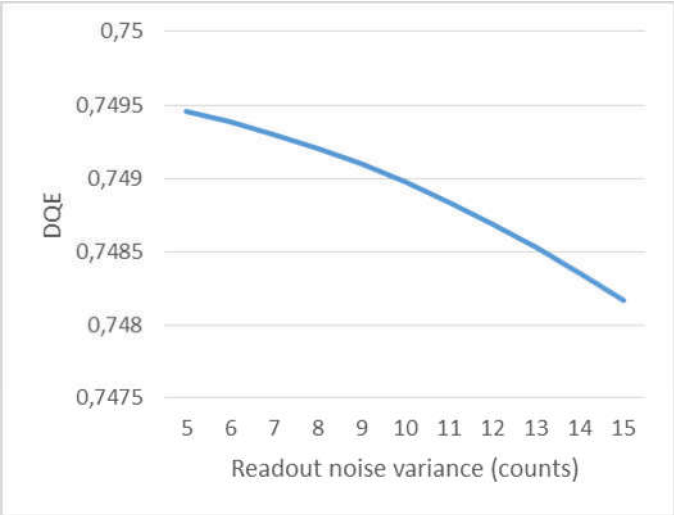

Fig. 10. Values of DQE in function of readout noise variance

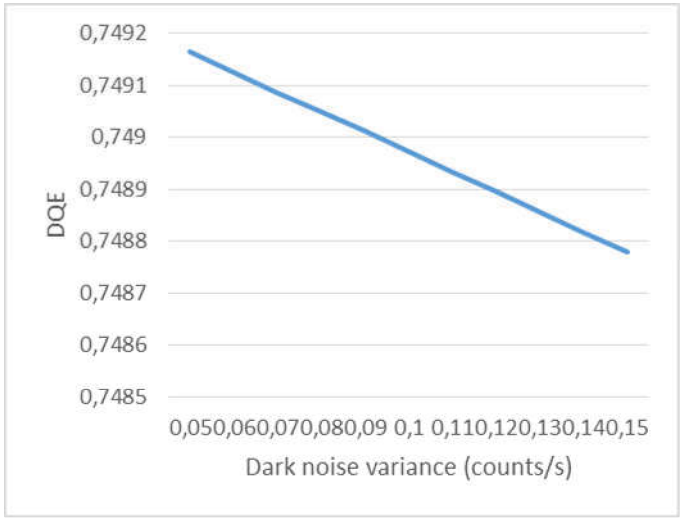

Fig. 11. Values of DQE in function of readout noise variance

Fig. 11. illustrates the values of DQE in function of dark noise variance. It is a negative function and it has linear relationship between the dark noise variance and the detective quantum efficiency.

V. Conclusion

Our paper describes some important aspects of the Detective Quantum Efficiency which has been taken into account for long distance free-space quantum key distribution including ground-satellite and satellite-satellite communications.

Acknowledgment

The research was supported by the Hungarian Scientific Research Fund – OTKA PD-112529.

References

[1] L. Hanzo, H. Haas, S. Imre, D. O'Brien, M. Rupp and L. Gyongyosi: Wireless Myths, Realities, and Futures: From 3G/4G to Optical and Quantum Wireless, Proceedings of the IEEE, Volume: 100 , Issue: Special Centennial Issue, pp. 1853-1888.

[2] L. Bacsardi. „On the Way to Quantum-Based Satellite Communication”, IEEE Comm. Mag.51:(08) pp. 50-55. (2013)

[3] C. H. Bennett and G. Brassard, “Quantum cryptography: Public key distribution and coin tossing,” in Proceedings of the IEEE International Conference on Computers, Systems and Signal Processing. Bangalore, India: IEEE, 1984

[4] C. H. Bennett,, “Quantum Cryptography Using Any Two Nonorthogonal States”, Phys. Rev. Lett. 68, 3121 (1992).

[5] E. H. Serna, “Quantum Key Distribution Protocol with Private-Public Key”, [online] arXiv:0908.2146v3 (2009)

[6] P. Villoresi et al., ”Experimental verification of the feasibility of a quantum channel between space and earth”, New Journal of Physics, Vol. 10, No. 3, p. 033038, 2008.

[7] Long March 2D launches world’s first quantum communications satellite, NASA SpaceFlight, https://www.nasaspaceflight.com/2016/08/long-march-2d-quantum-communications-satellite/

[8] A. Kiss and L. Bacsardi, “Analyzing a Satellite-based Quantum Key Distribution Network”, Global Space Application Conference, Paris, France, 2014

[9] A. Kiss, L. Bacsardi, “Quantum-based solutions in Low Earth Orbit Satellite Networks “, H-SPACE2016, Feb 25-26, 2016, Budapest, Hungary

[10] Rochester Institute of Technology, Noise and Random Processes, Detective Quantum Efficiency (https://www.cis.rit.edu/class/simg713/Lectures/Lecture713-09.pdf, Last accessed on Dec 20, 2016)

Analyzing energy efficiency of sensor networks deployed on the surface of a Solar System Body

Roland Béres, Péter Polgárdi, Árpád Huszák
Department of Networked Systems and Services
Budapest University of Technology and Economics
Budapest, Hungary
broland975@gmail.com, polpeti@freemail.hu,
huszak@hit.bme.hu

László Bacsárdi
Institute of Informatics and Economics
University of Sopron
Sopron, Hungary
bacsardi.laszlo@uni-sopron.hu

Following the exploration of Moon, the next step could be the exploration of Mars, since many man-made devices already sent measurement results from our closest planet. There is an interesting tendency that the private funding space researches are becoming more and more substantial next to state sponsored space programs. In the process of mapping a distant planet, cost efficiency is high priority since the available resources are limited. A cost-efficient method is using sensor networks to explore, which can be done on a lower budget compared to "single-probe" missions [1]. Human intervention is often not possible due to the great distances. Therefore, the usage of sensor networks can partly be a solution to the arising problems, since losing connection with the home base on Earth does not hinder the measurements [2]. Another advantage is that the failure of a device does not put the mission at jeopardy [3]. In our work, we assumed such a sensor network, which we examined from different points of view. Real Martian topographical data was used to create a Digital Elevation Model on which we studied different sensor movement algorithms. We analyzed the communication between sensors from the energy-efficiency aspect and we established an energy model to estimate the resource consumption of the sensors. A simulation program has been developed to examine our sensor network. In this simulation, we compared the efficiency of the algorithms and we investigated how the energy level of the sensors affect the time required to cover the measurement area.

Keywords—space exploration, sensors, energy efficiency

I. INTRODUCTION

There were many successful applications of wireless sensor networks on earth, for example; in healthcare, urban infrastructure development and agriculture [4]. They have important role in situations where human intervention is dangerous or not possible; like war zones or disaster areas.

In the next section, we provide an overview of wireless sensor networks. In Section 3, we describe the network examined in this paper. Section 4 is about reviewing the simulation program we created. The results are presented in the Section 5 and we conclude our paper in Section 6.

II. OVERVIEW OF WIRELESS SENSOR NETWORKS

A. Overview

From a physical point of view, sensors make up a sensor network, however from a network perspective these units are called nodes. A typical sensor network has three components; source, data sinks and exit points. There are many configurations but in most cases the source is the sensor which takes the measurements and relays the results. The task of the data sinks is to collect and process the data gathered by the sources. Because of this they require more processing capability and memory, however they are part of the network so their communication is like the sources. The exit points can communicate with the satellite, so their task is to send the data processed by the data sinks to the satellite [5]. It is considered best practice to divide larger networks into smaller parts called clusters. This division can be based on the small physical distance between a set of sensors or their place in the logical topology in the network.

B. Grouping of wireless sensor networks

1) Based on communication: Single-Hop and Multi-hop

As their name suggests, the difference between the two groups is in the flow of information. In single-hop networks, the source sends the information directly to the data-sink. In multi-hop networks the information goes through multiple participants before it reaches the data-sink [6].

2) Based on topology: Single-hop star, Multi-hop mesh, Two-tier hierarchical cluster

In wireless networks the simplest topology is the Single-hop star, when all nodes are directly connected to the exit point and there is no connection between the nodes themselves. The simplicity of this topology makes designing these networks easier. Great disadvantage is the lack of robustness and the limited expandability. To cover larger areas, multi-hop communication is necessary, which is used by the multi-hop mesh and the two-tier hierarchical cluster topologies. The former can be considered a single cluster, while the latter consists multiple clusters. Each cluster has a cluster head, which receives the data from the nodes [7].

3) Based on the event which triggers data relay: time-triggered, event-triggered, request-triggered

In the time-triggered case, the nodes send the data in predetermined time intervals, while in the event-triggered case the occurrence of some sort of event triggers the data relay. In a request-triggered network the nodes send data only when the data-sink asks for it.

III. THE EXAMINED SENSOR NETWORK

A. Structure of the network

In our sensor network, we differentiate two different kind of devices. One of them is the node, which makes measurements and processes the information extracted from the survey. This device is capable of movement and it can also forward the processed data. Every node has a probability of measurement value, which determines if the node measures or moves onward in the given simulation step. In our simulation, we set this step to a 6-minute time interval. The nodes have limited energy. The other device is the base station, there is only one of this in our network. In our paper, we did not examine the energy-relations of this unit, we assumed its energy to be undepletable. The base station is also capable of movement; however, it does not take any measurements. The task of this device is to forward the data gathered by the nodes to the satellite in orbit around the planet. A sample structure is illustrated in Fig. 1.

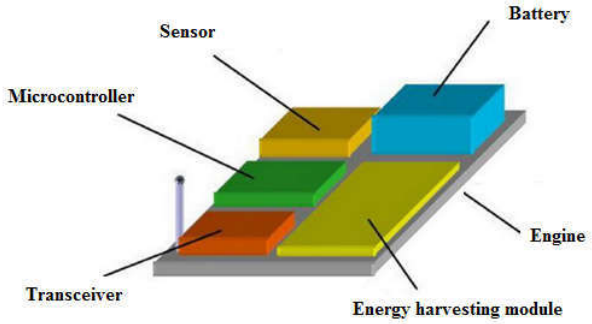

Fig. 1. Structure of a node

B. Energy model

Energy provisioning is critical in space exploration, due to the long-term measurements the devices need to take. When modeling a sensor network we must pay great attention to the examination of the energy-relations, because if a node runs out of energy it cannot take further measurements. To achieve this, in the design we must take into consideration the proper energy intake and storage. In our simulation, we used 2000 mAh battery, which means 43200 Joule energy [8]. Energy storages are often used due to the matters discussed above, supplemented by some sort of energy harvesting solution, which means using the environment to produce energy. In most cases replacing the batteries is not possible, so it is necessary to find an alternative source of energy. The most commonly used renewable energy sources are solar, wind, water, mechanical and thermal, however under the Martian circumstances their uses are limited. We only considered the energy gathered by the solar cells in our simulation [9]. The energy collected from outer sources means new challenges in the design of low consumption wireless sensors, due to the small size of these sensors.

We beared this factors in mind, while creating different energy models for the movement, measurement, data processing and communication.

In our simulation, we used the data of a simple engine [10] to move the nodes. Two state has been created; a standing and a moving state. The energy required for the moving was calculated from the multiplication of the rated voltage with the current without load. In our paper, we dismissed any outer factors, like drag.

According to their measurement probability, the nodes take measurements in intervals. In this case the do not move. In our simulation, we used the data of a temperature sensor [11]. We created two different states; one when the temperature sensor is turned off, the other is when it is turned on. To change states, some energy is required, which is calculated by:

$$e_{sensor-change} = \frac{1}{2} * T_{init-end} * (P_{init} + P_{end})$$

formula. In this formula $T_{init-end}$ represents the time needed for the state change, while P_{init} and P_{end} are the start and end state's power.

Following the measurement, the next step is the data processing, which is done with a microcontroller [12]. Here we created a sleeping state to reduce our energy expenses.

After processing the measured data, the nodes forward them to the base station. We used the data of a transmitter-receiver unit to calculate this [13].

IV. THE SIMULATION PROGRAM

A. Utilization of maps

There are several satellites in Mars orbit, which can take high resolution images. One of these units is the Mars Reconnaissance Orbiter with a device called HiRISE (High Resolution Imaging Science Experiment) [14] aboard. The pictures taken by the device and the relief map generated from the pictures are accessible to the public, through the internet [15], so we could use these. From the many obtainable pictures, we chose one taken of the Gale crater [16]. The Curiosity Mars rover landed in this area in 2012 [17]. The rover is still operational. From the map, we cut out an area of one square kilometer.

B. Creation of the digital elevation model

We modified the relief map created by the HiRISE project to a grayscale picture (as illustrated in Fig. 2.). Our program reads the RGB (Red, Green, Blue) values of the picture mentioned above and it constructs the digital elevation model. The (255,255,255)-white color code represents the lowest

point, while the (0,0,0)-black stands for the highest point. In order to properly calculate elevation data, another parameter was necessary, which defines the elevation change represented by one unit difference in the color value on a pixel. The resolution of the used map is 1 meter/pixel. Between the highest and the lowest point the elevation difference is 280,5 meters.

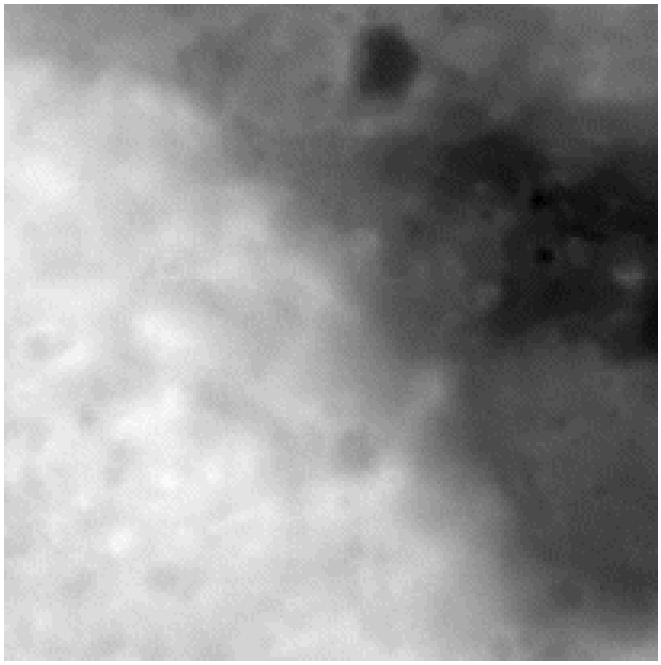

Fig. 2. Relief map of the examined area

The program read the map and it created a grid model to store the data in. We chose this model mainly because of its simplicity. The grid is constructed as follows: there is an elevation value assigned to every point of the map, it is a two-dimensional array. The arrays columns and rows represent the X and Y coordinates. The values stored in the array are the elevation values.

C. *Movement of the nodes*

In our sensor network the nodes are capable of movement. The simulation is terminated once all the Nodes leave the surveyed area, whilst moving on a predetermined path set for them. We implemented three algorithms to set the path of the nodes. Random-bouncing, base station-following and random-bouncing around the base station.

When the nodes follow the random-bouncing algorithm, they start from one side of the map and they set a random coordinate from the upper or lower side of the area as goal. When they reach the upper or lower end of the map, they set a new path from the other end of the map randomly (they "bounce back"). This goal is set in a way, that the node always moves forward, in other word they don't "bounce backwards". The results presented in this paper were acquired using this moving algorithm.

We have only one base station on our design, so losing it would mean that our network wouldn't be able to forward the gathered data. We must minimize every risk factor, which threatens this unit to maximize the chance of a successful mission. The repositioning of a device on the surface of a distant planet holds many risks, because the terrain is unknown and there is very limited human intervention if there is any at all. Our base station following algorithm sets the path of the base station in a way that the device tries to avoid movements which requires change in elevation. We used the Dijkstra [18] algorithm to achieve that. From the grid model, we created a weighted graph in which we could run the Dijkstra pathfinding. The vertices of the graph correspond to the coordinates of the digital elevation model. The weighted edges are calculated from the distance of the neighboring coordinates and from the height difference. The nodes move parallel to the base station.

Combining the first two algorithms mentioned above, we created a third one, when the path of the base station determines a zone in the map and inside this zone the nodes move like the random-bounce method. In this algorithm, the goal is to cover only a part of the map, so the "bouncing" of the nodes is triggered by reaching the end of the zone we intend to cover. We can see the path of the nodes, marked with red and the base station, marked with blue in Fig. 3.

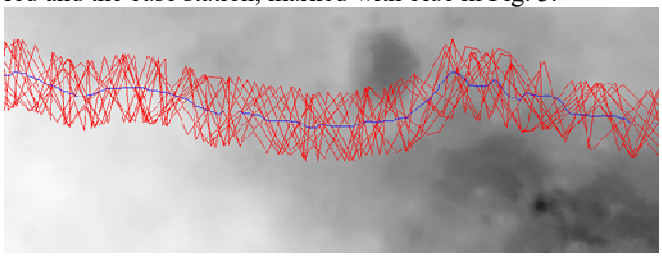

Fig. 3. Random-bouncing around the base station movement

V. RESULTS

A. *Effect of the terrain*

The movement is the operation, which has the most substantial effect on energy consumption, so the different paths the nodes take has different influence on the energy-relations. We couldn't ignore the height difference in the paths of the nodes, because we used a three-dimensional map in our simulation. The nodes movement is not only horizontal, but they move according to the terrain; if a node moves from a higher point to a lower point, it consumes less energy, while in the reversed situation it consumes more. We calculated the height difference in every simulation step because it affected the energy the node required to move and we summed up the elevation differences.

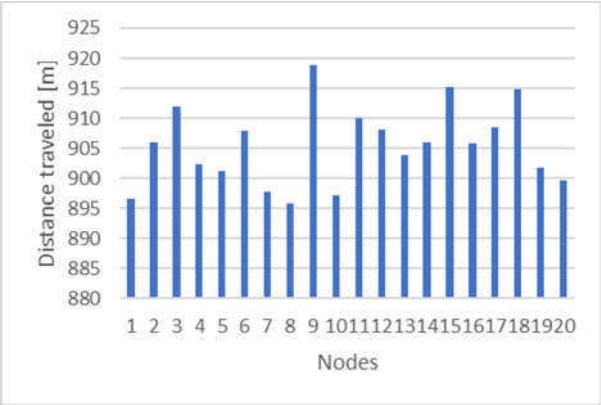

Fig. 4. Distance traveled by each node

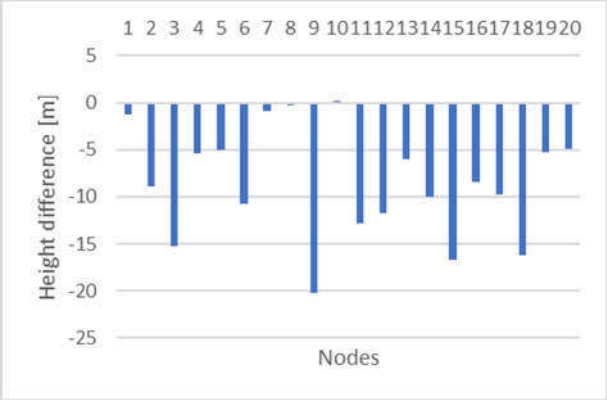

Fig. 5. Elevation change, the nodes took during the simulation

As expected; those nodes could move further, which moved downward on a slope for most of their paths. It can be observed that the nodes with less downward movement consumed more energy, that is the reason they traveled less distance.

B. *Effect of the battery*

In this examination, we were trying to find out, how the size of the battery affects the operation of the nodes. In the different scenarios, we used the following battery sizes; 43200 J, 86400 J, 21600 J.

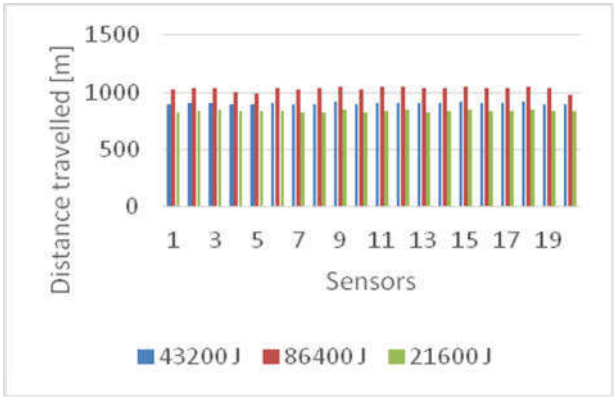

Fig. 6. Distances traveled with different battery sizes

It is a noteworthy observation that despite the fact we doubled the battery size, the traveled distance only grew by 9-15,5%. In the scenario where we reduced the battery size by half, the nodes traveled 7-8% less distance. The reason behind this result is that the movement of the nodes consumed much more energy than the solar energy could cover. During the simulation, discarding the starting period the energy level of the nodes were low. The conclusion we can draw from this is that the longer we run the simulation, the less effect has the battery size on the traveled distance.

In larger network when we talk about thousands of nodes, it should be considered to reduce the size of the batteries, seeing we can achieve similar results with less financial investment. The smaller battery size means smaller nodes, so we can send more of them in the cargo hold of the spacecraft to the distant planet. The reduced battery sizes also mean less mass, so we can save on the fuel cost of the rocket.

C. *Effect of the solar cell*

The nodes only have one source of energy, therefore the only way to increase the energy revenue is to expand the surface of the solar cell.

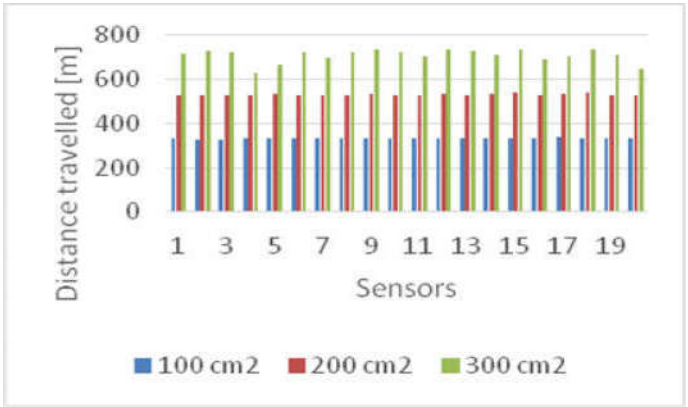

Fig. 7. Distances travelled with different solar cell sizes

It can be observed that if we double the size of the solar cells, the nodes traveled approximately 60% greater distances. On average the nodes made 110% further, when they had triple size solar cells. Of course, the size of the solar cells cannot be increased infinitely. The nodes operate both day and night resultantly, for them to move at night also, it is not enough to expand the solar cell, but we would have to increase the battery size. It must also be taken into consideration, that due to the small size of the sensors, the solar cells have a limited expandability.

VI. CONCLUSION

In a wireless sensor network operating on the surface of the Mars, to make effective use of the devices we must consider the energy relations. In our paper, we reviewed the architecture of the wireless sensor networks and some of the grouping possibilities. We created a simulation model, in which we examined the factors influencing the energy consumption. The replacement of the batteries in the devices is not possible due to the absence of human intervention, so it is necessary to use energy efficient methods.

References

[1] C.Sergiou, A. Paphitis, C. Panagiotou, P. Ktistis, K. Christou: "Wireless Sensor Networks for Planetary Exploration: Issues and Challenges through a Specific Application", SpaceOps 2014 Conference 5-9 May 2014, Pasadena, CA

[2] P. Rodrigues, A. Oliveira, F. Alvarez, R. Cabás, G. Oddi, F. Liberati, T. Vladimirova, X. Zhai, H. Jing: Space Wireless Sensor Networks for Planetary Exploration: Node and Network Architectures - 2014 NASA/ESA Conference on Adaptive Hardware and Systems (AHS)

[3] A. Szeile, A. Huszak, L. Bacsardi. „Advanced sensor based positioning and monitoring system", Global Space Application Conference, Paris, France (2014)

[4] G. Anastasi, O. Farruggia, G. Lo Re, M. Ortolani: „Monitoring High-Quality Wine Production using Wireless Sensor Networks", Proceedings of the 42nd Hawaii International Conference on System Sciences – 2009

[5] P. Rodrigues, A. Oliveira, F. Alvarez, R. Cabás, G. Oddi, F. Liberati, T.Vladimirova, X. Zhai, H. Jing: Space Wireless Sensor Networks for Planetary Exploration: Node and Network Architectures - 2014 NASA/ESA Conference on Adaptive Hardware and Systems (AHS)

[6] Vincze Zoltán, Vida Rolland: „Mobil eszközök alkalmazása szenzorhálózatokban", Híradástechnika LXI/12, pp. 13-17. *(in Hungarian)*

[7] F. Nack: An Overview on Wireless Sensor Networks

[8] http://bydit.com/doce/products/Li-EnergyProducts/
(Date of last visit: Jan 9, 2017)

[9] Winston K:G: Seah, Zhi Ang Eu, Hwee-Pink Wan: Wireless Sensor Networks Powered by Ambient Energy Harvesting (WSN-HEAP) - Survey and Challenges - Institute for Infocomm Research, Singapore

[10] http://www.mcmanis.com/chuck/robotics/tutorial/h-bridge/datasheets/mabuchi_rc280rasa.pdf
(Date of last visit: Jan 9, 2017)

[11] https://datasheets.maximintegrated.com/en/ds/DS18S20.pdf
(Date of last visit: Jan 9, 2017)

[12] http://www.ti.com/product/MSP430F4794
(Date of last visit: Jan 9, 2017)

[13] http://www.ti.com/product/CC2420
(Date of last visit: Jan 9, 2017)

[14] McEwen, A. S., et al., Mars Reconnaissance Orbiter's High Resolution Imaging Science Experiment (HiRISE), Journal of Geophysical Research, 2007

[15] HiRISE project website:
http://hirise.lpl.arizona.edu/index.php
(Date of last visit: Jan 9, 2017)

[16] HiRise: Possible MSL Landing Site in Gale Crater:
http://hirise.lpl.arizona.edu/PSP_010573_1755
(Date of last visit: Jan 9, 2017)

[17] NASA's website about the Curiosity mission:
http://mars.nasa.gov/msl/mission/timeline/prelaunch/landingsiteselection/aboutgalecrater/
(Date of last visit: Jan 9, 2017)

[18] Katona Gyula Y., Recski András, Szabó Csaba: A számítástudomány alapjai Typotex publisher 2006, pages 52-54. *(in Hungarian)*

Introducing E-GNSS navigation in the Hungarian Airspace

The BEYOND experience and the relevance of GNSS monitoring and vulnerabilities

Rita Markovits-Somogyi
Technical Development Division
HungaroControl Hungarian Air Navigation Service Provider
Budapest, Hungary
rita.somogyi@hungarocontrol.hu

Alberto de la Fuente
Aeronautical Systems Division
GMV
Madrid, Spain
afuente@gmv.com

Bence Takács
Department of Geodesy and Surveying
Budapest University of Technology and Economics
Budapest, Hungary
takacs.bence@epito.bme.hu

Peter Lubrani
Service Provision Unit
ESSP SAS
Madrid, Spain
peter.lubrani@essp-sas.eu

***Abstract*—The use of GNSS solutions and the satellite based augmentation system, EGNOS, the European Geostationary Navigation Overlay Service, can provide a cost-efficient alternative to instrument landing systems at airports. Until the year of 2016, the market uptake of E-GNSS navigation solutions in the Hungarian airspace was hindered by a lack of the relevant approach procedures. It was with the aim of filling this gap that the European H2020 framework of project, BEYOND, managed by the European GNSS Agency (GSA) and led by the European Satellites Service Provider (ESSP) was launched.**

The overall project concept of BEYOND lies in developing capacity building in the field of multimodal applications, especially focused on aviation, and based on E-GNSS (EGNOS and Galileo) in different Eastern European and Euro-Mediterranean countries.

In aviation specifically the transfer of knowledge has been consolidated through a four stepped methodology (training sessions, guided exercises, technical workshops, flight trials) applied within six key knowledge domains (Performance Based Navigation, Safety, Procedure Design, GNSS Monitoring and Ground Validation, Flight Validation and Future GNSS scenarios). With the help of this process, a PBN implementation plan has been developed; and having carried out the relevant cost benefit analyses, a regional airport, Debrecen, has been selected as the candidate of the procedure design and flight validations tasks. During spring 2016, LPV approaches were designed for Debrecen, which then were also flight validated in the summer.

The project also included GNSS Monitoring exercises, where the performance (accuracy, continuity, availability, integrity) parameters of EGNOS coverage were investigated. This issue is particularly interesting in Eastern Europe, within the boundary zone of available EGNOS corrections. The article presents how the data collected by permanent GNSS stations can be used to calculate SBAS corrections, and how these corrections enhance the efficiency of GNSS bases navigation. Apart from and inspired by the obligatory tasks within the project, the research team conducted extra investigations and measurements as well. Coverage parameters in the Debrecen area were investigated, and the vulnerability of the system was tested by interference monitoring. The paper presents the results of these investigations which do not only show that Debrecen is located in a well performing EGNOS area, but also highlight and measure the vulnerability that GPS jammers may pose to GNSS solutions. The authors also venture to examine the potentially achievable efficiency of the future Galileo solutions.

Keywords—GNSS; EGNOS; Galileo; air navigation; LPV procedure design; flight validation; GNSS Monitoring and Vulnerabilities

I. INTRODUCTION

System *integrity* (i.e. the capability of self-monitoring), the *reliability* of the positions provided need to be ensured within all safety critical applications of the GPS technology. This is even more vital in the aviation sector, where safety of life is of utmost priority. Here, integrity and reliability may be achieved by statistical means conducted by the receivers and utilizing the redundant measurements (*Receiver Autonomous Integrity Monitoring, RAIM*). Alternatively, augmentation systems may also be employed.

Augmentation systems are based on the idea of ground monitoring stations (called RIMS, *Ranging and Integrity Monitoring Stations*) continuously monitoring the signals of the satellites, which are then screened for outlier data. Should such data be observed, users are notified within very short

time, within the timeframe of some seconds, of the anomaly. This information may be provided to the users by means of geostationary satellites (*Satellite Based Augmentation System*, SBAS) or by radio transmitters located on the ground (*Ground Based Augmentation System*, GBAS). These systems enable an increase in the accuracy of the measurements as well, in as much as they model the major regular errors elicited from the data obtained by the ground monitoring stations. Subsequently, the parameters of these models are made available to the users, while, in the form of corrections, the effect of the regular errors are taken into account when raw data are processed. Characteristically, SBAS augmentation systems provide correction data to whole continents, and several such systems are operated worldwide. In Europe it is EGNOS (*European Geostationary Navigation Overlay Service*), which, with its declaration in 2011 [1] of the Safety of Life service, provides the aforementioned to the aviation community. The EGNOS Safety of Life Service (SoL) [2] consists of an augmentation signal to the Global Positioning System (GPS) Standard Positioning Service (SPS) intended for most transport safety critical applications. This declaration enables precision approaches and renders air navigation safer. In the same way, this accessible Service contributes to reducing delays, diversions and cancellations of flights while the airport capacities are increased and operating costs reduced [3].

To be able to use satellite navigation for air transport safely, e.g. for the landing and approach of aircraft, satellite navigation has to fulfil strict criteria in terms of accuracy, integrity, availability and continuity. The benefits of satellite navigation include an increase in flight safety, the possibility to decommission or to cater for the lack of ground navigational equipment otherwise financially not feasible to install or maintain (e.g. ILSs – *Instrument Landing Systems*), while it might also facilitate approaches at smaller aerodromes under adverse meteorological conditions [4].

The number of SBAS based approaches are rapidly growing in Europe. As based on data from ESSP, the enterprise providing EGNOS, the European SBAS solution [5, 6], Fig. 1 shows the number of aerodromes where LPV (*Localizer Performance with Vertical Guidance*) approaches are planned or are already in place within Europe.

In Hungary, Liszt Ferenc Budapest International airport already possesses LPV based approach procedures, and within the European funded research and development project, BEYOND (*Building EGNSS capacity On EU Neighbouring multimodal Domains*), LPV approaches have been designed for LHDC Debrecen airport as well, however the latter has not been published in the AIP (*Aeronautical Information Publication*) yet. The work performed in BEYOND is a pre-implementation step which requires further more work to be done in order for the procedure to fulfill aviation's stringent international rules and regulations.

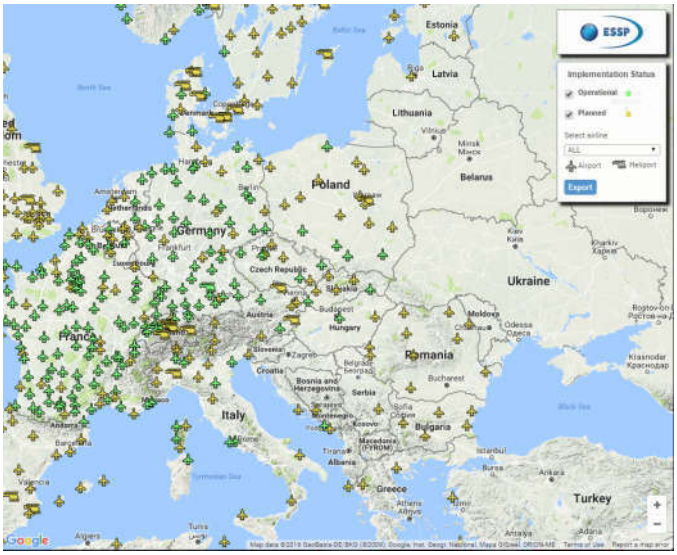

Fig. 1. Planned and operational LPV procedures in Europe (October 2016, source:https://egnos-user-support.essp-sas.eu/new_egnos_ops/?q=lpv200_maps)

II. Measuring Navigational Efficiency

Visual navigation is still paramount within aviation. Approaching the airport, there is always a height where the pilot needs to see the runway or its lights; and has to decide as based on this whether she will land, or, due to the lack of visibility, she will go around. This height is by definition the decision height (DH). The relationship between the landing categories and the values of runway visual range (RVR), just as well as decision height are summarized by Fig. 2.

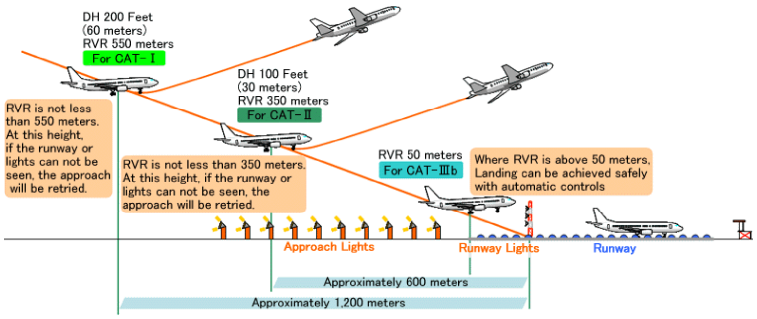

Fig. 2. Decision heights (DH) and Runway Visual Range (RVR) within the different categories (source:www.mlit.go.jp/koku/15_hf_000077.html)

The requirements for satellite navigation are specified in the Standards and Recommended Practices (SARPS) Annex10 Volume I (Radio Navigation Aids) by ICAO (*International Civil Aviation Organization*) , see Tab. 1. It shall be noted that LPV-200 corresponds to a CAT-I Approach [7].

To determine accuracy, the real position of the points measured need to be known. One of the obvious solutions is to process the measurements of the permanent stations; while, in case of kinematic experiments, another one is to identify the flight path with positioning much more precise than allowed by

original navigational means (e.g. with precise point positioning).

Protection level is a notion introduced to be able to assign a numerical value to the reliability of navigation. The accuracy values (mean errors) resulting from the models used to reduce the effect of standard errors are calculated. Using these mean errors multiplied by protection values are protection levels defined [8]. If the protection level reaches the alarm limit, then satellite navigation can be seen as not fulfilling the required criteria. In theory, position error is to be below protection level at all times. If this is not the case then we talk about an integrity event. Based on our experience, this happens only very rarely, and it has its reasons in the local surroundings.

TABLE I. SERVICE ELIGIBLITY CRITERIA WITHIN AVIATION

Service	APV-1.	CAT-I.
Horizontal accuracy [m] 95%	**16**	**16**
Vertical accuracy [m] 95%	**20**	**6 to 4**
Horizontal Alarm limit [m]	**40**	**40**
Vertical Alarm Limit [m]	**50**	**35 to 10**
Continuity	**1-8x10^{-6} within 15 seconds**	**1-8x10^{-6} within 15 seconds**
Availability	**0.99-0.99999**	**0.99-0.99999**

To calculate availability, those epochs are taken into account, in which case the EGNOS augmented positioning fulfils all the requirements. Namely, positioning is accurate enough, and the protection level remains both horizontally and vertically below the alarm limit. As based on the prerequisites, availability should be at least 99%.

If positioning or the criteria to be fulfilled by the positioning solution are interrupted, a continuity event is at hand. Continuity risk is calculated by dividing the number of continuity events with the number of epochs in the given interval. Experience shows that continuity requirements are generally not easy to meet. This is why, as based on ICAO specifications, satellite based procedures may be published even if continuity requirements are not fulfilled[1].

[1] Annex 10 of the Chicago Convention, Attachment D, 3.4.3.4: "For those areas where the system design does not meet the average continuity risk specified in the SARPs, it is still possible to publish procedures. However, specific operational mitigations should be put in place to cope with the reduced continuity expected. For example, flight planning may not be authorised based on GNSS navigation means with such a high average continuity risk".

III. THE BEYOND PROJECT

A. Background

Horizon 2020 is the European Union financial instrument implementing the Innovation Union, a Europe 2020 flagship initiative aimed at securing Europe's global competitiveness.

This program offers opportunities for the development of applications to use with EGNOS and Galileo which is crucial to meet the overall objectives of the Galileo program and to foster the uptake of E-GNSS (European Global Navigational Satellite programs, including EGNOS and Galileo).

The BEYOND project is a two year project, part of the European H2020 framework of projects, managed by the European GNSS Agency (GSA) and led by the European Satellites Service Provider (ESSP), the EGNOS Service Provider.

Strong of nineteen partners among which we find industry, academia, Air Navigation Service Providers, research institutes and Civil Aviation and Transports Authorities, the BEYOND consortium is supported by the companies ESSP, GMV and Telespazio in the roles of coordinator/leadership and technical expertise.

There are three main project goals:

1. Promoting the use of EGNSS and growing the interest towards EGNSS outside EU (i.e. in EU neighboring countries),

2. Preparing them towards an optimal adoption of EGNSS, and thus contributing to the growing of know-how, capacity and knowledge in relation to EGNSS outside EU;

3. Supporting networking and liaisons between EU and non-EU players thus creating the basis for cooperation, the establishment of relationships possibly evolving into business opportunities.

B. Methodology and steps in aviation capacity building.

The methodology is based on the fulfillment through three distinct educational steps of the following key knowledge domains:

- PBN Strategy on GNSS
- GNSS Monitoring
- LPV Procedures design
- Safety Assessment of LPV procedures
- Ground and Flight Validation of LPV procedures
- Future Scenarios

Step by step:

1. each company creates an expert team while applying a collaborative approach;
2. the team is trained in the various aspects of PBN and the specific domains through the training sessions,
3. They are thus proposed guided exercises with the support of an expert and are finally required to

show their work and share their results with the other teams and the tutors.

The results of the aforementioned steps converge in the flight trials at the chosen airport. Finally the flight trails are performed to ensure the procedures pre-implementation maturity.

C. *Achievements*

The strength of this methodology relies on mimicking the real areas of knowledge and cycle required for the development of an SBAS/LPV procedure from the very start to the operational implementation: among other things identifying the necessary stakeholders and human interfaces; taking account of the international/local caveats and problems; stimulating preemptive thinking while proposing solutions that pave the way for a smoother implementation of PBN based on GNSS enabling technology in their organization and the country's airspace.

IV. Processing Data from the BME EGNOS Monitor Station

First, the raw data from the EGNOS monitoring station located at the top of the central building of Budapest University of Technology and Economics (BME) were processed, and these results were analysed. This EGNOS monitoring station may basically be considered as a permanent station, recording the raw measured data every second in 24 hours a day. The station disposes of a NovAtel ProPak V receiver, capable of receiving GPS L1 and GLONASS G1 signals. It is also capable of receiving and recording the EGNOS corrections. Basically, the data recorded by any permanent station may be used for the sake of such an investigation, and the necessary EGNOS corrections may later also be downloaded from the ftp servers of the EDAS[2] service of ESSP. The raw data were post-processed, at 24 hour intervals. The positions received were compared with the position of the station's aerial. The position of this may be considered as known very accurately. This comparison yielded the accuracy indices. The software also calculated the protection levels, and further numbers characterising e.g. availability and continuity. It must be noted that the data can be processed in a fully automated manner as well; the results may be presented and published in a report format as well.

The main indices are shown in Tab. 2 and 3. Regarding accuracy, protection levels and availability, as compared to the values shown in Table 1, it can be stated that the results fulfil the requirements. Several companies (among these, the ESSP) offer(s) solutions to monitor the efficiency that can be attained by EGNOS corrections. At their website, the accuracy, integrity, availability and continuity parameters measured at any desired RIMS station can be downloaded. These main parameters may be displayed on maps and graphs as well. The data and results obtained by the authors are in line with the parameters delivered by the service provider.

TABLE II. Statistical Data of the Main Accuracy Values and Protection Levels Measured at the Permanent Station of BME

Date	Horizontal Accuracy [m] 95%	Vertical accuracy [m] 95%	Horizontal Protection Level [m] 99%	Vertical Protection Level [m] 99%
16.10.2016.	0.85	1.48	14.26	19.14
17.10.2016.	0.71	1.33	14.94	21.54
18.10.2016.	0.74	1.32	13.40	18.89
19.10.2016.	0.80	1.22	15.16	19.06
20.10.2016.	0.73	1.24	12.76	18.76
21.10.2016.	0.80	1.28	12.55	20.46
22.10.2016.	0.87	1.41	12.67	20.13

TABLE III. Availability and Continuity Values Processed from Raw Data of the BME EGNOS Monitoring Station

Date	Availability APV-I [%]	Continuity APV-I
16.10.2016.	99.5715	1-0.0000e+00
17.10.2016.	99.1522	1-1.6354e-04
18.10.2016.	99.1533	1-1.6553e-04
19.10.2016.	99.5715	1-0.0000e+00
20.10.2016.	99.5715	1-0.0000e+00
21.10.2016.	99.5715	1-0.0000e+00
22.10.2016.	99.1429	1-1.6355e-04

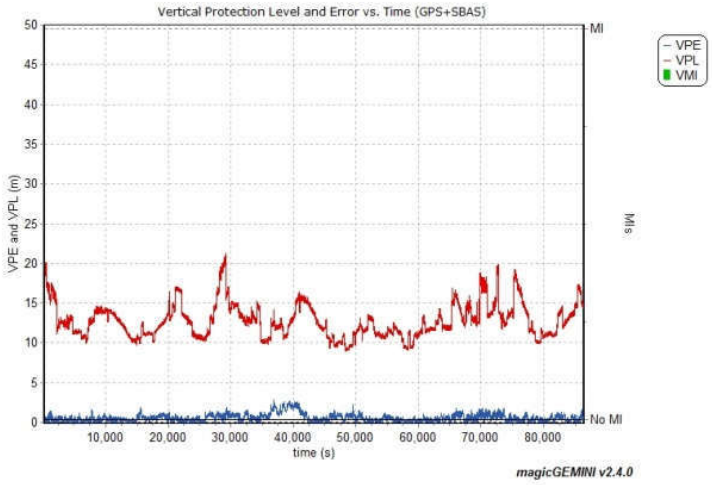

Fig. 3. Vertical Protection Level, Vertical Protection Error and Vertical Misleading Information gained from post-processing raw data of 16th October 2016, from the BME EGNOS monitoring station (source: own research)

A typical daily change in the position error and protection levels are shown in Figure 3.

It is interesting to note that availability only reaches 99.5715% on several days, although the system is fully available during the analysed days. Our experience shows, that in the course of data processing, the software cannot calculate

[2] (EDAS service – https://egnos-user-support.essp-sas.eu/new_egnos_ops/content/edas-service)

the position for exactly the first 370 epochs, some sort of initialization is taking place here; and this is why availability is short of being 100%. On some days, the continuity in positioning is interrupted for some measurement events, some local effect may be the cause of this. On these days, availability is also eventually showing a decreased value.

Investigating the issue at 22 October 2016, we found that the first continuity event appeared at 16:58:43. Around this epoch, for a short period, the number of measured satellites decreased to 2 or 3, although earlier and later 10 satellites were measured. The signal-to-noise ratio also decreased significantly (Fig. 4.). There is no clear evidence, since the spectrum has not been tracked, but the effect looks very similar to interference events [9].

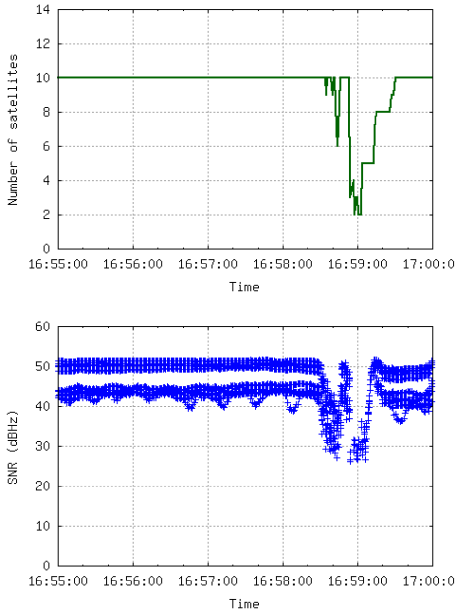

Fig. 4. Number of satellites and signal strength during a continuity event (source: own research)

V. Analysing Data from the LHDC Flight Trials

Having processed and analysed static data, kinematic data were collected by a GNSS receiver mounted on a general aviation aircraft. Similarly to the previous examinations, these raw data were post-processed. First, the LPV procedures were designed for LHDC airport, and then, within the framework of a flight trial these were tested. The aim of the measurements was not only to test the flight procedures, but also to process and analyse the kinematic GNSS measurements. The flight trials were carried out on the 12th and 13th of July 2016, flying 6 times along the predefined flight paths. The device used for the measurements was a dual-frequency TOPCON GR3 receiver, capable of receiving both the GPS L1 and L2 and the GLONASS G1 signals. The receiver was mounted on top of the dashboard of the PA-34 220T Piper Seneca aircraft.

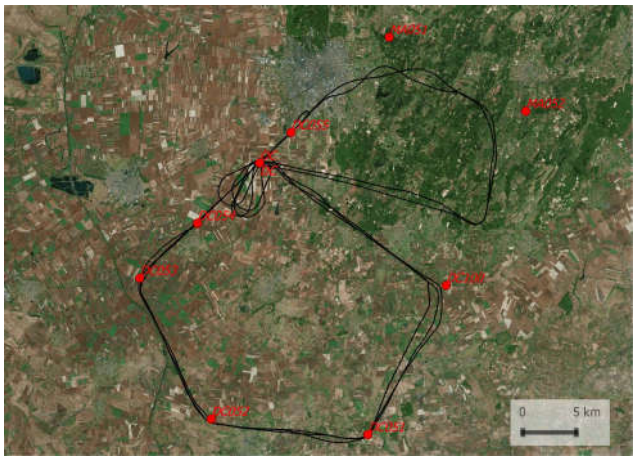

Fig. 5. Path of the kinematic measurements (source: own research)

The dual-frequency raw measurements were used to determine the flight path as accurately as possible (Fig. 5.). To this end, precise point positioning was applied. The accuracy of the coordinates determined are in the order of few centimeters. Then, the measurements were also processed using the EGNOS corrections. Subsequently, comparing the two results yielded the NSE (Navigation System Error) of the EGNOS augmented positioning (Fig. 6). The NSE obtained was 0.65 m horizontally, and 0.81 m vertically, these values are somewhat more favorable than the results gained from processing the data from the permanent station (Table 2.). Protection levels can be calculated in this case as well (Fig. 5.). The protection levels are basically similar to those experienced before.

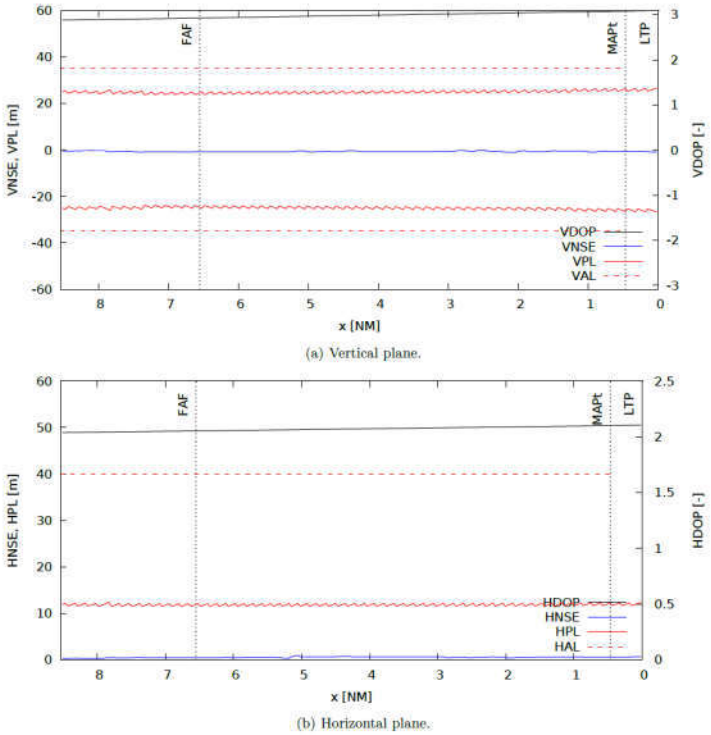

Fig. 6. NSE, protection levels and DOP values of the data recorded during the kinetic measurements (source: own research)

VI. Investigation with simulated GALILEO data

As based on the results presented above, the criteria to carry out LPV-200 approaches are already helped along and fulfilled by EGNOS augmented positioning. Nonetheless, there is a growing demand of EGNOS being able to meet even stricter navigational criteria to lower the decision height. In order to do so, it is mainly the protection levels that need to be decreased significantly, especially in the vertical sense. The values of the protection levels may, on the one hand, be reduced by increasing the accuracy of the models determined to decrease the effect of standard errors. Another, to some extent even more efficient solution may, on the other hand, be to raise the number of satellites used for positioning. This also makes satellite geometry more favorable. This is important because there is basically a linear correlation between the DOP values, used to characterize satellite geometry, and the protection level values (Fig. 7.).

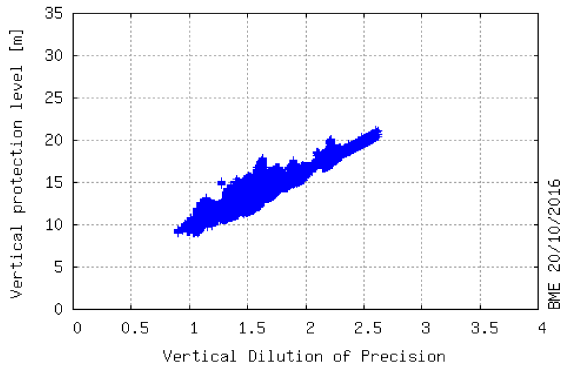

Fig. 7. Correlation between protection levels and satellite geometry just for the case of GPS satellites (source: own research)

Besides the GPS constellation, the number of satellites may be increased by integrating those of other systems (e.g. those of Galileo and GLONASS). Even today the signal of several Galileo satellites may be measured already, and it is a much welcome fact that their number is growing[3]. However, there are not enough Galileo satellites available yet to enable us to carry out the same measurements; hence, simulated Galileo measurements are used in the investigations described below (Fig. 8. and 9.).

The position errors of EGNOS augmented relying also on the simulated Galileo-measurements were determined, and compared to the position errors as carried out using GPS satellites only (Fig. 10. and 11). Positioning errors decreased only slightly, from 0.59 m to 0.42 m horizontally, and from 1.03 m to 0.97 m vertically (at 95%).

[3] The actual status of the Galileo constellation may be monitored at the following website: https://www.gsc-europa.eu/system-status/user-notifications.

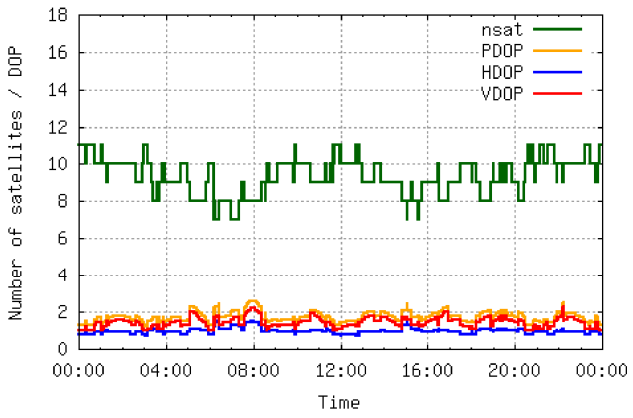

Fig. 8. Number of real GPS satellites, and DOP values I. (source: own research with [10])

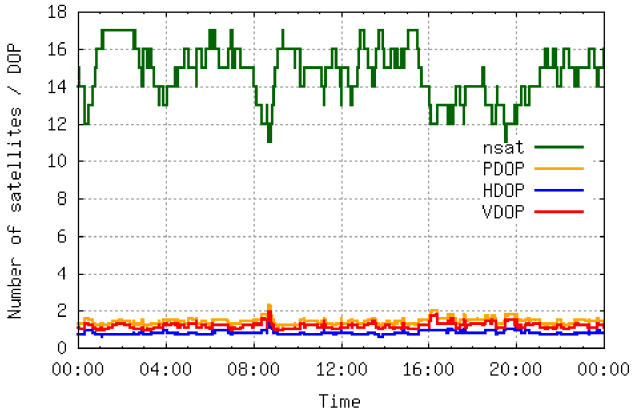

Fig. 9. Number of real GPS and simulated Galileo satellites, and DOP values II. (source: own research with [10])

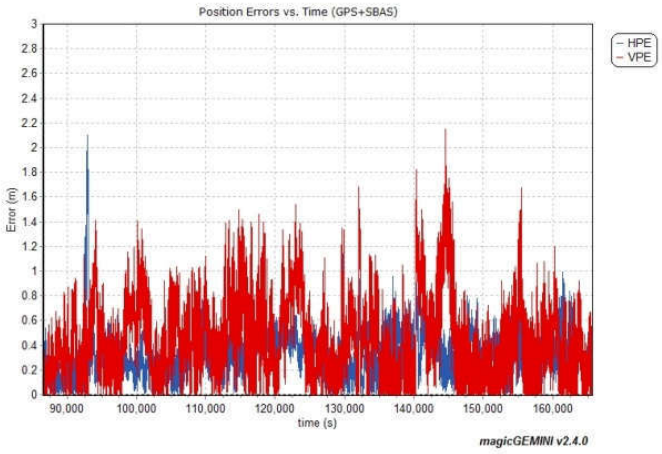

Fig. 10. Position errors of EGNOS based postioning using the GPS satellites only (source: own research)

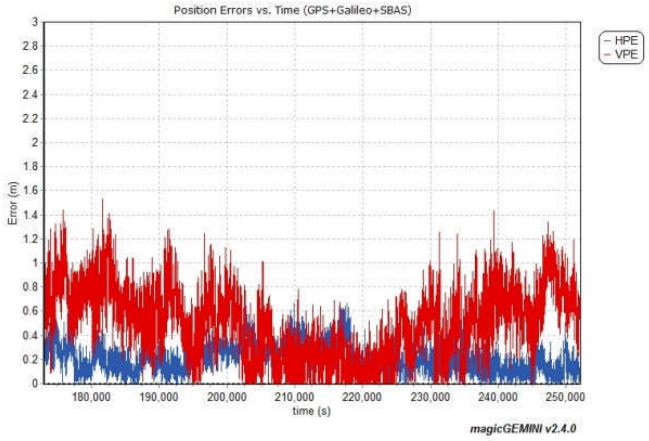

Fig. 11. Position errors of EGNOS based postioning using both the GPS and the simulated Galileo satellites (source: own research)

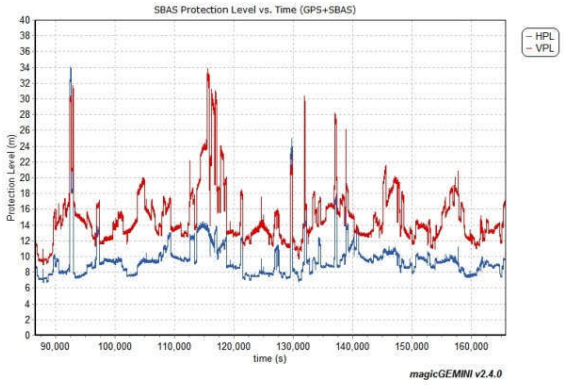

Fig. 12. Protection levels using the GPS satellites only (source: own research)

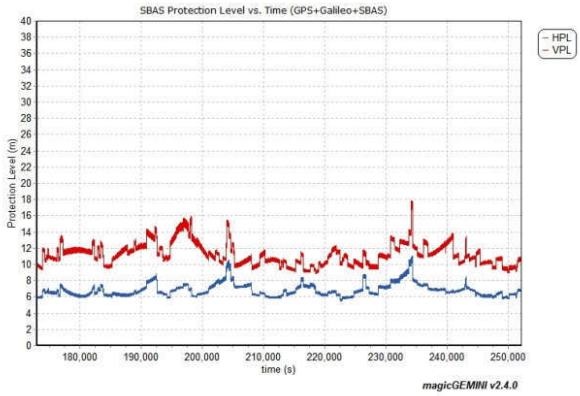

Fig. 13. Protection levels using both the GPS and the simulated Galileo satellites (source: own research)

Protection levels were also determined in both cases. Integrating the Galileo satellites enables a significant decrease in the protection levels, from 13.43 m to 9.87 m horizontally, and from 21.34 m to 15.05 m vertically. It is particularly important to note that the high values of the protection levels observed for short time intervals are basically eliminated, the functions show quasi stable values, unvarying with time (Fig. 12. and 13.)

VII. Conclusions

Parallel to the LPV procedure design tasks performed within BEYOND, the performance of EGNOS augmented navigation was analyzed as based on the knowledge transferred by the project partners and using the data from the Hungarian permanent station. Based on these measurements and their evaluation, the accuracy, integrity and availability parameters of APV-I and LPV criteria are thoroughly fulfilled. There are minor insufficiencies regarding continuity. According to our experience, these might be due to GNSS interference phenomena. However, there is further research needed to justify these assumptions.

With the advent of the GALILEO constellation, the number of visible satellites will roughly double. This will entail a much more favorable satellite geometry (with a drop in VDOP to below 2). This will have also result in a VPL value of less than approximately 16 meters. Nonetheless, as based on our present knowledge, this will still not be adequate enough to meet CAT-II criteria.

Acknowledgment

The authors gratefully acknowledge the support of the GSA through the H2020 framework.

References

[1] ESSP SAS Press Release 0.1 - ESSP-PR-R006 on the 02-03-2011

[2] EGNOS Safety of Life (SoL) – Service Definition Document 3.0. 22/09/2015, European Global Navigation Satellite Systems Agency

[3] Navpedia Item on EGNOS Safety of Life Services (Last accessed on 4th January 2017, URL: http://www.navipedia.net/index.php/EGNOS_Safety_of_Life_Service

[4] 63rd SINGLE SKY COMMITTEE: SSC/16/63/5: Agenda Item 4.1: Discussion on a EU Air Navigation Strategy, 28 November 2016

[5] P. Pintor, T. Seoane, R. Chaggara, R. Roldan, "SBAS CAT-I available in Europe" , Coordinates, 2006, Vol. XII. No. 5.

[6] R. Roldan, P. Pintor, M. Aguilera, J. Gómez, C. de la Casa, R. M. Fidalgo, "The EGNOS Performance monitoring activities performed by the ESSP"

[7] International Civil Aviation Organization – ICAO – Standards and Recommended Practices (SARPS) Annex 10 Volume I (Radio Navigation Aids).

[8] Radio Technical Committee for Aeronautics (RTCA) "Minimum Operational Performance Standards for Airborne Equipment Using Global Positioning System/Wide Area Augmentation System", Doc. DO-229D, 2006, with Change 1, 2013, Washington, DC. URL: http://www.rtca.org

[9] S. Pullen, G. Xingxin Gao, "GNSS jamming in the name of privacy", InsideGNSS, March/April 2012. pp. 34-43.

[10] T.Takasu, RTKLIB: Open Source Program Package for RTK-GPS, FOSS4G 2009 Tokyo, Japan, November 2, 2009

Inspiring space enthusiast students and young professionals

István Arnócz, László Bacsárdi, Dorottya Milánkovich*
Space Generation Advisory Council, Vienna, Austria
istvan.arnocz@spacegeneration.org, laszlo.bacsardi@spacegeneration.org, dorottya.milankovich@spacegeneration.org

***Abstract*— Nowadays people's lifestyle has accelerated and it is not an easy task to inspire the students and young professionals, compete with distractions from the internet and make extra courses. Fortunately, space and space research is still a mysterious topic for the public. It provides wild range of new and exciting knowledge for curious minds. In addition, hopefully, the space industry is developing gradually and it will continue in the next years and decades, therefore, it will need qualified experts and engineers. The UN-established Space Generation Advisory Council (SGAC) provides opportunity for university students and young professionals between age of 18 and 35 years to expand their knowledge of international space policy issues and space research, build relationships and think creatively about the future [1]. SGAC Hungary in collaboration with the Hungarian Astronautical Society would like to foster Hungarian youth to take part in the process and share the knowledge and experience with the enthusiast young generation. In Hungary, they organize several events during the year for their audience. The goal of these programs is to develop and maintain a platform for the young generation in our country and give them the chance to learn more about space research and economy. Here they can connect with space experts and entities, share ideas and get involved in the national and international space sector. Based on our four years of experience, lessons learned will be discussed in our presentation.**

***Keywords*— space generation, outreach, dissemination, students and young professionals**

I. INTRODUCTION

Members of Generation Y—people born between 1980 and 1999—would like to get new knowledge after receiving their college/university degree. In Hungary, there are several possibilities for this in the space field. The UN-established Space Generation Advisory Council (SGAC) provides opportunity for university students and young professionals between age of 18 and 35 years to expand their knowledge of international space policy issues and space research, build relationships and think creatively about the future [1]. With SGAC Hungary and MANT our goal is to bring space to student and young professional in a more understandable way. Space is a domain based on complex technology. This is complex, however during the years it has been mystified by the people and they assume a higher complexity as it really is.

II. THE ORGANIZERS

In the last 3 years, the *SGAC Hungary* activities were carried out with collaboration and active help of the members of the *Hungarian Astronautical Society*. This is the oldest Hungarian non-profit space association, founded in 1956. This society gathers Hungarian space researchers, users of space technology and everyone who is interested in the interdisciplinary and state-of-the-art uses and research of outer space. The aim of the association is to raise public awareness about space exploration and uses. It also provides opportunity for space enthusiasts to meet, exchange ideas and work together.

MANT, through its members from various fields of science, organizes conferences, youth forums, summer space camps, issues periodicals, releases media material and holds lectures about space research and connected scientific fields [3]. The association is a voting member of the International Astronautical Federation (IAF) since 1959. Members of this society participated in the UNISPACE III conference when SGAC was established. Memorandum of Understanding between MANT and SGAC was signed on Sep 30 2014 during the International Astronautical Congress in Toronto, Canada.

The *Space Generation Advisory Council* (SGAC) is a global non-governmental organization and network, which aims to represent university students and young space professionals to the United Nations, space agencies, industry and academia. SGAC was established as a recommendation from the Third United Nations Conference on the Exploration and Peaceful Uses of Outer Space (UNISPACE III) held in Vienna in 1999. SGAC has Permanent Observer Status in the UN Committee on the Peaceful Uses of Outer Space (UN COPUOS) and is regularly present at its annual meeting and its two subcommittee meetings. These presentations cover the outcomes of SGAC's annual conferences and projects throughout the year. This includes the reporting the recommendations and outcomes gathered at the annual Space Generation Congress (SGC) and the annual Space Generation Fusion Forum (SGFF), bringing together top young minds from around world to focus on key space topics [4].

III. Target Audience and methodology

The Y generation grew up together with the information technology. They are digitally natives, enjoy to work with modern technology, internet based cooperative systems etc. They are accustomed and trained to expect immediate results. If they do not reach their expectations, they lose interest in the given field much faster than previous generations. On the other hand, to work with them in traditional cooperative forms can be something new for them. While reaching out to them, we needed to consider this as well.

We reach out to the Generation Y on their native channels – the Internet and social media. We attract their interest and ask them to come to physical events where they can meet real space researchers. We ask them to work in working groups in smaller still interesting topics. This ensures to give them an insight on the topics of Aerospace and destroy the idealized image of unreachable distances of complex space research.

III. Reaching out to the audience

We use multiple ways of communication to the audience. Facebook, emails, website, and event landing pages. All supporting each other.

A. Email communication

Emails were used to communicate to specific persons. This of course is good to reach out to an earlier reached member of audience. Earlier in MANT it was the only way of communication. At the moment we use two types of emails. One is a more informative mail with text only design. This is easier to read through – if the reader has the motivation already to read it. We recently implemented Mailchimp ™ to send out colorful emails. With these emails we tend to reach the expectations of generation Y. We always reach out to communicate our physical event. We organize the content following the AIDA method (Attention, Interest, Decision, Action). We start with an interesting title, and an image that draws attention. This is followed by the description of the given event in a QA form. We strengthen the decision with the section "Why to come". And we add a sign up button and a direct order "Click here to register".

B. Social media / Facebook

We are in the implementation of a continuous Facebook communication. The first semester this activity was the test phase of the best practices learned from other industries. Not all the post types perform the same success rate than others. We need to focus on the initial goal of creating the facebook page: to reach out to our target audience. We need to communicate to our target audience with the right content. This content will draw the attention of the sensitive audience, and will be less attractive to those who are less motivated to learn new things. Important to notice: the goal of our social feed is not to get the most likes, but to get the most likes from the right audience. Therefore, we use the following post structure

i. Short Space News

Interesting news from mainstream media which is commented by an expert.

ii. Job offers

Offers from space agencies, mainly ESA. Offers from space related companies in Hungary and abroad. This is a key part of our communication. This demonstrates that we are not simply communicating about the topic, but through SGAC & Űrakademia, the listener can enter the Space economy.

iii. Events

We communicate mainly our events. This is a useful tool to reach out to those who are on our mailing list but missed the mail communication about the event. Also, to get new audience, we can redirect new people to our physical events. On the events, we offer them to sign up to the mailing list.

iv. Hungarian space information

To strengthen the idea that our country has ongoing space activity and research. This may seem obvious for those who work in it, but it is far from evident for the broad audience.

v. Anniversaries

Historical aspect is good to look back where we really are. To value how much interest the space topic gets now from press and citizens, compared to the 50's 60's 70's. Usually the audience is aware of achievements of the past. This is a good way to connect present researches and technologies to start with a historical topic that is well understood. We save the time to explain things and ensure the connection to the target, not to loose their attention.

Important to notice that we tend to keep the funny content low. That could draw the attention of personnel that are not the target audience.

To segment the content between platforms, we will follow the conventions. Instagram – Images with text, Facebook – shorter and longer posts, sometimes videos. Pinterest – Images of the events. We do not use twitter. This platform is not so much penetrated to the Hungarian user's every day.

IV. National events

To inspire the young generation, SGAC Hungary in collaboration with the Hungarian Astronautical Society (MANT) organizes several events during the year for their audience [2]. These events are advertised through the social media and also through interpersonal relations. We still measure a majority of participants who was invited by one of their friends and they never met a Facebook advertisement or received an e-mail from us.

A. Space Academy Club

The first Space Academy Club was held in August of 2014 in Budapest. It was a two-hour-long open and free workshop with two lectures followed by a Q&A session. Since the first event, considering the interest of the audience, we organize the workshop in every second month during the academy year in different universities in Budapest. The two lectures are usually chosen from the most relevant and up and coming space topics, which are sometimes presented in front of the public for the first time. The topics covers a wide range of space research, *from the European space policy, through the climate change and space industry, till the space flight an space travel, which could be interesting from a scientific, an engineering or a manager point of view. Some examples from the lectures we had so far: European Space Agency and the space policy of the European*

Union, Job opportunities in space industry, Neuro- and cognitive science experiments on board the International Space Station, Use of satellites for the climate change, The MarsOne program, Possibilities and limits of interstellar space travel, Radiological risks of manned space flights, European Space Agency's Earth Observation programmes, Possibilities of appearance of liquid water on the Mars nowadays, The past and the future of Solar System research in Wigner Research Centre for Physics, What happened to the light? Does an alien megastructure block it or something else?, SMOG-1 student satellite, The almighty GPS, BME Space Technology Laboratory, Scientific results in 30 seconds

In addition to the fascinating topics, we also lay emphasis on the lecturers. One of our invited speakers is usually a representative of the national space sector, the other speaker is a Hungarian university student or young professional. Thus we provide a unique opportunity to the curious students to gain insight into the latest space-related researches and news.

Up to now this event series was held in September, November, February and April in Thursday afternoons in three different universities, namely the Budapest University of Technology and Economics, the Eötvös Loránd University and the Óbudai University. For the first events, number of participants mostly depended on the location and the topic. This transferred to be topic dependent as our follower base is growing. Apparently there is interest of the young generation to these events. Right now we are investigating the possibility to hold this series outside of Budapest as well. At the moment the two candidate cities are Debrecen and Szeged.

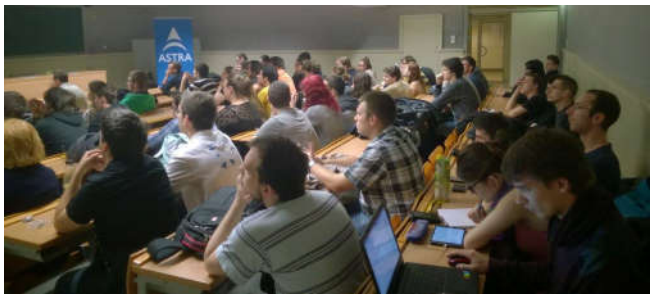

Fig. 1. Audience of the bimonthly event, the Space Academy Club held in the Eötvös Loránd University in 2015. The event is held in different universities across Budapest for university student and young professionals between age of 18 and 35.

B. Space Academy

During the summer the four-day-long Hungarian Space Academy is another unique possibility for the enthusiastic Hungarian students and professionals, where they can work together on a space related project and learn about space in tutorial lectures given by Hungarian professionals from national industry and academy.

During the second Space Academy - which was held between 11-14th of August 2016 - the participants listened lectures about the main Hungarian space research projects on ISS and a presentation about SGAC. They also designed an experiment and created a detailed proposal about it and explicated what are the benefits for Hungary of this projects. The Space Academy was very successful and we managed to build a great team of young space enthusiasts.
The proposal was presented by a participant on Day of the Space Research on the 21th of October (one-day event organised for people interested in the activities of the Hungarian space sector).

Fig. 2. Participants of the MANT Space Academy 2016, a four-day-long event organized by the MANT and SGAC for university students and young professionals interested in space research.

C. Space Academy Free Talk

This event is an informal meeting with a talented and successful Hungarian space expert. The first Free Talk was held on the 14th of July with a remote sensing expert form the German Aerospace Center (DLR).

D. Yuri's Night Budapest

Yuri's Night parties and events are held around the world every April in commemoration of Yuri Gagarin becoming the first human to venture into space on April 12, 1961, and the inaugural launch of the first Space Shuttle on April 12, 1981.
Yuri's Night events combine space-themed partying with education and outreach. Hungary joined to this global celebration series and within this program we spend a night in Budapest with a special guest and young people interested in space activities.

V. International Opportunities

A. European Space Generation Workshop (ESGW)

This event is a two-day regional workshop, which was created for the purpose of bringing together university students, young professionals, and experts; primarily from the European region. The 1st E-SGW with 56 delegates from 24 countries was held between 26-27 February, 2016 in Budapest, Hungary organized by SGAC and MANT.

Fig. 2. Participants of the first E-SGW in 2016

During the two days, there were also three working groups with the aim to make recommendations that could help shape and provide insight into the future of the European space sector and SGAC. The topics were as following: „European collaborations in small satellites", „Knowledge sharing between young professionals and experts at the European level", „Young Entrepreneurship in Europe - the Space Perspective". The workshops were led by three subject matter experts. Overall, the insight and ideas given in each working group were well represented by the final presentations and gave thought-provoking points to consider for both SGAC and the European space sector.
In 2017 the Headquarters of the European Space Agency in Paris will host this event.

B. Space Generation Congress (SGC)

The SGC is the annual meeting of the Space Generation Advisory Council held in conjunction with the International Astronautical Congress every year. Top university students and young professionals with a passion for space will travel from all around the globe to attend three days of SGC.
With SGC, SGAC aims to hone and promote the voice of the next generation of space sector leaders on the topic of international space development.

C. Space Generation Fusion Forum (SGFF)

This two-day event immediately preceding The Space Foundation's Space Symposium in Colorado Springs. Held in partnership with the main Symposium, this event brings together international perspectives of a select group of approximately 50 university students and young professionals from across the world to discuss the important and pressing issues for the space sector.

The Forum is an intellectual exchange between the delegates and senior leaders representing industry, academia and U.S. and international government entities. Exceptional international delegates are supported through the SGAC's Global Grants Program to ensure diversity of ideas and discussions amongst participants. Attendees come from a variety of space-related fields such as aerospace medicine, space law, space policy, engineering, and space science.

D. Project Groups

SGAC also acts as the forum for the next generation of space sector leaders to discuss and debate current topics in international space policy. The 8 SGAC Project Groups produce papers with input from a broad sample of SGAC members and embodies SGAC's purpose as envisioned from our beginnings at the United Nations. From perspectives on space situational awareness and space law to thoughts on exploration and space disaster management, the members of the young space community have opinions to share, and the project groups provide a perfect platform for the international collaboration via teleconferences.

E. Competitions and Grants

SGAC with its partners hosts several competitions and scholarships for talented students and young professionals to attend the space events like SGC, SGFF or the International Astronautical Congress. This opportunies are also open for the Hungarian SGAC members.

VI. Conclusion

The increasing number of the Hungarian members of SGAC, the Úrakadémia mailing list subscribers, the Úrakadémia Facebook page followers and the participants on the Hungarian events shows the need of the space related forums for the young generation.

MANT and SGAC Hungary are constantly working on developing and sustaining a dynamic forum for the university students and young professionals, where the potential members of the next generation of the national space sector can study, connect, share knowledge and get involved in the national and international space research. Taking advantage of the possibilities offered by the Internet, social media and different multimedia technologies, we can offer a unique platform for the Hungarian space enthusiasts.

REFERENCES

[1] Website of the Hungarian Astronautical Society, http://www.mant.hu (Last retrieved: January 4, 2017)

[2] Website of the Space Generation Advisory Council, http://www.spacegeneration.org (Last retrieved: January 4, 2017)

[3] L. Bacsárdi, M. Horváth, „Unforgettable Memories in the Hungarian Space Camp – Lessons from 18 years of Organization", in *Proc. 62nd International Astronautical Congress*, Cape Town, South Africa, 2011

[4] C. Dubois et al.. „Policy Considerations for New Human Space Exploration Strategies: the Space Generation Perspective", In Proc. *66th International Astronautical Congress, Jerusalem, Israrel, 2016*

[5] S. Ayres, How to each the Millennial Generation With Social Media, http://www.postplanner.com (Last retrieved: January 4, 2017)

[6] A mail sending service: MailChimp, http://www.mailchimp.com, (Last retrieved: January 4, 2017)

[7] An online meeting platform: the Gotomeeting, http://www.gotomeeting.com (Last retrieved: January 4, 2017)

Comparative analysis of tropospheric delay models using reference data derived from ray tracing numerical weather model

Szabolcs Rózsa[1], Bence Ambrus[2], Ildikó Juni[3]
Department of Geodesy and Surveying
Budapest University of Technology and Economics, Faculty of Civil Engineering
Budapest, Hungary
[1]rozsa.szabolcs@epito.bme.hu, [2]ambrus.bence@epito.bme.hu, [3]juni.ildiko@epito.bme.hu

***Abstract*—Electromagnetic signals broadcast by GNSS satellites suffer considerable delays while travelling through the atmosphere. The tropospheric delay depends on the actual meteorological parameters of the atmosphere and also on the elevation angles of the satellites. There are numerous models for calculating the tropospheric delay, however, these models deviate quite significantly from each other, either in the meteorological parameters used during the calculation or whether they take into account the periodic perturbation of some meteorological parameters. We studied the wet and hydrostatic part of the tropospheric delay separately and also differentiated between blind and site mode of all the models. In blind mode the model uses its own meteorological dataset while in site mode in situ measurements of the parameters are applied. Our goal was to test the accuracy of four troposphere models, employing the ray tracing method, using input data from numerical weather models. For the analysis we calculated statistical parameters to evaluate the performance of each model.**

Keywords—troposphere, tropospheric delay, GNSS, ESA, GPT2, GPT2w, RTCA-MOPS, ray tracing, numerical weather model

I. Introduction

Using the global navigation satellite systems is becoming part of more and more walks of our everyday life. The troposphere and the electrically neutral zone above it in the atmosphere cause significant signal delays in GNSS observations. The tropospheric delay can be separated into two parts, the hydrostatic and the wet delay. Both of these can be calculated using different delay models. Our aim in this paper is to analyse four tropospheric delay models: the RTCA-MOPS [1], the model developed by ESA for the Galileo satellite system [2], the GPT2 [3] and GPT2w [4] models developed by the Technical University of Vienna. In order to do this, we created a reference model, using input data from a numerical weather model for the period of 2010-2011 and a ray tracing algorithm. Besides the meteorological parameters, the tropospheric delay depends on the elevation angle of the observed satellite as well, so in the analysis we studied the model performance in different elevation angles: 3°, 5°, 10°, 45° and 90°.

II. The effect of the troposphere and the models used in the study

The tropospheric delay effect comes from the change in refractivity along the signals propagation path. The total tropospheric delay can be calculated with the Thayer-integral [5], using (1):

$$T = 10^{-6} \int N \, ds \tag{1}$$

where N denotes the refractivity. The total tropospheric delay in zenith direction (ZTD) can be divided into two parts, the hydrostatic delay in zenith direction (ZHD), which is the effect of gases in hydrostatic equilibrium and the wet delay in zenith direction (ZWD) which is caused by the water vapour content of the air. ZHD and ZWD depend on different meteorological parameters in different tropospheric models, such as pressure, temperature, water vapour pressure, temperature lapse rate, water vapour lapse rate and so on. We have to take into account the elevation angle of the satellite, because the delay grows significantly if the satellite is closer to the horizon. The delay is usually calculated in the zenith direction and then converted to any slant direction, using a mapping function. When calculating with different troposphere models, we have to distinguish between blind mode and site mode. The models use their own built-in meteorological data in blind mode and apply user supplied measurements of meteorological parameters in site mode to improve the model performance in ground based augmentation systems. In our analysis, both operation modes were used for each model.

A. RTCA-MOPS model

The tropospheric delay TD_i for satellite i takes the form described in [1], using the following formula:

$$TD_i = (ZHD + ZWD) \cdot m(E_i) \tag{2}$$

where $m(E_i)$ is the mapping function to scale the delays to the satellite's elevation angle.

ZHD and *ZWD* are calculated from the receiver's height above the mean sea level, refraction coefficients, the gas

constant of dry air, the mean gravitational acceleration, and five meteorological parameters: air pressure, air temperature, water vapour pressure, temperature lapse rate and water vapour lapse rate. In blind mode the values of each of the five meteorological parameters, applicable to the receiver latitude and day of year (starting with 1 January), are computed from the average and annual variation values which are built into the model. The model calculates and applies the mapping function described in [6] to give the total delay, which is valid for satellite elevation angles not less than 4°. If the elevation angle is less than 4° but not less than 2°, an expanded version of the formula is used.

B. ESA model

The calculation of the zenith hydrostatic and the zenith wet delays for a receiver on the surface is similar to the method used in the RTCA-MOPS model [2]. In contrast however, the gravity acceleration is not a constant anymore, but rather a function of latitude and height of the receiver above mean sea level. Tropospheric hydrostatic and wet delays are calculated in the zenith direction. In order to obtain the tropospheric delay for any elevation angle, the Niell mapping function [7] is applied. The input parameters for the ESA-model in blind mode are derived from a re-analysis dataset of the European Centre for Medium-Range Weather Forecasts (ECMWF), the ERA15 statistical analysis and stored in climatological maps. In total 21 maps are utilized, where the mean values, daily and annual fluctuations of all the climate parameters are given. The tropospheric delay at any receiver position is calculated using bilinear interpolation based on delay values at the four closest grid points surrounding the receiver.

C. GPT2 model

The GPT2 (Global Pressure and Temperature Model) is a global empirical model of surface meteorological parameters. GPT2 provides pressure, temperature, temperature lapse rate, water vapour pressure and mapping function coefficients [3]. The Vienna Mapping Function 1 (VMF1) [8] is used to transform the zenith delay into slant delay. In blind mode, when only the coordinates of the station and the date of the observation are given, all the meteorological parameters are calculated from the model. In this case, the mean values, annual and semi-annual variations of all the hydrostatic climate parameters are given on a global grid with a resolution of 1° x 1°. The meteorological data are derived from ECMWF Re-Analysis monthly mean profiles between 2001-2010 using 37 pressure levels. These meteorological parameters are then used as input data for the Saastamoinen troposphere model [9] to calculate the hydrostatic part of the delay and the Askne-Nordius troposphere model [10] in order to calculate the wet part of the delay.

D. GPT2w

The GPT2w [4] is an upgraded version of the GPT2, providing mean values, annual and semi-annual variations for pressure, temperature, temperature lapse rate, water vapour pressure and its decrease factor, weighted mean temperature as well as hydrostatic and wet mapping function coefficients for the VMF1. The model uses a global grid of a resolution of 1° x 1° to store the mean values, annual and semi-annual variations of the hydrostatic and wet climatological parameters used in blind mode. The hydrostatic delay can be calculated like in the case of GPT2 and the wet tropospheric delay is determined using the Askne-Nordius formula [10].

III. Generating the reference data using ray tracing

A. Input data

ECMWF ERA-Interim monthly mean solutions were used for both the ray tracing and in the site mode computation for the different troposphere models. The dataset contained relative humidity, temperatures and geopotential values for 37 pressure levels, ranging from 1000 hPa to 1 hPa. The mean values for each month are computed and interpolated onto a global grid with a resolution of 1° x 1°. The ERA-Interim data is expanded up to the height of 86 km with values given in the International Standard Atmosphere (ISA).

B. The ray tracing algorithm

Using this method, the path of a satellite beam is traced throughout the neutral atmosphere, starting at a certain elevation angle and continuously refracting at different layers of the atmosphere Besides calculating the total length of the path the refracted beam takes (which gives us the geometric delay), we also compute the hydrostatic and wet refractivity values of each layer and use them in (3).

In order to achieve accurate results with ray tracing, the resolution of the input data must be increased [8]. The resolution of the height used for the interpolation varies according to the gradient of the interpolant parameter in a pre-defined manner. The interpolation is done linearly for the temperature and exponentially for the air pressure and water vapour pressure values. If the lowest pressure level is located above the topography, an extrapolation step is carried out using the values of the two pressure levels that are closest to the surface in order to start every ray tracing computation from the level of the topography.

In the next step the hydrostatic and wet refractivity values are calculated. The total refractivity at each level is the sum of the hydrostatic and wet parts [11]. From these values, we can derive the length of the refracted beam in each layer. The distance travelled by the ray and therefore the delay caused by the troposphere can be calculated using the refractivity of each layer and the distance travelled by the beam in that given layer:

$$ds_h = \sum_{i=1}^{k-1} s_i \cdot N_{h,i} \qquad ds_w = \sum_{i=1}^{k-1} s_i \cdot N_{w,i} \tag{3}$$

In the formula s_i is the length of the refracted beam, $N_{h,i}$ is the hydrostatic refractivity and $N_{w,i}$ is the wet refractivity in the i-th layer.

As a result of the ray tracing computation, a global grid was created with a resolution of 1° x 1° for each month (24 in total), using the vertical profiles obtained from the numerical weather data. For each grid point, the hydrostatic and wet tropospheric delay values were determined. These grids served as the reference of the comparison for each troposphere model.

IV. Comparative analysis of the troposphere models

A. Statistical parameters used in the analysis

Having created the reference dataset, we had a common basis to which each of the troposphere models could be compared. In order to assess the goodness of the models, three different statistical characteristics were calculated from the data. The input generated to be used in the computations was the differences ($d_i = D_{r,i} - D_{m,i}$) between the reference delay values ($D_{r,i}$) obtained with ray tracing and the delay values calculated using the various troposphere models ($D_{m,i}$). The bias of the model denoted the arithmetic mean of the differences. In addition to this, we computed the root mean square and the corrected standard deviation for each model.

The statistical parameters were calculated for both blind and site operation modes of each of the models using a two year dataset (2010-2011) with one sample per month. The delay values were calculated for the elevation angles of 3°, 5°, 10°, 45° and 90°. The bias and the σ values were computed for every grid point of a worldwide grid with a resolution of 1° x 1°, while the RMS was represented for each model and operation mode by a single average value. When operated in site mode, we calculated the weather parameters on the ground level using the method described in section III/B.

In the following section of the paper, we present the results of the comparisons for each of the troposphere models and their operation modes.

B. Comparison of the troposphere models to the ray tracing data

1) RTCA-MOPS model

As the model only contains the annual variation of the meteorological parameters, the expected results of comparing the RTCA-MOPS model to the ray tracing dataset were moderate at best. The blind mode results show heavy biases for the wet delays in an approx. 30° wide swath around the equator (Fig. 1), which only start to disappear above 10° of elevation.

The σ and RMS values become substantial at lower elevation angles for both the hydrostatic and the wet delays and tend towards zero around 45° elevation (Table I.), however, the σ of the wet part of the delay remains relatively high around the equator.

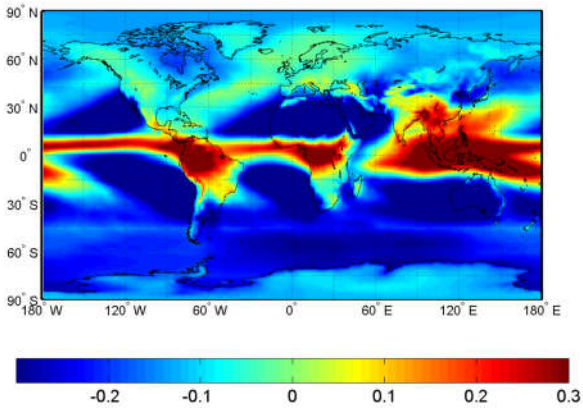

Fig. 1. Bias values of the wet delay from the RTCA-MOPS model at the elevation angle of 10°, computed using blind mode.

In good agreement with the expectations, the site mode results show considerable improvements of both the bias (Fig. 1), σ and the RMS values of the hydrostatic delay (Table I.). While there is noticeable development regarding the statistical parameters of the wet delay, both values remain rather significant along the equator.

Table I. below shows the RMS values of the hydrostatic and wet delays calculated from the RTCA-MOPS model for both operation modes.

TABLE I. RMS values of the RTCA-MOPS model in meters

Operation mode and type of delay	Elevation angles				
	3°	*5°*	*10°*	*45°*	*90°*
Blind mode hydrostatic	1.210	0.568	0.221	0.041	0.028
Blind mode: wet	0.792	0.527	0.286	0.072	0.051
Site mode: hydrostatic	1.054	0.434	0.126	0.008	0.005
Site mode: wet	0.570	0.330	0.166	0.041	0.029

2) ESA model

The troposphere model developed by ESA improves upon the results of the RTCA-MOPS model. Its meteorological dataset contains not only the annual but the diurnal variations of the core parameters as well. In blind mode, the bias of the hydrostatic delays, while still high at lower elevation angles, diminishes around 10° (Fig. 2a). The decrease of the blind σ and RMS values becomes faster as well (Table II.). The bias of the wet delays calculated in blind mode is substantially lower than the values of the RTCA-MOPS model (Fig. 2b and Fig. 1), even at the elevation angle of 10°. The same trend can be noticed for the standard deviation as well.

Using the site mode of the model, further improvements can be noted in the hydrostatic delays. The bias becomes increasingly lower even at the elevation angle of 10° and while there is some fluctuation in the σ values at lower elevations, the results become consolidated at approx. 10° of elevation. As for the wet part of the tropospheric delay, both the bias and the σ values remain relatively high up to the elevation angle of 10° and decreasing to approx. the same levels as in blind mode at higher elevations (Table II.).

Table II. shows the calculated RMS values for each of the operation modes of the ESA model.

TABLE II. RMS values of the ESA model in meters

Operation mode and type of delay	Elevation angles				
	3°	*5°*	*10°*	*45°*	*90°*
Blind mode hydrostatic	0.697	0.266	0.085	0.017	0.012
Blind mode: wet	0.405	0.261	0.136	0.034	0.024
Site mode: hydrostatic	0.692	0.252	0.066	0.010	0.007
Site mode: wet	0.361	0.235	0.123	0.031	0.022

3) The GPT2 model

As described in Section II, when we talk about the GPT2 model, we mean the Saastamoinen [9] and the Askne-Nordius [10] troposphere models to calculate the hydrostatic and the wet parts of the delay respectively, using the meteorological parameters supplied by the GPT2 as input data. While the GPT2

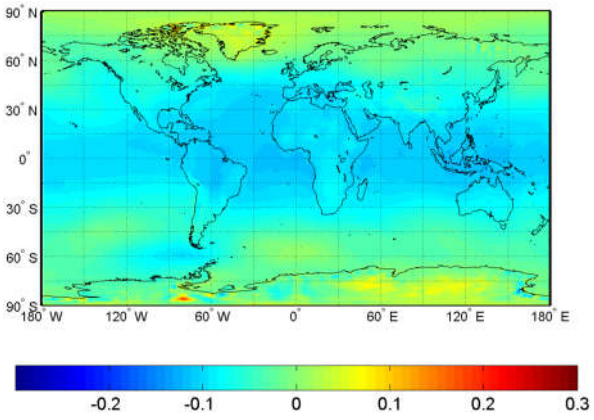

(a)

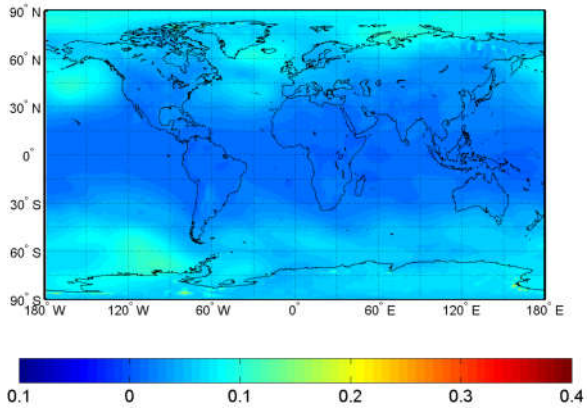

(b)

Fig. 2. Bias of the hydrostatic (a) and wet (b) parts of the tropospheric delay, calculated using the blind mode of the ESA model.

itself was developed after the ESA model, it cannot be considered a direct improvement on it. This is due to the fact, that even though it contains the annual and semi-annual variations of the parameters, this is only valid for the parameters used for the hydrostatic delay calculation.

The bias for the hydrostatic part computed in blind mode show little difference between the ESA model and GPT2, with the GPT2 being slightly more coherent at lower elevation angles. The σ values are practically identical for both troposphere models. As for the wet part calculated in blind mode, the bias of the GPT2 results are significantly higher up to 10° of elevation and remain so around the equator even above that. In terms of the σ values, little to no improvement can be noticed (Table III.).

Similar results can be seen when the model is used in site mode. The hydrostatic bias values show no development, while there is some improvement in coherence of the σ results. The higher bias values of the wet delays are more concentrated around the equator in case of the GPT2, as opposed to the ESA model and continue to remain higher at elevation angles above 10° as well. Similarly, the high σ values are condensed more noticeably in a 60° swath around the equator and remain slightly larger at higher elevation angles (Fig. 3).

According to the RMS values in Table III., even at higher elevation angles, the GPT2 model deviates slightly more from the reference data than the ESA model.

TABLE III. RMS VALUES OF THE GPT2 MODEL IN METERS

Operation mode and type of delay	Elevation angles				
	3°	*5°*	*10°*	*45°*	*90°*
Blind mode hydrostatic	0.724	0.275	0.085	0.017	0.012
Blind mode: wet	0.498	0.316	0.163	0.040	0.029
Site mode: hydrostatic	0.710	0.258	0.067	0.010	0.007
Site mode: wet	0.435	0.276	0.142	0.035	0.025

4) The GPT2w model

The GPT2w can be considered a direct improvement of the GPT2 model, with the aim of enhancing the accuracy of modelling the wet part of the tropospheric delay. The model contains the annual and semi-annual variations for the parameters used to calculate the wet part of the delay as well.

Comparing the bias of the hydrostatic delay calculated using the blind mode of the model to the ESA model, we receive similar results with the GPT2w having more consistent deviations from the reference dataset at lower elevation angles. The σ values show little difference as well. The improved wet delay modelling of the GPT2w shows significant improvement in the bias of the differences at lower elevation angles, however,

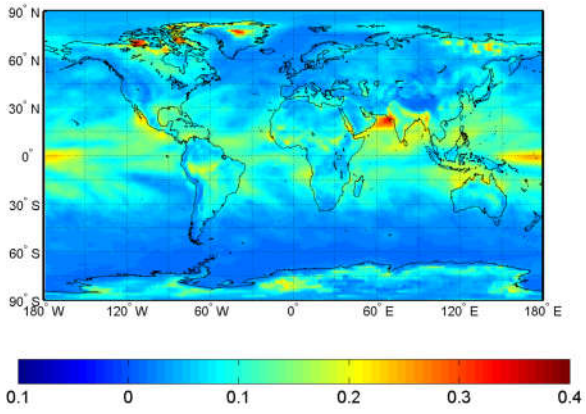

(a)

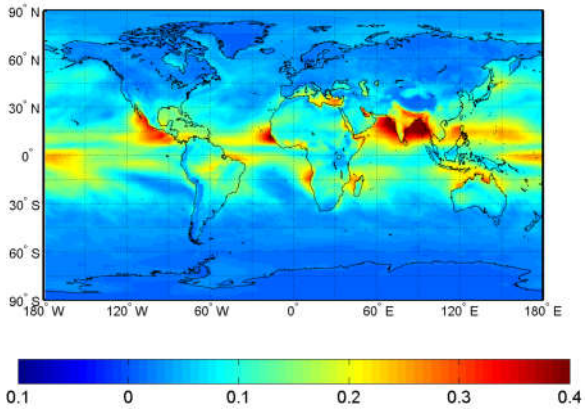

(b)

Fig. 3. σ values of the wet tropospheric delay computed using the ESA (a) and the GPT2 (b) models in site mode at the elevation angle of 10°.

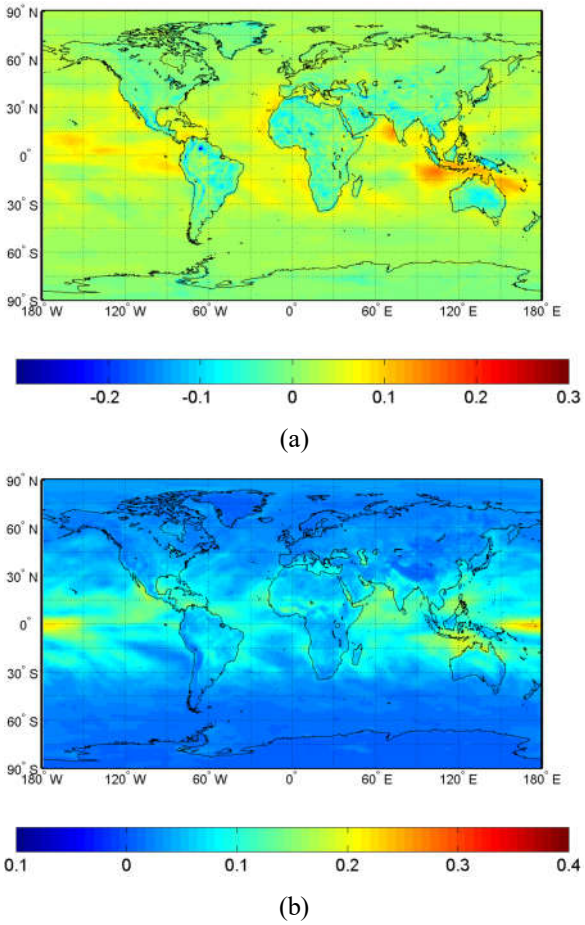

Fig. 4. Bias (a) and σ (b) values of the wet tropospheric delay computed using the site mode of the GPT2w model at the elevation angle of 10°.

it tends to remain a bit higher at the equatorial region than the ESA model. The σ values show the same trend, at lower elevation angles, the GPT2w indicates improvement compared to the ESA model, even though the results become rather similar at higher elevation angles.

When using the site mode of the model to calculate the hydrostatic delay, it shows little to no improvement compared to the ESA model or the GPT2 in terms of both bias and σ values. However, when modelling the wet part of the delay, the difference is quite significant with the GPT2w giving smaller bias values even at lower elevation angles. The σ values display improvement as well up to the elevation angle of 45°, above which the difference is no longer noticeable (Fig. 4).

The RMS values presented in Table IV. indicate that the model data from the GPT2w generally better resembles the reference dataset, however much of the improvement can be noted in modelling the wet part of the tropospheric delay in both blind and site modes.

TABLE IV. RMS VALUES OF THE GPT2W MODEL IN METERS

Operation mode and type of delay	Elevation angles				
	3°	*5°*	*10°*	*45°*	*90°*
Blind mode hydrostatic	0.719	0.272	0.083	0.016	0.012
Blind mode: wet	0.267	0.172	0.089	0.022	0.016
Site mode: hydrostatic	0.710	0.258	0.067	0.010	0.007
Site mode: wet	0.197	0.128	0.067	0.017	0.012

V. SUMMARY AND CONCLUSIONS

In the paper we presented the comparative analysis of troposphere delay models currently applied in high precision processing of GNSS observations. The reference dataset used in the study was generated employing a ray tracing algorithm and meteorological data from a numerical weather model as input. Comparing the computed delay from each model to the ray tracing data, we determined statistical parameters for every studied model to assess their quality. While the models produce increasingly good results at higher elevation angles, in case of integrity considerations, accurate performance at lower elevations is key. Out of the four models analysed in the paper, the troposphere model developed by ESA and the GPT2w model developed by the Technical University of Vienna proved to give results that best fit the reference dataset. Both models have similar characteristics concerning the hydrostatic part of the delay with the GPT2w supplying significantly improved results for the wet part of the tropospheric delay even at lower elevation angles.

REFERENCES

[1] "MOPS-DO-229D with Change 1 - Minimum Operational Performance Standards for Global Positioning System/Satellite-Based Augmentation System Airborne Equipment," Radio Technical Commission for Aeronautics, December 2006.

[2] A. Martelucci, ESA Galileo Programme, "Galileo Reference Troposphere Model for the user receiver," 2002, ESA-APPNG-REF/00621-AM, ver. 2.7, 2012

[3] K. Lagler, M. Schindelegger, J. Böhm, H. Krásná and T. Nilsson, "GPT2: Empirical slant delay model for radio space geodetic techniques," 2013, Geophysical Research Letters, 40(6), 1069-1073. doi: 10.1002/grl.50288

[4] J. Böhm, G. Möller, M. Schindelegger, G. Pain, and R. Weber, "Development of an improved empirical model for slant delays in the troposphere (GPT2w)," 2015, GPS Solutions, 19(3), 433-441. doi: 10.1007/s10291-014-0403-7

[5] J. Ádám, L. Bányai, T. Borza, Gy. Busics, A. Kenyeres, A. Krauter, B. Takács, "Műholdas helymeghatározás," Műegyetemi Kiadó, Budapest, 2004, pp. 100-103.

[6] H. D. Black and A. Eisner, "Correcting satellite Doppler data for tropospheric effects," 1984, Journal of Geophysical Research. 89, pp. 2616-2626

[7] A.E. Niell, "Global mapping functions for the atmosphere delay at radio wavelengths," 1996, J. Geophys. Res. 101(B2):3227-3246.

[8] J. Boehm and H. Schuh, " Vienna Mapping Functions," 2003, 16. Working Meeting on European VLBI for Geodesy and Astrometry 131-143.

[9] J. Saastamoinen,. "Atmospheric correction for the troposphere and stratosphere in radio ranging of satellites," 1972, The Use of Artificial Satellites for Geodesy, 15, pp. 247-251.

[10] J. Askne and H. Nordius, "Estimation of tropospheric delay for microwaves from surface weather data," 1987, Radio Science, 22, 379-386, DOI: 10.1029/RS022i003p00379

[11] E. K. Smith and S. Weintraub, "The constants in the equation for atmospheric refractive index at radio frequencies," 1953, Proceedings of the Institute of Radio Engineers 41, pp.1035-1037.